# Organic Photorefractive Materials and Applications

**ARTICLE** *in* ADVANCED MATERIALS · NOVEMBER 2011

Impact Factor: 17.49 · DOI: 10.1002/adma.201100436 · Source: PubMed



**3 AUTHORS:**

Sebastian Köber
Qiagen
**64** PUBLICATIONS **247** CITATIONS
SEE PROFILE

Michael Salvador
Friedrich-Alexander-University of Erlangen-…
**36** PUBLICATIONS **299** CITATIONS
SEE PROFILE

Klaus Meerholz
University of Cologne
**324** PUBLICATIONS **10,056** CITATIONS
SEE PROFILE

# Organic Photorefractive Materials and Applications

*Sebastian Köber, Michael Salvador, and Klaus Meerholz**

**This review describes recent advances and applications in the field of organic photorefractive materials, an interesting area in the field of organic electronics and promising candidate for various aspects of photonic applications. We describe the current state of knowledge about the processes involved in the formation of photorefractive gratings in organic materials and focus on the chemical and photo-physical aspects of the material structures employed in low glass-transition temperature amorphous composites and organic photorefractive glasses. State-of-the art materials are highlighted and recent demonstrations of photonic applications relying on the reversible holographic nature of the photorefractive materials are discussed.**

## 1. Introduction

The term "photorefractive" (PR) loosely characterizes a material that exhibits a temporal change of its refractive index induced by illumination. In turn, the same definition describes the creation of a phase-hologram, the most effective way to simultaneously store amplitude and phase of any arbitrarily shaped light wavefront. Moreover, the transient nature of the PR effect enables the fully reversible control of the propagation properties of one light beam by another light beam in the material, which is the basis of optical computing and regarded as a promising mechanism for various kinds of holographic, or more general, photonic applications.

Since the first description of the PR effect in inorganic crystalline materials in 1966,[1] several material systems exhibiting the PR effect have been discovered. However, despite the huge diversity of material approaches, all PR materials share the same basic mechanism (see **Figure 1**): non-uniform illumination of the material (e.g. through a laser interference pattern) leads to the generation of oppositely charged carriers in the bright regions. One carrier type is mobile, which is subsequently displaced and trapped in the regions of low light intensity. The resulting space-charge field in turn alters the refractive index through second- or higher-order non-linear optical effects.

Since the first demonstration of the PR effect in an organic material in 1991,[2] tremendous improvements regarding their general performance, shelf life-time and also the theoretical description of the underlying physics have been obtained through combined achievements of scientist in the fields of chemistry, physics, material science and optical engineering. Several review/feature-articles[3–10] and book chapters[11–16] clearly highlight the maturation of this dynamic field. It should be stressed that these improvements go along with recent advances in the field of organic electronics, like organic light emitting diodes (OLED), organic field-effect transistors (OFET) and organic photovoltaic devices (OPV). Especially the latter, in the well-known bulk hetero-junction configuration, shares several photo-physical aspects similar to electronic processes in organic PR materials.

Today, organic PR materials are considered as an equal alternative to inorganic PR crystals. This is due to the benefits from their organic heritage, like low-cost, ease in processability, the possibility to tune their properties through modification of their chemical or compositional properties, to name just a few. Moreover, organic PRs benefit from the extensive research on organic electronic materials (organic semiconductors) and molecules with high optical nonlinearity.

The fundamental difference between crystalline inorganic and amorphous organic materials arises from the difference in their dielectric constants (high in inorganics, low in organics), which renders charge generation and transport in the organic materials highly field-dependent. Thus, the description of the photo-physical mechanisms in these materials is generally more complicated. Moreover, typical inorganic semiconductor band-type models are unable to describe the behavior of organic materials, which are characterized by highly confined, discrete distributions of energetic states. On the other hand, the field-dependence of chromophore orientation introduces features unknown to inorganic PRs, like the amplification of the refractive index change by the "orientational enhancement mechanism".[17]

This review highlights recent advances in the field of organic PRs since the last comprehensive review by Ostroverkhova et al.[4] in 2004. We focus on low glass-transition temperature ($T_g$) amorphous composite materials, which constitute the most investigated and most successful class of organic PR materials to date. After a rather brief introduction to the theory and general material aspects in Section 2, we present recent achievements in the research of new materials and physical effects in Section 3 and 4, respectively. Section 5 is devoted to the recent demonstration of holographic applications in organic PR

Prof. K. Meerholz, Dr. S. Köber, Dr. M. Salvador[+]
Department of Chemistry
University of Cologne
Luxemburger Str. 116, 50939 Cologne, Germany
E-mail: klaus.meerholz@uni-koeln.de
[+]Present adress: Department of Chemistry, University of Washington, Box 351700, Seattle, WA 98195, USA

**DOI: 10.1002/adma.201100436**

materials. We conclude the review with an overview on sample fabrication and measurement techniques in Section 7.

## 2. The Photorefractive Effect in Organic Materials: Theoretical Description

A PR material requires three basic properties: (1) photosensitivity at the operating laser wavelength, which leads to photogeneration of charges, (2) charge mobility, which should differ for electrons and holes, and (3) electro-optic activity, which basically describes a field-dependent refractive index in non-centrosymmetric bulk materials. In contrast to PR crystals and PR semiconductor materials, in amorphous composite materials, each of these functionalities is introduced by a specific molecule in the blend. It should be pointed out that the following description is applicable to other organic PR materials like organic glasses, fully-functionalized materials and liquid-crystal (LC) doped polymeric structures as well.

A step-wise description of the formation of a PR grating in organic materials is depicted in Figure 1.

The dc-biased PR material is illuminated by a stationary interference pattern $I(x)$ originating from the superposition of two coherent laser beams. In the bright regions of the interference pattern, geminate charge carrier pairs are created which either recombine or escape their counterpart beyond their coulombic attraction by assistance of an electric field. Since both charge-carriers exhibit a different mobility in the material, typically only one carrier is displaced via field-induced drift into the regions of lower light intensity,[13] which results in a relative displacement of the centre of charges. In organic materials, most commonly the hole is displaced. Due to the presence of a strong applied electric field, the contribution of carrier diffusion to the transport of charges is usually neglected. The holes drift by hopping between adjacent sites provided by the charge-transporting agent (CTA), until the mobile charge eventually gets trapped in the areas of lower light intensity. Trapping generally refers to a process hindering the mobile charge to further participate in charge transport. A deeper insight into trapping in organic materials is presented in chapter 2.1.3. Poisson's equation of electrostatics requires that the derivative of the distribution of charge-carrier density $\rho(x)$ leads to the formation of a modulated space-charge field $E_{SC}(x)$, which therefore exhibits a phase-shift $\varphi$ relative to the illuminating interference pattern $I(x)$. In the diffusion limit (PR crystals without applied poling field), $E_{SC}$ is phase-shifted by $\varphi = \pi/2$, which corresponds to one quarter of the grating spacing $\Lambda$. In drift-dominated materials, the phase-shift is $\varphi < \pi/2$ and depends on the charge transport capabilities of the material and the grating spacing of the interference pattern.

The final step of the recording process is the translation of the space-charge field into a refractive index modulation through the linear electro-optic effect (Pockel's effect) in non-centrosymmetric media. In amorphous media, application of a poling field is employed to break the centrosymmetry of the bulk material through orientation of the electro-optic species, usually referred to as chromophores. Additional contributions from modulated birefringence

**Klaus Meerholz** studied chemistry at the Universities of Bielefeld and Freiburg and he received his Ph.D. in 1991. He was a postdoctoral fellow at SUNY Buffalo/USA and an Assistant Research Scientist at the Optical Sciences Center, University of Arizona (1993–1995). In 1995 he moved to the University of Munich, where he finished his Habilitation in 1998. Since 2001 he holds a Chair of Physical Chemistry at the University of Cologne/Germany. His research interests are organic light-emitting diodes for display applications, organic solar cells for photovoltaics, organic nonlinear optics, organic holographic storage media for optical data processing, smart sensors for high-throughput screening, and organic electrochemistry.

**Michael Salvador** graduated from University of Cologne with a M.S. (Diploma) and Ph.D. in Chemistry (2002, 2008). His doctoral research focused on photorefractive polymer composites for coherence-gated holographic imaging. Subsequently, Michael worked with Prof. Changhuei Yang (Caltech) on optical phase conjugation for turbidity suppression in tissue models. Recently, he joined Prof. David Ginger at University of Washington where he investigates colloidal-enhanced organic solar cells.

**Sebastian Köber** studied Chemistry at the University of Cologne and completed his diploma degree in physical chemistry in 2005. His PhD under the supervision of Klaus Meerholz focuses on the development and characterization of photorefractive polymer composites for real-time NIR applications, with emphasis on depth-resolved imaging through scattering media.

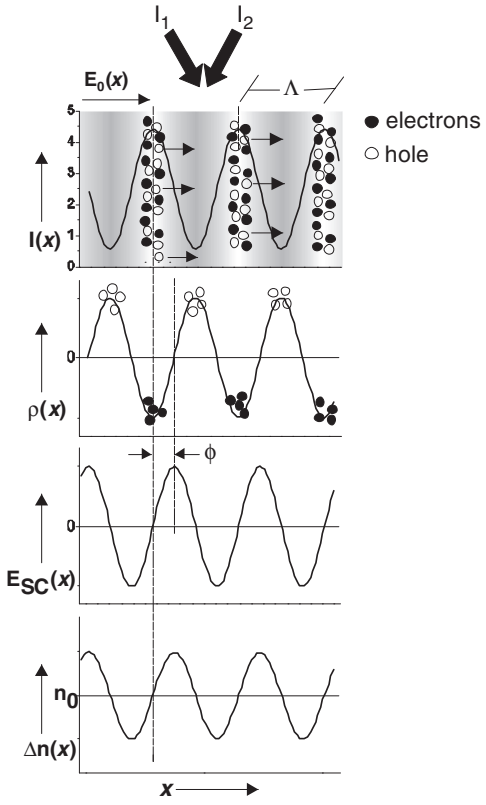


**Figure 1.** Stepwise description of the photorefractive effect in organic media (only holes are considered mobile), under an applied field $E_0$ and illumination by coherent write-beams $I_1$ and $I_2$.

through the orientational enhancement mechanism in low-$T_g$ organic materials will also be discussed in Section 2.1.4. As depicted in Figure 1, the final refractive index modulation is in phase with the space-charge field and thus, also phase-shifted relative to the interference pattern. This phase-shift leads to asymmetric energy transfer between the write beams (see Section 7.2.3). The phase-shift distinguishes the PR effect from in-phase ($\varphi = 0, \pi$) light-induced refractive index changes, e.g. formed through photochromism, photoisomerization, photobleaching, thermochromism, density gratings (photopolymerization) etc.

## 2.1. Photo-Physical Mechanisms

In this Section, we will provide a rather brief introduction on the photo-physical mechanisms underlying the description of the PR effect as presented above. For a more rigorous treatment, the reader is referred to recent book chapters.[13,14] The description of the mechanisms for photoconductivity (which is the convolution of charge-carrier generation and transport) will be based on a polymeric hole-conductor (p-type charge transport agent, CTA) doped with little amounts of an electron accepting species (n-type sensitizer), since this constitutes the most common situation in organic PR materials.

### *2.1.1. Charge-Carrier Photogeneration*

The charge-generation process in biased p-type PR materials involves photo-excitation upon absorption of light in the bright regions of the interference pattern. Owing to the low intrinsic absorption of most organic photoconductors in the visible and NIR, sensitizers are incorporated into the material. The field-independent generation of coulombically bound electron-hole pairs (excitons) upon absorption is followed by electron transfer and subsequent trapping of the electron on the lowest unoccupied molecular orbital (LUMO) of the sensitizer. The mobile hole is subsequently injected into the highest occupied molecular orbital (HOMO) of the charge transporting manifold. The dissociation of the exciton to yield free charges has thereby to compete with geminate recombination processes, which are affected by the screening of the charges by the surrounding matrix. A measure for this screening is the effective coulomb radius $r_C$, which is inversely proportional to the dielectric constant $\varepsilon$. The latter is generally small in organic polymeric materials ($\varepsilon < 10$) as compared to inorganic systems ($BaTiO_3$: $\varepsilon = 3600$). This leads to relatively high recombination rates in organic materials and to poor internal charge generation quantum yields $\varphi$, which is the fraction of the number free charge carriers created by the number of absorbed photons. To obtain a reasonable amount of charges in organic composites, strong external fields are applied to the material. This suppresses geminate recombination by reducing the coulombic attraction between the carriers in accordance with the Poole-Frenkel effect.[18]

### *2.1.2. Transport*

The physical quantity describing the ability of a material to transport charges is the mobility μ. Recent publications about charge transport in organic materials with a broad scope on organic electronics can be found in Refs. [18–20]. In contrast to band-like transport in ordered inorganic semiconductors, the low intermolecular coupling in organic materials leads to highly confined, localized charge transport sites. Thus, charge transport in amorphous and highly disordered organic media is highly field and temperature dependent. Displacement of charges is usually described in terms of temperature-activated molecular hopping between adjacent redox sites of similar energy. Those sites are chemically identical, but physically different. Due to fluctuations in intermolecular potentials and relative positions the charge transport manifold is subject to a distribution in energetic (diagonal) and positional (off-diagonal) disorder. A very successful model to describe the temperature and field dependence of the charge carrier mobility is the Gaussian disorder or hopping model by Bässler and co-workers.[1]

With regard to PR composites, it is worth noting that the described model is valid for temperatures below the glass-transition temperature $T_g$. At this temperature the material is characterized by a rubber-like state with sufficient free internal volume. By that, thermally induced fluctuations of the molecular arrangement may induce further variations in the energetically distribution of transport sites. Moreover, PR composites are often doped by large amounts (20–50 wt.%) of dipolar molecules (chromophores, see below), which induce

further energetic disorder and thus generally lower the charge mobility.[22]

### 2.1.3. Evolution of the Space-Charge Field: Influence of Trapping Parameters

A central necessity of photorefractivity is the presence of trapping sites in the material, which describe entities in the material that hinder charges to participate in transport by capturing charges for some time. Trapping and de-trapping rates are important properties for the dynamic build-up and the steady-state amplitude and phase of the space-charge field $E_{SC}$ in the material. Compared to the nature of traps in inorganic PR crystals, the situation is more complex in organic materials, since a single trapping species is insufficient to describe $E_{SC}$ formation here. Still, the nature of traps in organic materials is still not fully understood.

One trapping process in organic photorefractives is due to the recombination of the mobile hole with a radical anion of the sensitizer moiety, formed upon the charge generation process. An apparent implication of this trapping mechanism is the fact, that the number of recombination traps, which are formed due to the charge generation process, are thus not constant but dynamic and depend on the measurement (illumination and applied field) and the material ($T_g$, sensitizer concentration, thermally accessible traps) conditions. An additional intrinsic trap level stems from the dispersive nature of charge transport in organic materials, as pointed out in chapter 2.1.2. Every transport site of lower potential energy than its surroundings (the tail of the DOS) is thus capable of trapping charges. These traps are uncharged and thermal energy is usually sufficient for de-trapping of the carriers (field dependent process due to the Poole-Frankel effect).

Schildkraut et al.[23,24] introduced an analytical model to provide solutions for the steady-state space-charge field amplitude and phase. It included the uncharged trap species as derivation from the Kukhtarev model[25] for inorganic crystals, together with the field-dependence of the main photoconductivity parameters, namely charge generation efficiency and mobility. **Figure 2** depicts an energy level scheme of the original Schildkraut model.

Analytical solutions for the build-up dynamics of $E_{SC}$ were given by Yuan et al.,[26] for erasure dynamics by Cui et al.[27] Recently, Ostroverkhova et al.[22] expanded the Schildkraut model by introducing two thermally de-trappable trap levels, shallow and deep traps. The trap-depth is solely determined by the escape conditions, the detrapping rate. The authors distinguish the trap depth by a more than one order of magnitude slower detrapping rates for deep traps in contrast to shallow traps.

Through time-dependent photo-physical measurements under pulsed conditions, Kulikovsky et al.[28] were moreover able to independently determine trapping rates and trap densities of a PR composite. A comprehensive overview and mathematical treatment of the mentioned models so far are given in Ref. [13].

Traps may be intrinsic to the material or extrinsic due to doped components. One frequently encountered example is the use of chromophore molecules with lower ionization

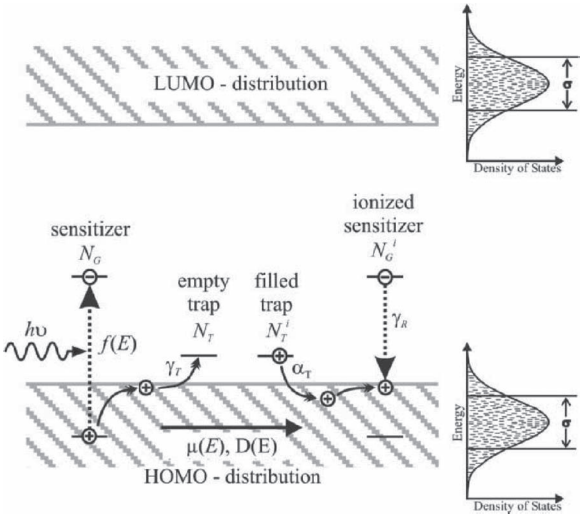


**Figure 2.** The Schildkraut model. Upon absorption of a photon of energy h$\nu$, a sensitizer molecule is excited; subsequently a mobile hole is injected into the HOMO of the hole-conductor and displaced by drift or diffusion along its density of states (DOS). The hole is captured by an uncharged trap (density $N_T$, trapping rate $\gamma_T$) and may be released from the filled trap with the de-trapping rate $\alpha_T$. The mobile hole may also recombine with an excited sensitizer radical anion in its proximity with the rate $\gamma_T$. Reproduced with permission.[13] Copyright 2006, Springer.

potential than the CTA.[22,29,30] A linear dependence between optimum trap-depth and energetic disorder of the charge transport manifold for efficient space-charge field formation is predicted through Monte-Carlo (MC)-simulations.[31] A similar linear dependence is obtained for trap concentration and trap dipole,[32] but no experimental verification of the predictions is given so far. Recently, Oh et al. presented a model[30] which modified the Schildkraut–model to include rate constants of trapping, de-trapping, recombination and trap density dependent hole-mobility. This model yielded good agreement for simulated photocurrent and space-charge field amplitudes for different trap densities and gathered experimental data on a PSX-Cz-based material doped with DB-IP-DC-chromophores, which acts as an extrinsic trap in this particular material. Moreover, Samiullah[33] discussed the possibility of the development of a space-charge field in the hypothetical absence of any trap states and the influence of exciton diffusion on the formation of space-charge fields.

Finally, the photo-electromotive force technique (photo-EMF, see Table 5) was employed by Gather et al.[34] to obtain a complete set of photoconductivity parameters. The low external voltage requirements of this technique even allowed for probing of the Einstein relation between drift mobility and diffusion coefficient in the materials.[34,35]

### 2.1.4. Electro-Optic Response

The final step in the formation of a PR grating is the translation of the space-charge field into an in-phase refractive index modulation. For a comprehensive review of the topic, the reader is referred to.[14] In inorganic crystals, this change arises from the polarization of the crystal lattice and forms solely through

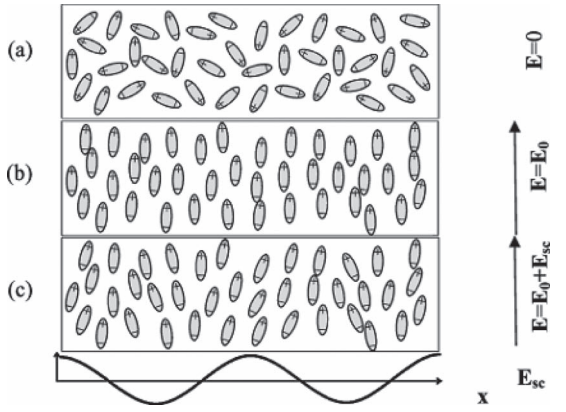


**Figure 3.** Chromophore orientation and the orientational enhancement effect in low-$T_g$ photorefractive composites. a) random orientation of the chromophores in the matrix, the bulk material is therefore centrosymmetric and does not show even-order non-linear effects. b) the application of an external field $E_0$ orients the chromophores (degree of orientation is exaggerated for illustration purposes), the material is now non-centrosymmetric and birefringent. This allows for refractive index changes through the second-order non-linear (Pockel's) effect. c) the modulation of the chromophore orientation by the static external field and the spatially varying space-charge field $E_{SC}(x)$ gives rise to a refractive index change by the orientational Kerr-effect. A significant fraction of the overall effect hereby stems from the modulation of birefringence in the material. Reproduced with permission.[4] Copyright 2004, American Chemical Society.

the electro-optic (EO) or Pockels effect (field-dependent refractive index). In organic materials, the non-linearity is achieved by doping the material with EO dyes, so-called chromophores, which will be further discussed in Section 3.4.

With regard to the glass-transition temperature of the organic composite, two different material classes have to be distinguished:

(1) **hard materials** with a $T_g$ above room temperature. Here, the material is usually heated above $T_g$, an electric field $E_{ext}$ is applied to induce orientation of the chromophores to break centrosymmetry and the material is subsequently cooled. This freezes the orientation of the chromophores, the non-linear response of the material is solely due to the Pockels effect. Since repeated heating and cooling cycles are detrimental for the lifetime of organic films due to formation of cracks, these materials are largely omitted in recent literature in favor of

(2) **soft/plasticized materials** with a $T_g$ near or below room temperature. Here, the chromophores have sufficient orientational mobility to be oriented in situ during recording. The electric field experienced by the chromophore is then due to the total electric field $E_T$, which denotes the superposition of the static applied electric field $E_{ext}$ and the space charge field $E_{SC}$ upon grating recording. Due to the modulation of $E_{SC}$, $E_T$ and thus the degree of poling are modulated periodically in amplitude and direction, the refractive index change becomes quadratically dependent on the electric field (orientational Kerr effect). As a result, the poling induced birefringence becomes also modulated and contributes to the refractive index modulation. This improvement was first described by Moerner et al.[17] and is referred to as "orientational enhancement mechanism" (OEM), see **Figure 3**.

The birefringence contribution accounts for a significant amount of the refractive index modulation (up to 70–80% of the whole NLO effect, depending on the nature of the chromophore), and thus requires a refinement of the chromophore figure of merit (FOM) for PR low-$T_g$ composites (see Section 3.4).

## 3. Materials

### 3.1. Photorefractive Material Classes

In principal, every system combining photoconductivity and nonlinear optical response is capable of featuring the PR effect. Several PR systems are described in the literature: besides a huge variety of inorganic crystals ($BaTiO_3$,[36] $KNbO_3$,[37] $LiNbO_3$,[38,39] $Sn_2P_2S_6$ (SPS)[40] to name just a few prominent examples (for a comprehensive overview, the reader is referred to Ref. [15]), the PR effect was demonstrated in compound semiconductors (GaAs, InP, CdTe etc.[41,42]), III-V and II-VI semiconductor multiple quantum wells (MQWs),[43,44] organic crystals (COANP doped with TCNQ, MNBA, DAST[15]), liquid crystalline materials (containing doped photorefractive LCs and polymer dispersed LCs (PDLC), see below), and amorphous materials. A more or less direct comparison of the different approaches in terms of performance and properties can be found in Ref. [15].

The huge diversity of approaches to the PR effect gives rise to materials with fundamentally different properties and accordingly diverse possible areas of application. In order to differentiate between the different concepts, important material characteristics and properties are given in **Table 1**. The aim is to provide the reader with a general overview instead of establishing a direct quantitative comparison.

#### *3.1.1. Sensitivity (Diffraction Efficiency and Response Time)*

For almost all applications relying on the dynamic and reversible properties of the PR-materials, the sensitivity is of uttermost relevance. Several definitions of sensitivity can be found in the literature.[15] Generally, materials which need less time at a lower irradiance to reach a specified refractive index modulation feature the respective higher sensitivities. The amplitude of the refractive index modulation and hence obtained diffraction efficiency can be defined due to the necessities of the target application of the material. To account for absorption losses of the materials, usually external diffraction efficiencies are taken for calculation (see Section 7.2.4). Most definitions of sensitivity do however not include the value of the applied external field used to achieve a certain dynamic response.

The sensitivity does not lend itself for comparison of the material classes above, since the huge differences in dynamic range and device thicknesses of the different approaches impede the definition of a significant $\Delta n$ reference. For reasons of clarity, we refrain from scaling individual data to some reference arrangement. Instead, the sensitivity is broken down

**Table 1.** Comparison of different PR materials: amorphous composites, polymer dispersed liquid crystals (PDLC), inorganic crystals, and photorefractive multiple quantum well (MQW) structures in the transverse geometry (field applied parallel to the wells). The materials are contrasted on applied field requirements under operational conditions, wavelength range at which materials were demonstrated, material thickness, typical device cost, achievable sample aperture, diffraction efficiency, refractive index modulation and response time (fitting constants, if not explicitly stated).

| | amorphous | PDLCs | inorg. crystals | MQWs |
|---|---|---|---|---|
| % diffraction efficiency | 90–100[a] (532–1064 nm), 40 (1550) | 60–100 | up to 90 ib-PR[b]:0.1 | 0.1–1, 2[c] |
| refractive index modulation | $10^{-3}$[d] $10^{-2}$[e] | $10^{-3}$ | $10^{-5}$–$10^{-3}$ ib-PR[b] $10^{-5}$–$10^{-4}$ | $<10^{-2}$ |
| response time | 300 μs,[f] 5 ms,[g] 50 ms,[h] 35 ms[i] | 100 ms–10s | <1 s[j]–300 s[k] 10–100 ms[l] ib[b] 1-50 μs | 0.4 ms,[m] 1–100 kHz |
| field requirements [V μm$^{-1}$] | 20–100 | 5–50 | 0–2 | 0.1–1 |
| wavelength range [nm] | 532–1550 | 450–780 | UV-NIR | 600(II–VI), 830-840, 1064(III–V) |
| aperture [cm$^2$] | up to 900[n] | 10 | 1 | 0.04 |
| thickness [μm] | 20–200 | 10–100 | $10^4$[o] | 1–2 |
| cost | cheap | cheap | expensive | expensive |

[a]100% internal diffraction efficiency is never reached in practice due to internal losses. Complete internal diffraction usually refers to over-modulation of the signal (see experimental Section) in transmission geometry at $\eta > 90\%$; [b]interband photorefraction, here SPS at 480/532 nm; [c]microcavity enhanced;[44] [d]composites and [e]glasses; [f]pulsed recording, 4 mJ cm$^{-2}$ 532 nm, 95 V μm$^{-1}$ bias;[45] [g]cw-647 nm, 1 W cm$^{-2}$, 100 V μm$^{-1}$;[46] [h]cw-830 nm, 0.6 Wcm$^{-2}$, 57 V μm$^{-1}$, $\tau_{50}$-value;[47] [i]11.4 μJ fs-pulses, 1550 nm, 93 V μm$^{-1}$; [j,k]Rh-doped $KNbO_3$, 2BC dynamics; [j]$\lambda < 500$ nm; [k]$\lambda = 1064$ nm;[37] [l]SPS, $\lambda = 1064$ nm;[40] [m]25 kHz repetition rate under imaging conditions;[48] [n]holographic display, see Section 5.6; [o]the penetration depth in case of interband photorefraction is severely limited due to high absorption, with absorption coefficients $\alpha$ up to several thousand per cm.

into maximum achievable diffraction efficiency, obtainable refractive index modulation amplitude and the response time of the materials.

### 3.1.2. Field Requirements

Contrary to inorganic crystalline systems, all organic PR materials (except organic crystals) require the application of external dc-fields in order to induce bulk non-centrosymmetry and/or to enable/enhance photoconductivity. It should be pointed out, that in these materials, a trade-off between the magnitude of the applied field with respect to the enhancement of field-dependent effects and the operational lifetime of the sample exists, which is limited by dielectric failure.

Inorganic crystals, however, show the PR effect without any applied external field, yet in some instances electric fields are applied to enhance the performances of the crystals. In the case of MQWs, the photoconductivity is not given by photoionization, but by direct interband transitions upon irradiation. In the transverse geometry, in which the MQW behaves most similar to other PR materials, the applied field leads to ionization of the quantum confined excitons and lifetime broadening of the excitonic transition (Franz-Keldysh effect). The change of absorption upon application of an electric field (electroabsorption) subsequently leads to a change of the refractive index (electrorefraction) through the Kramers-Kronig relation.

### 3.1.3. Wavelength

Amorphous organic materials are flexible with regard to the range of operational wavelength, solely limited to the availability of appropriate sensitizing agents (red/NIR) and to the transparency of the composite (<532 nm). For inorganic crystals, the operational wavelength depends on the properties of the respective crystal and its doping and processing (wide bandgap ferroelectrics). Some crystals exhibiting small bandgaps were also demonstrated to reveal interband photorefractive effects (e.g. SPS, $E_g = 2.3$ eV, interband transitions for $\lambda < 532$ nm). While the direct transition between the valence and conduction band in the crystals gives rise to remarkable fast PR effects, the penetration depth and thus the effective thickness of the crystal is severely limited due to the increased absorption.

For PR-MQW, the wavelength is confined to a few nanometer wide spectral range close to the excitonic transition, due to the necessity of a resonant enhancement of the electro-optic effects induced by the applied electric field (see below).

### 3.1.4. Aperture

Aperture refers to the active material area which is available for the light beams to interact with each other. For inorganic PR materials, the area is mainly limited due to restrictions originating from the preparation of the material itself (PR crystal growth, semiconductor fabrication process). It should be noted that for MQWs operated in the transverse-field geometry the aperture equals the separation of the electric contacts.

Despite the inherent possibility to scale the aperture of amorphous organic materials without material restrictions, the manageability of the sample fabrication process in typical laboratory environments proves to be limiting. Enhancements due to typical plastic processing techniques (injection molding) were demonstrated (Section 7.1).

While most holographic applications do not require large apertures, they may be limiting in terms of storing gratings in the Fourier-domain (and thus low-pass filtering the spatial information) or direct image processing task carried out in the Image-domain (reducing the achievable field of view (FOV)-resolution product). Any defects in the sample structure due to the fabrication process (up to 2000 defects cm$^{-2}$ for MQWs[49]) may impose similar restrictions.

On the other hand, display applications (Section 5.6) scale in attractiveness with larger device apertures.

#### 3.1.5. Thickness

The thickness of the recording medium is (besides the grating spacing and thus the geometry) the crucial parameter determining the validity and the selectivity of the Bragg-condition (see Sections 7.1 and 7.2). Moreover, the product of the amplitude of the refractive index modulation and device thickness (more specifically the propagation length $l$ of the beams in the medium) determine the achievable diffraction efficiency of the device. The extent of amplification of one beam in PR materials showing net gain also depends on the thickness of the device ($\Gamma l$-product, see Section 7.2.3).

While the dimensions of inorganic crystals are solely limited by the crystal growth conditions, the thicknesses of organic amorphous and PDLC materials are restricted due to the necessity of the external field to be applied in direction of beam propagation. Thick materials thus require high-voltage sources, which is impracticable in light of applications. MQWs inherently are thin-film devices that operate in the Raman-Nath regime (see Section 7.2.1). The same applies to doped LC PR materials, which are typically operated at large grating spacings (50–100 μm) at thicknesses of 5-50 μm. It should be pointed out, that gratings written in the Raman-Nath and the Bragg regime are not directly comparable.

#### 3.1.6. Cost

The major difference in cost for the different material classes is due to the the fabrication processes involved in the preparation of the respective devices. The amorphous nature of the organic materials principally allows for low-cost high volume fabrication processes. Inorganic crystals growth however is a slow (two weeks for a 2 $cm^3$ SPS crystal boule[40]), and thus cost intensive process. MQWs are fabricated by periodically depositing up to hundred layers of around 10 nm thick semiconductor materials of different compositions, which requires clean-room conditions, specialized equipment and energy-intensive semiconductor fabrication processes (vapor epitaxy).

### 3.2. Organic Amorphous PR Systems

Due to the flexibility of organic chemical synthesis, approaches to the PR effect in amorphous organic materials are numerous. In addition to generally distinguish the materials due to their glass-transition temperature (soft and hard materials, see Section 2.1.4), a further means to categorize the materials is due to their structural components. Please note, that the border between categories may not be sharp in every case, but a rather smooth transition.

**Monolithic or fully functionalized materials** usually contain one single structural motif exhibiting photoconductive and electro-optic moieties. This group includes fully functionalized polymeric materials, where all functional groups are attached to an organic backbone. Similarly, organic sol/gel materials fall into this category, which are considered to be fully functionalized materials with an inorganic backbone. In some cases, very small amounts of a sensitizer or plasticizer are added to the monolithic materials. A feature article on this topic can be found in Ref. [10]. An apparent advantage of those systems is their phase stability and thus long shelf lifetimes, which happens to be a fundamental problem of the second main category.

**Compositional or multi-component approaches** describe distinct low-molecular-weight (LMW) molecules, which are doped into polymeric hosts. Despite the fact, that the first material of this "guest-host" combination was demonstrated on a nonlinear optical polymer doped with charge-transport molecules,[2] this approach was abandoned in favor of the higher performance of charge-transport polymers doped with EO-chromophores. Benefits of this approach include the simple tuneability of the composition and exchange of individual functional components of the blend. Due to that, polymer composites form the most investigated and successful category of organic PR materials. Hence, the following discussion will focus on this material class.

Nevertheless, composites of polymers and LMW dopants, which in the case of chromophores are of significantly higher polarity than the host matrix, are thermodynamically metastable, resulting in phase-separation of the individual components and the subsequent loss of optical quality of the material. In this review, several approaches to overcome this problem and to enhance the lifetime of the composites are discussed in the respective material sections.

Another category of organic photorefractives are **low-molecular-mass glasses**, in which the material blend consists of one or more components of low molecular weight, which forms an amorphous glassy solid. In some cases, a polymeric binder without further functionality is added to enhance the dielectric strength of the materials. Several publications describe blends, in which charge-transporter and chromophore form bi-functional moieties, either provided by a single molecule (chromophore with hole-transport capability) or by covalently attaching hole-conductor- and chromophore-molecule (dyads). Depending on the resultant composition, the material may either be regarded as monolithic or composite. Some materials from this category are discussed below.

The last category belongs to the area of **liquid-crystal-containing photorefractives**, which initially described doped liquid-crystalline PR systems, like low-molecular-weight nematic liquid crystals, liquid crystalline polymers and ferroelectric liquid crystals. The observation of high refractive index changes due to the orientational enhancement effect of *in situ* poled low-*Tg* PR polymers triggered the interest in liquid crystal materials, which is due to their comparably large Kerr effects and their collective reorientation under low applied fields. Grating formation in these materials is due to space-charge field formation by drift and diffusion of ions. "Photorefractive"-like refractive index changes in these materials are furthermore discussed to be due to conductivity and dielectric anisotropy, thermal diffusion, surface and interface effects.[16] However, in comparison to polymer composites, the EO component in doped LC materials is interacting over macroscopic distances. Thus, the length of the oriented liquid crystalline phase subsequently limits the achievable resolution and grating spacing. This is due to the inability of the weak elastic restoring forces to ensure efficient orientational modulation at higher grating frequency.

In order to increase the resolution, liquid crystals were dispersed in photoconductive matrices. This describes a photoconductive or doped inert polymer hosting phase-separated droplets of liquid crystalline molecules in high concentrations. Gratings in these materials are written analogously to the mechanism discussed above. However, polymer dispersed liquid crystals (PDLCs) feature effects unknown to photorefractive composite materials, as memory effects, switching from opaque to transparent state etc.

For a comprehensive overview on this topic, the reader is referred to recent book chapters,[16] review articles,[4,9] and highlight articles[50] on the matter. Recent publications on applications based on LC containing materials can be found in Refs. [51,52].

### 3.3. Chemical Approaches to the Photorefractive Effect in Organic Materials

In this Section, chemical approaches to the PR effect in amorphous organic materials from the current literature are discussed.

Organic PR materials have greatly benefited from research on organic electronic materials. Several materials and material classes from organic light emitting diodes (OLED) and organic solar cells (OSC) were implemented in PR materials, among them $Alq_3$ (OLED-emitter),[53] PCBM and derivatives (OSC-n-type conductor),[47] PF6-TPD (OLED- p-type conductor)[47,54,55] as one representative of TPD photoconductors, etc. A comparison of fundamental characteristics of OLEDs, OSCs and PR materials is depicted in **Table 2**. It is obvious, that OSCs and PR composites actually show a great level of structural similarity, despite their pronounced difference in active material thickness. The underlying photo-physical mechanisms, namely photo-charge-generation in the bulk material, recombination as a limiting mechanism, transport of charges through disordered random solids under an applied potential, are basically the same in both material classes, which presupposes an inherent similarity of the respective blend components. Due to that fact, Kronenberg et al.[56] recently fabricated OSCs from PR LMW-glass materials (see Section 3.4.4).

As outlined above, we will focus the further discussion here on low-$T_g$ guest-host composite materials, which is the widest investigated and most successful material class. This approach allows for a separate discussion on recent research on charge-conducting materials, sensitizer, chromophore, and other dopant molecules in individual chapters. As for the photoconductor, according to the dominant design strategy in literature, we emphasize on p-type hole-conductors. Accordingly, the discussion on the sensitizing agent will be accentuated on n-type electron-accepting materials, which are usually of very low content in the blends and thus do not provide a complementary path for electron conduction. Finally, the influence of further dopants on the photoconductivity will be discussed, followed by an overview on nonlinear optical dyes, so-called chromophores.

The materials will be compared on basis of results extracted from holographic measurements. A description of two- and four-wave mixing experiments are given in Sections 7.2.3 and 7.2.4, respectively.

#### *3.3.1. Transport: Charge Mobility*

The spatial displacement of the mobile charges upon photogeneration and the subsequent trapping of the charge carriers in areas of lower light intensity is a key requirement of PR materials in general. In recent publications on organic PR materials (except for research on low-molecular-weight glasses), it is common to incorporate a polymeric material with charge transport units in its main- or side-chain. In this way, the polymer also serves as a host matrix to provide the resultant composite material with a sufficient viscosity for reasons of processing. The photoconductor provides a pathway for the charge carrier to migrate by subsequent redox processes through the bulk material. In the case of amorphous organic materials, a field-assisted hopping motion of the charge carriers according to the Gaussian-Disorder-Model is usually assumed. Transport in amorphous materials is known to be highly dispersive. The quantity to describe the performance of charge displacement is the (field-dependent) mobility $\mu(E)$. Simulations based on the rate equation model by Ostroverkhova and Singer[22] support the intuitive notion, that besides the photo-generation efficiency, the charge carrier mobility has a major influence on the dynamic performance of the PR materials.

It is common to prepare PR materials based on a monopolar photoconductor, which means that the charge mobility for hole and electron in the materials are different by several orders of magnitude. Most guest-host composites demonstrated in the literature so far were based on hole-conducting polymeric materials. Nevertheless, complementary electron transport along the chromophore,[53,57] or sensitizing molecules under certain experimental conditions was described. Electron or bipolar transport has been reported in some cases.[58,59]

##### *3.3.1.1. Hole-Conductors*

Hole-only transport implies that the charge is transported along the HOMO of the polymer. Subsequently, trapping of the charge (which basically describes any mechanism to detain the charge from transport) in sites of lower potential is affected by the dispersity of the hole-conductor (any site in the low potential tail of the density of states may represent a trap). Thus, the dispersity and the mobility is influenced

**Table 2.** Comparison of organic light emitting diodes (OLED), organic low-$T_g$ photo-refractive compsite materials and organic solar cells (OSC) with regard to fundamental characteristics.

| | Organic LED | Organic PR materials | Organic Solar Cells |
|---|---|---|---|
| material thickness | 80–120 nm | 30–200 µm | 60–250 nm |
| charge generation | injection | absorption | absorption |
| charge transport distance | hopping < 100 nm | hopping few µm[a)] | hopping 100 nm |
| current flow | yes (10s mA/cm$^2$) | no (pA/cm$^2$) | yes (1–10 mA/cm$^2$) |
| recombination | desired | undesired | undesired |
| emission | yes | no | no |

[a)]the actual value in this case may depend on the employed geometry and thus the grating spacing $\Lambda$ of the interference pattern.

by the nature of the dopant mixed into the polymer, as well as the dopant content (which in the case of guest-host materials may exceed 50 weight% of the composite) due to the increase of positional disorder induced broadening of the DOS.[60] As a rule of thumb, the mobility decreases as the concentration of charge-transport moieties decreases and the polarity and concentration of the dopant increases. Also, the relative position of the polymer HOMO with respect to the ionization potential of the other components of the blends determines the extent of extrinsic hole traps in the material, which was found to limit the performance of the composites under prolonged optical exposure.[61] Thus, besides the mobility, the knowledge about the ionization potential ($I_p$) of the polymer and the respective dopants is of fundamental importance.

A compilation of polymeric hole-conductors used in PR composites is given in **Figure 4**.

The vast majority of guest-host PPCs in the literature are based on carbazole-containing polymers like poly-(N-vinylcarbazole)[62] (PVK (**1**), sometimes denoted as PVCz) and polysiloxanes (PSX **5a**),[80] the former being a well studied system for applications in xerography[81] and commercially available. Throughout the 90s, PVK-based PR composites formed the dominant system, producing milestone materials like the first polymeric material to show net gain,[82] complete internal diffraction efficiency,[62] the first demonstration of millisecond response times[46] and a huge variety of applications based on these materials (novelty filtering,[83] image amplification,[84] optical correlation,[85] imaging through scattering media,[86] vibration analysis,[87] self-pumped phase conjugation,[88] amongst others). For a detailed overview on PR materials based on carbazole systems, including polymeric structures, sol-gel approaches, and multifunctional carbazole chromophores, the reader is referred to Ref. [89]. PVK is characterized by a quite high glass-transition temperature $T_g$ in pristine form ($T_g$ = 200 °C), which necessitates the introduction of plasticizers if low $T_g$ materials are envisioned. Plasticizers may hereby be inert molecules, like phthalates (BBP, DPP, DOP) or of further functionality, like participating in charge transport in the case of the monomeric ECZ often found to plasticize PVK based materials.[62,90] A comparison of materials comprising a conductive plasticizer and BBP-plasticized materials was conducted in Ref. [63]. The plasticization of the composite by EO chromophores is discussed in Ref. [91,92].

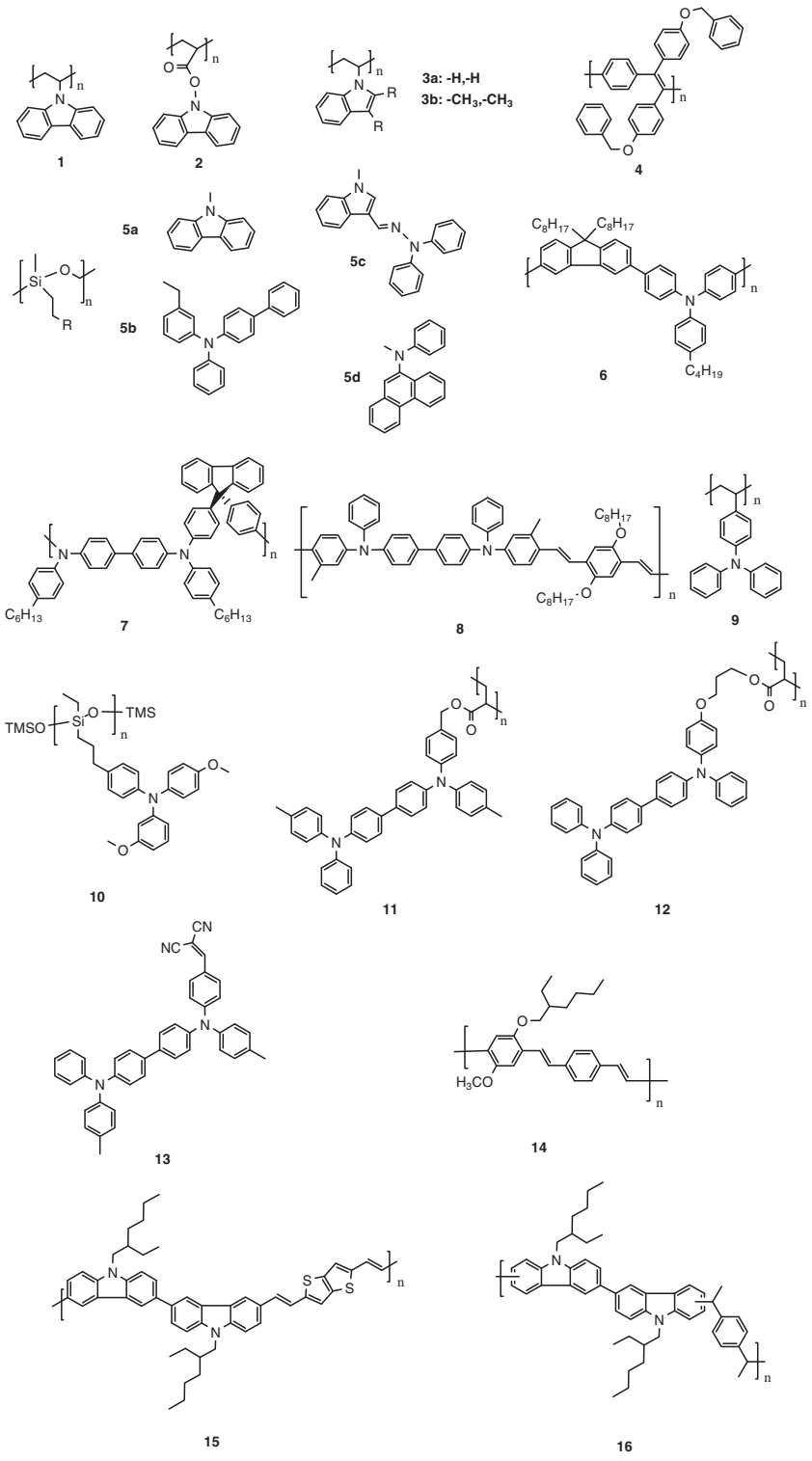


**Figure 4.** Chemical structures of hole-conductors employed in photorefractive materials: **1** PVK,[62] **2** PCzEA,[63] **3a** PVI,[60] **3b** PVDMI,[60] **4** DBOP,[64] **5a** PSX-Cz,[65] **5b** PSX-bTPA,[66] **5c** PSX-IDEH,[67] **5d** PSX-PhPA,[67] **6** TFB,[68] **7** PF6-TPD,[47,54,55,69] **8** TPD-PPV,[70,71] **9** PDAS,[72] **10** MM-PSX-TAA,[73] **11** TPDac,[74] **12** PATPD,[75,76] **13** MDCETPD,[77] **14** p-PMEH-PPV,[78] **15** EhCzThThZ,[79] **16** DiCz.[79]

PSX, first introduced as a PR host material by Zobel,[80] and its derivatives (arylamine-derivative PhPA (**5d**) and hydrazone-derivative IDEH (**5c**),[67] PSX-bTPA (**5b**)[66]), are

frequently employed due to their lower $T_g$ compared to PVK, which stems from the larger bond lengths and bond angles of the siloxane backbone compared to vinyl polymers[66] and the possible variation of alkyl spacer length between the backbone and the carbazole unit. This enables the preparation of soft composite materials with a lower concentration of plasticizer molecules. The hole mobility of PSX is comparable to that of PVK. In a similar attempt to reduce the $T_g$, Tsutsumi et al.[63] investigated composites based on polycarbazoylethylacrylate (PCzEA **2**), but with no notable performance increase over similar PVK-based systems.

Alternatively, Ribierre et al.[93] investigated the possibility to optimize the $T_g$ by variation of the avarage molecular weight ($M_W$) of the polymeric host, and concluded that the free internal volume and thus the orientational mobility of the chromophores increases when $M_W$ decreases, but no PR measurements were conducted in this work. In contrast, in Ref. [94], PVK with an averaged $M_W$ of 412 000 g mol$^{-1}$ gave PR composites with slightly better steady-state and dynamic diffraction efficiency results compared to blends with lower $M_W$ (23 500 g mol$^{-1}$ and 113 000 g mol$^{-1}$). The 2BC gain however was found to be unaffected by $M_W$.

As indicated above, an important property of the polymeric material in the guest-host-approach is the miscibility of the matrix with the other components of the blend. The miscibility ultimately determines the shelf lifetime of the composites, since the mixtures are prone to phase separation. This is especially true for the compatibility of the matrix with the chromophore load of the composite, due to the usually high concentrations used and the large dipole moment of the NLO-molecules (see Section 3.4). A design rationale is to exchange the carbazole group in PVK for the more polar indolyl-group (electric dipole moment of 2.45 D in contrast to 1.65 D of carbazole).[60] Here, differential scanning calorimetry (DSC, see Section 7.2.5) analysis confirmed a better compatibility of poly-(1-vinylindole) (PVI **3a**) and poly-(2,3-dimethyl-1-vinylindole) (PVDMI **3b**) to the frequently used EO-chromophore DMNPAA (dipole moment = 7D), than PVK. Unfortunately, both materials were found[60,95] to feature a lower photoconductivity $\sigma$ than PVK ($\sigma_{PVK} > \sigma_{PVDMI} > \sigma_{PVI}$), which is partly ascribed to the higher ionization potential of PVI and PVDMI with regard to PVK. Subsequently, gain values $\Gamma$ for PVI and PVDMI were found to be inferior to PVK-based polymers ($\Gamma = 41$ cm$^{-1}$, $\Gamma = 72$ cm$^{-1}$, and $\Gamma = 112$ cm$^{-1}$, respectively). All blends in this study were doped with 50 wt.% DMNPAA (**45**), 1 wt.% TNFM (**19**), 685 nm illumination and 90 V μm$^{-1}$ applied field.

Several publications treated the influence of main-chain conjugated polymeric materials, such as derivatives of poly(phenylenevinylene), on the PR performance.[64,70,71,78] Here, the ability of the polymer to displace charges through their delocalized $\pi$-electron structure was taken as an approach for high-charge mobility hosts. The results, however, do not stand up to the high expectations. A direct comparison of the $\pi$-conjugated host polymer DBOP-PPV (**4**) with PVK-based devices revealed a similar dynamic PR performance, despite the higher hole-drift mobility of pristine DBOP-PPV with regard to PVK.[64] This is explained by the inefficient charge generation of the DBOB-PPV sensitized by PCBM (**31**). A similar explanation is given for mixtures of TPD-PPV (**8**) with PCBM, which show response times in the order of seconds under 830 nm illumination and 57 V μm$^{-1}$.[70,71] Pre-illumination of the material with 633 nm light prior to the actual measurement ("gating"), however, was found to relieve the constraint of low charge generation and lead to a 40-fold increase of dynamic grating growth. The influence of pre-illumination will be discussed in Section 4.3.

A direct comparison of the $\pi$-conjugated host EHCzThThZ (**15**) to similar materials based on the non-conjugated DiCz (**16**) (both materials sensitized by $C_{60}$ (**17**), DB-IP-DC (**54**) as chromophore) was conducted by Moon et al.[79] A high dark conductivity was measured for the EHCzThThZ-composite; the lower photoconductivity subsequently led to lower steady-state diffraction efficiency in comparison to the blend based on DiCz (37% and 82%, respectively at 50 V μm$^{-1}$ and 633 nm). The response time for the conjugated material was found to be faster (fast time constants from bi-exponential fits gave $\tau_1 = 0.16$ s for EHCzThThZ and $\tau_1 = 1.18$ s for DiCz, respectively), however, the comparison may be obscured by the fact that, due to the lower $I_p$ of EHCzThThZ with regard to DiCz, the chromophore was found to form traps in the DiCz material only, which may have diminished the PR performance of the latter.

Despite the apparent success of PR composites based on PVK, the major drawback of carbazole containing polymeric materials is their notoriously low hole mobility. Pristine films of PVK have a hole mobility of $\mu = 10^{-7}$–$10^{-6}$ cm$^2$ (Vs)$^{-1}$[74] (**Figure 5**), which drops by more than one order of magnitude to $\mu = 7 \times 10^{-8}$ cm$^2$ (Vs)$^{-1}$ when doped with 55 wt.% dopants[35] (50 wt.% ECZ plasticizer and 5 wt.% EO chromophore DMNPAA). Therefore, many recent reports focused on the replacement of carbazole-based polymers in favor of high mobility materials based on triarylamine or TPD (often referring to all materials carrying the tetraphenyldiaminophenyl (triphenylamine-dimer

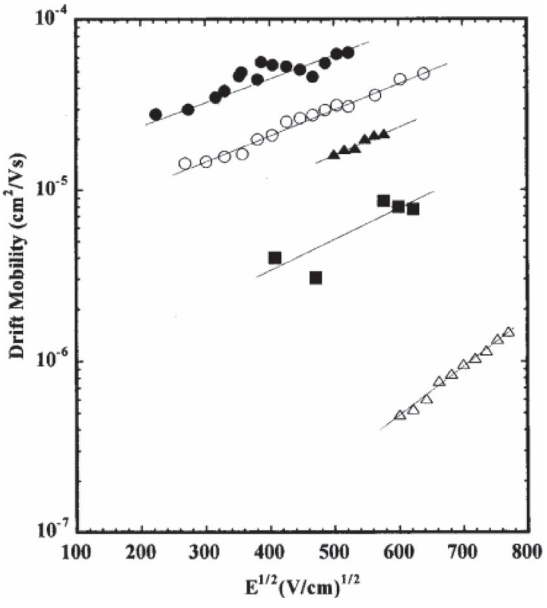


**Figure 5.** Field dependent drift mobility of PTPDac copolymers (TPD-content: 65% solid symbols, 58% open circles), PTPDac copolymer doped with 10%(solid triangles) and 15%(solid squares) DEANST, PVK (open triangles). Reproduced with permission.[74] Copyright 1997, American Chemical Society.

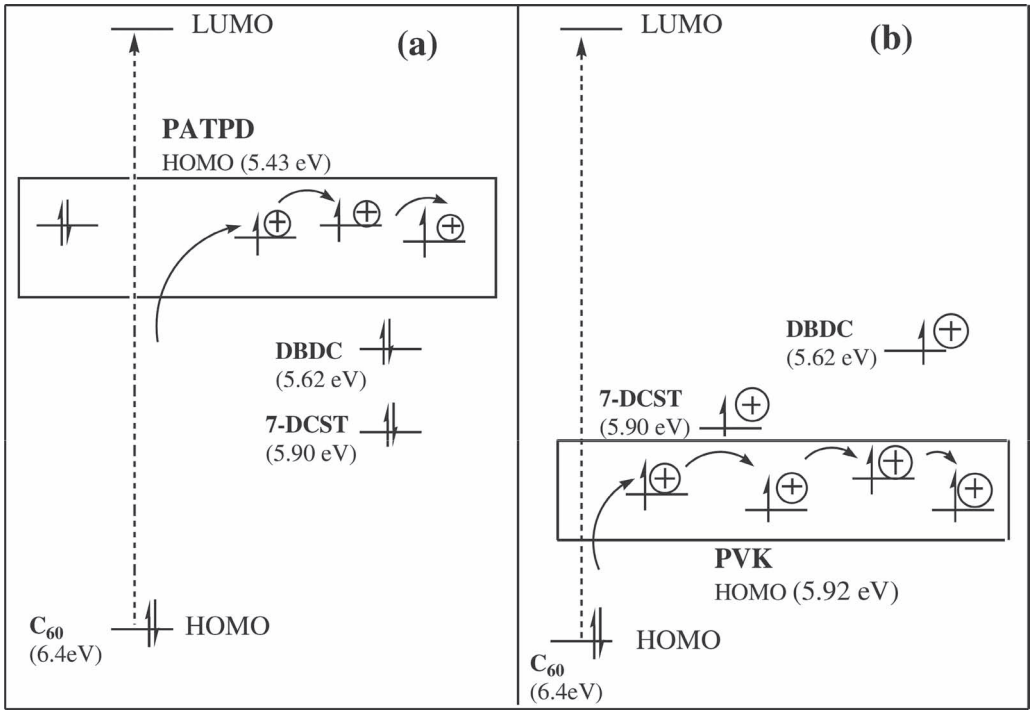


**Figure 6.** Electronic states of a PATPD (a) and PVK (b)-based composite with DBDC and 7-DCST as chromophores and $C_{60}$ as sensitizer. Reproduced with permission.[76] Copyright 2004, Wiley-VCH.

in some publications) functional group). These materials include homo-polymers like vinyl-type PDAS (**9**),[72] fluorene-bridged PF6-TPD (**7**),[47,54,55,69] siloxane based PSX-bTPA (**5b**)[66] and MM-PSX-TAA (**10**),[73] acrylate-type PTPDac (**11**)[74] and PATPD (**12**).[3,75,76] Acrylate-based TPD-polymers were also demonstrated as block co-polymers of TPD and various amounts of n-butyl-acrylate plasticizer (PTPDac-BA1-4[74]) and a carbaldehyde aniline group (PATPD-CAAN[3,96]). A fluorene-triarylamine-copolymer (TFB **6**) as PR host was demonstrated in.[68] Also, bi-functional charge-transport/chromophore molecules based on TPD were demonstrated (MDCETPD **13**.[77]) The nematic-like mesophase photoconductive polymer PPT-TPA, which features triarylamine side-groups attached to an aromatic rigid backbone was introduced by Kwon et al.[97]

Generally, TPD-based materials are known to exhibit higher charge-carrier mobilities and lower ionization potentials relative to carbazole-based materials. Hole-mobilities in the range of $10^{-4}$–$10^{-5}$ $cm^2$ $(Vs)^{-1}$ were reported for PTPDac-based co-polymers[74] and $10^{-5}$ $cm^2$ $(Vs)^{-1}$ for the TFB-based material with 59 wt.% polymer in the blend, which is roughly two orders of magnitude higher than that of PVK under the same experimental conditions (see Figure 5). Drop-cast films of PF6-TPD showed hole-mobilities of $\mu = 4 \times 10^{-5}$ $cm^2$ $(Vs)^{-1}$ (all mobility data was derived by means of time of flight (TOF) measurements).

TPD-based polymeric materials are known to feature a lower density of hole-traps compared to PVK-based materials,[77] which led to inferior space-charge fields and subsequently lowered diffraction efficiencies in some composites. The influence of providing external traps by introducing molecules of appropriate ionization potential will be discussed in Section 3.3.4.

PVK features a ionization potential of $I_p$ = 5.9 eV, which is higher than many chromophore molecules (ATOP **63**, 7-DCST **49**, etc), which states that the chromophore is easier oxidized than the charge-transport manifold and thus serves as a hole trap. These chromophores are identified as compensator sites for growing concentrations of sensitizer radical anions upon prolonged illumination, which is generally accompanied by a detrimental drop in performance and an undesired illumination history of the materials.[98] Besides adjusting the ionization potential of the chromophore,[61] the generally lower oxidation potential of TPD-compounds in comparison to PVK are considered to evade this problem[72,75,76] (see **Figure 6**). Materials with charge transporters as compounds of lowest ionization potential have thus featured stable material performance under prolonged exposure, manifested through 160,000 write-erase cycles without degradation of performance.[75]

The low ionization potentials of the TPD- and PDAS- based materials were also found to greatly enhance the photoconductivity of the materials.[66,72] This is in part ascribed to the enhanced complexation of the hole-conductor, which is an electron donor, with the sensitizing agents (electron acceptors) in the respective blends. The influence of the donor ionization potential on the charge transfer (CT)-spectra for a series of indole-derivatives with TNFM as acceptor can be found in Ref. [95]. Hendrickx et al.[99] demonstrated the influence of ionization potential of the hole-transport molecule on the photo-generation efficiency of the CT-complex between the aromatic donor molecule and a sensitizer acceptor (here, $C_{60}$ **17**). The results suggested a dramatic increase of the photo-generation efficiency from 0.3% to 100% (at 50 V $\mu m^{-1}$, 633 nm

illumination) by lowering the ionization potential from 5.90 eV (PVK) to 5.39 eV (alkoxy-functionalized TPD-derivative). The findings were rationalized on the basis of the Marcus electron-transfer theory, which states a higher electron transfer rate with increased complexation enthalpy between the donor and acceptor moiety in the blend. The actual experiments, however, did not involve PR characterizations.

In a subsequent publication, Choi et al.[65] demonstrated an increase of PR speed for lowering the $I_p$ of polysiloxane-based PR polymers. The reader however should keep in mind that, despite some statements in recent publications, no actual connection between low ionization potential and high mobility exists, thus simply lowering the $I_p$ of the donor does not constitute the ultimate recipe for faster PR materials. Exchanging both alkyl-groups of PF6-TPD for alkoxy-groups lead to a lower $I_p$, but also negatively affected the hole-drift mobility of the polymer ($\mu = 4.0 \times 10^{-5}$ and $\mu = 1.2 \times 10^{-6}$ cm$^2$ (Vs)$^{-1}$, respectively), which subsequently lowered PR response time.

Nevertheless, TPD-based materials feature the currently fastest PR materials in the literature, combining millisecond response times with complete internal diffraction efficiency for illumination in the region from 532 to 1064 nm.[45,47,54,69,100]

### 3.3.2. Sensitization

From the standpoint of chemistry, the most important contribution to the field of PR material research has been the search of novel and more efficient sensitizing molecules. Besides reports on PR response without the use of a sensitizing agent,[101,102] the sensitizer is understood to have a major impact with regard to the field-dependent steady-state and, even more pronounced, dynamic performance of the composites.

As indicated above, the sensitizer assists in the generation of charges and has thus to be compatible with the host in terms of solubility and must be selected with regard to the frontier orbital energy level distribution of the materials in the composite. Moreover, the sensitizer has to absorb at the targeted spectral region of operation for initial exciton formation. On the other hand, absorption is a loss mechanism, attenuating the transmitted power of the light beams. Thus, it is imperative to find an optimum concentration of sensitizer molecule with respect to the electrical and optical performance of the material.

Finally, since in the usual p-type configuration of PR composites (the space-charge field formation is dominated by hole-conduction through the polymeric matrix), the sensitizer serves as trap for the immobile electrons created upon charge generation. These radical anions are known to constitute recombination traps for mobile holes within their coulombic radius. This implies that the sensitizer influences the recombination dynamics of the mobile hole with the radical anion. Thus, the chemical and photo-physical nature as well as the density of the sensitizer plays a crucial role in the dynamic and field-dependent formation of the PR grating through its significant influence on all photoelectric parameters.

Three major approaches to sensitize PR polymers can be distinguished in the recent literature: organic molecules, metal containing organic complexes, and inorganic semiconductor nanoparticles. Due to the inherently different peculiarities of the named approaches, we discuss the corresponding results separately.

#### 3.3.2.1. Organic Sensitizers

When implementing organic molecules into polymeric hole-conducting systems, three different modes of bulk absorption of the final composite must be considered. The absorption of the composite may thereby originate from direct excitation of the sensitizer species, from nonlinear two-photon absorption or from donor-acceptor complexation of the CTA and the sensitizer, known as charge-transfer complexes. Those complexes give additional features to the pristine spectra of the sole components, e.g. additional absorption bands at longer wavelength. The singlet state CT complex of PVK with $C_{60}$ and $C_{70}$ was identified as the main source for generated charges.[103] Charge-transfer complexes used in literature so far provide absorption in the visible and the near infrared up to 830 nm.

Since most materials are p-type hole-conducting systems, most of the employed sensitizers are rather strong n-type electron acceptors. The most common sensitizers are organic molecules based on fluorenones, like TNF (**18** visible range absorption),[111,62,105] TNFM (**19** VIS-NIR range absorption),[70,104,112] both well characterized in combination with carbazole hole-conductors.[113,114] In addition, fullerenes emerged as a versatile and powerful class of organic sensitizers. Within the literature on organic photorefractives, $C_{60}$ (**17**)[53,98,115] was partially replaced by the soluble derivative [6,6]-phenyl $C_{61}$-butyric acid methyl ester([60]PCBM **31**).[64,47] **Figure 7** displays the chemical structures of the organic sensitizers discussed in this review.

In order to combine the apparent advantages of TNF and $C_{60}$ for PVK-based composites, namely high compatibility, strong electron accepting capability and high photogeneration yield due to low recombination rates, a series of TNF-$C_{60}$-Dyads (**37**–**40**) were synthesized.[110] The absorption spectra were found to be a superposition of both independent moieties, thus excluding electronic ground-state coupling between both acceptors. The PR properties under 633 nm illumination were compared to a composite sensitized with $C_{60}$ alone. Due to a slightly higher absorption and better solubility, an improvement of the dynamic performance by a factor 2-3 was obtained in 2BC-experiments for the dyads. In a subsequent paper, the same group introduced a flexible polyether linker, to enhance both solubility and interaction between both moieties,[109] but the authors did not observe a significant enhancement compared to the $C_{60}$ sensitized reference.

Several publications were devoted to examine the influence of the sensitizer on the steady-state and dynamic properties of the PR composites through measuring systematic series of organic materials similar to TNF, TNFM and $C_{60}$. A series of quinones (**23**-**27**), TNF, and TNCB (**28**) were measured in a PVK/7DCST-material at 633 nm.[105] As expected, a direct correlation between the absorption coefficient resulting from the formation of a CT-complex and the photocurrent of the bulk sample under illumination was identified. Also, the response time of the composite related to the density of charge carriers and thus the achieved photocurrent, giving the fastest response to the TNF and DDQ (**27**) based material. Interestingly, the dynamic performance and photocurrent were reduced for quinone derivatives with lower electron affinity.

Similarly, a series of PSX-Cz/DB-IP-DC (**54**) based materials with TeNFM (**20**), TNFM, TNF, TCNE (**22**) and TCNQ (**21**) were

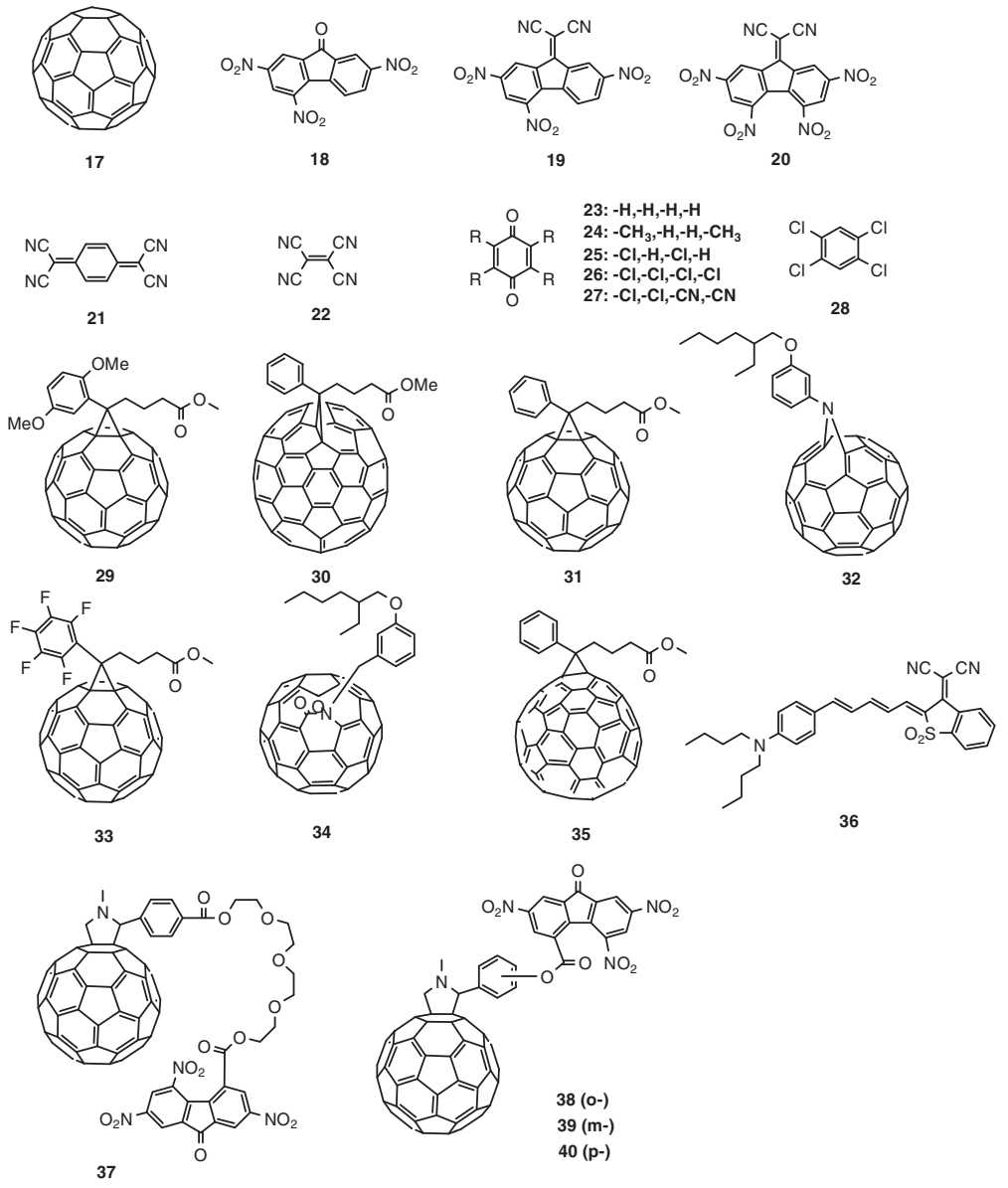


**Figure 7.** Chemical structures of organic sensitizers:**17** $C_{60}$, **18** TNF, **19** TNFM (TNFDM in some publications), **20** TeNFM,[104] **21** TCNQ,[104] **22** TCNE,[104] **23** BQ,[105] **24** MQ,[105] **25** $Cl_2Q$,[105] **26** Chloranil,[105] **27** DDQ,[105] **28** TCNB,[105] **29** 2,5-OMePCBM,[47] **30** [70]PCBM,[47] **31** PCBM,[47] **32** azafulleroid,[47] **33** $F_5$-PCBM,[47] **34** ketolactam,[47] **35** [84]PCBM,[47,54] **36** DBM,[100,106,107] **37** TNF-$C_{60}$-dyad with polyether linker,[108,109] **38-40** TNF-$C_{60}$-Dyads.[110]

investigated under 633 nm illumination.[104] The authors also found absorption related changes to constitute the dominant difference between the materials, giving higher photocurrent and faster holographic response time going from TeNFM over TNF to TNFM, in agreement to their increased absorption coefficients. Conversely, the dynamic response was reduced in TCNE and TCNQ, despite their even higher charge generation efficiency. This finding was explained on the basis of the concomitant formation of a higher concentration of radical anion traps upon illumination, degrading the photocurrent dynamics. In both references, no concise connection of the influence of the sensitizer on the steady-state PR properties of the materials is described.

In order to investigate the influence of the electron accepting capability on the materials, a series of fullerene-doped (**29-35**) PF6TPD-based materials was measured at 830 nm.[47] At this wavelength, as opposed to the series described above, the change of the absorption coefficient was found to be negligible and furthermore, all materials featured similar steady-state performances, i.e. complete internal diffraction efficiencies at moderate applied fields ($\eta$ > 90% at 60 V $\mu m^{-1}$). This allowed the direct correlation of the reduction potential to the sensitivity of the composites, giving higher performance through faster response times to materials doped with stronger electron acceptors, see **Figure 8**.

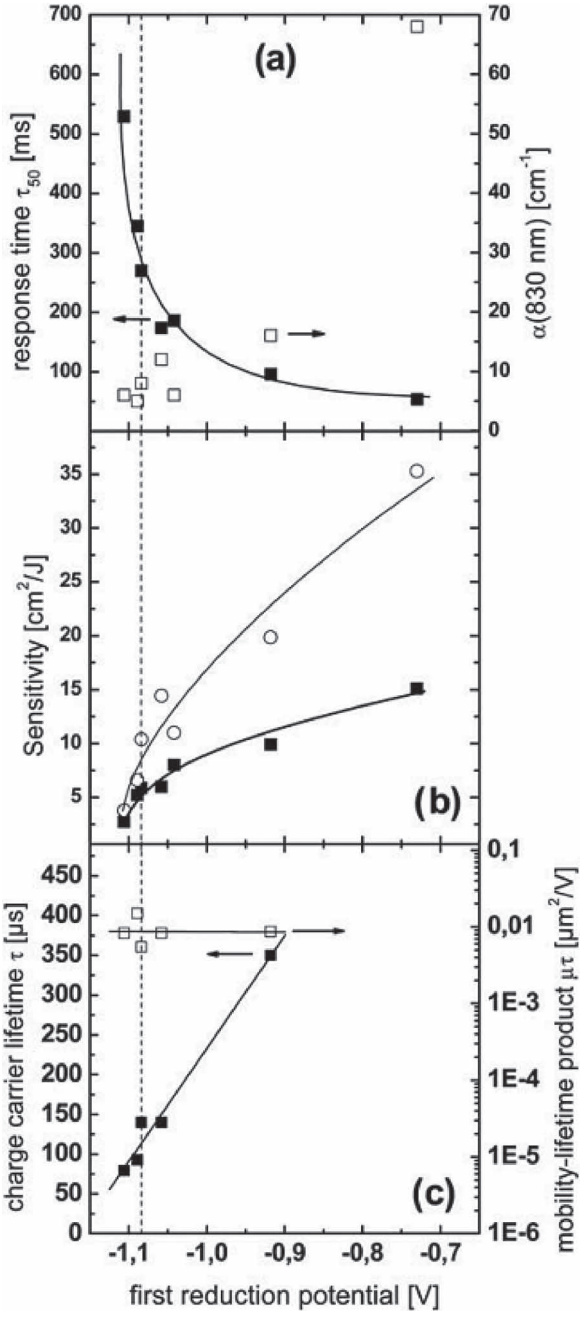


**Figure 8.** Dependence of the response-time $\tau_{50}$ (a), sensitivity $S_{1\%}$ with and without pre-illumination (b, filled and open symbols, respectively), charge carrier lifetime $\tau$ (c, solid symbols) and mobility-lifetime product $\mu\tau$ (c, open symbols) on the reduction potential of the incorporated fullerene sensitizer. All data were taken at $I_{WB}$ = 0.64 W cm$^{-2}$ and 57 V µm$^{-1}$ applied field. Reproduced with permission[47] Copyright 2010, Royal Society of Chemistry.

Supplementary photo-EMF measurements confirmed the influence of the reduction potential on the dynamic characteristics by lowering the recombination rate between mobile hole and fullerene radical anion. Interestingly, the charge generation rate was found to be constant within the series. The beneficial dynamic effect was eventually enhanced through pre-illumination of the sample (see Figure 8, b). The materials described in this publication are among the most sensitive NIR composites to date, featuring response times ($\tau_{50}$) in the 50 ms region at 57 V µm$^{-1}$ applied field and $I_{ext}$ = 0.6 W cm$^{-2}$ $\lambda$ = 830 nm irradiance.

Several recent papers were devoted to produce all-organic photorefractives for operation in the region above 830 nm, which allows for NIR applications like biomedical imaging and the processing of telecommunication signals. Eralp et al. introduced the near-infrared dye DBM (**36** 1 wt.%) into a PATPD/7-DCST composite device for sensitization at a wavelength of 975 nm.[100] The device featured good steady-state performance ($\eta$ = 60% and $\Gamma_p$ = 120 cm$^{-1}$ at 95 V µm$^{-1}$) and remarkably fast response times ($\tau$ = 33 ms for the fast component of a bi-exponential fit, 1 W cm$^{-2}$ irradiance). This was discussed to be due to the efficient linear absorption of the dye and the high photoconductivity of the PATPD-based material. Due to the favourable absorbing capabilities in the near-infrared and the high charge generation efficiency when doped into hole-conducting polymers, the higher fullerene-derivative [84]PCBM (**35**) was successfully capable to sensitize a PF6-TPD-based PR material to achieve high sensitivity under low intensity (1 W cm$^{-2}$) 1064 nm irradiance.[54] The results were shown to improve for enhancing the sensitizer content from 1 wt.% to 5 wt.%. The measurements revealed a complete internal diffraction efficiency ($\eta$ = 81% at 60 V µm$^{-1}$) and fast response times of $\tau_5$ = 36 ms (regarding the build-up of 5% internal diffraction efficiency) for 5 wt.%[84]PCBM. This corresponds to a 44 times faster response compared to high-$T_g$ organic PR materials doped with carbon nanotubes (CNT) under the same conditions and wavelength.[116]

Further extension of the operation of all-organic PR composites to the important telecommunication wavelength of $\lambda$ = 1550 nm were enabled by the use of 10 wt.% DBM as a two-photon-absorption (TPA) sensitizer. Following an initial report on TPA by a chromophore in a PVK-based composite at 650 nm 130 fs illumination,[117] gratings were written at 1550 nm in the PATPD/7-DCST/DBM-composite using an optical parametric amplifier, pumped by a femtosecond Ti:sapphire laser.[106] A diffraction efficiency of 3% at $E_{ext}$ = 60 V µm$^{-1}$ was achieved for an average power of $I_{ext,av}$ = 9.9 W cm$^{-2}$. As noted in the publications, a potential benefit of the two-photon approach is the possibility of non-destructive read-out of the grating by a cw-source of the same wavelength, since no linear absorption occurs. In a subsequent publication,[107] the authors were able to further improve the performance of the material through optimization of the material composition and taking into account peculiarities of the pulsed writing operation, e.g. the beam walk-off effect through the small effective overlap area of the pulsed beams in the sample (see Section 5.5). The latest results featured 40% diffraction efficiency and $\Gamma_p$ = 11 cm$^{-1}$ at $E_{ext}$ = 60 V µm$^{-1}$ and a fast time constant of $\tau$ = 35 ms at $E_{ext}$ = 93 V µm$^{-1}$ and a pulse energy of 11.4 µJ.

The extended absorption ranges of CNTs were utilized to fabricate a series of $\lambda$ = 1550 nm sensitive high-$T_g$ composites. Here, the absorption of single-wall and oxidized single- wall CNTs were shown to provide PVK based materials with a linear NIR-absorption of $\alpha_{1550}$ = 3.3 cm$^{-1}$ [118] and $\alpha_{1550}$ = 4.6 cm$^{-1}$,[119] respectively. Despite net gain values of $\Gamma_{net}$ ~ 5 cm$^{-1}$ and $\Gamma_{net}$ ~ 15 cm$^{-1}$

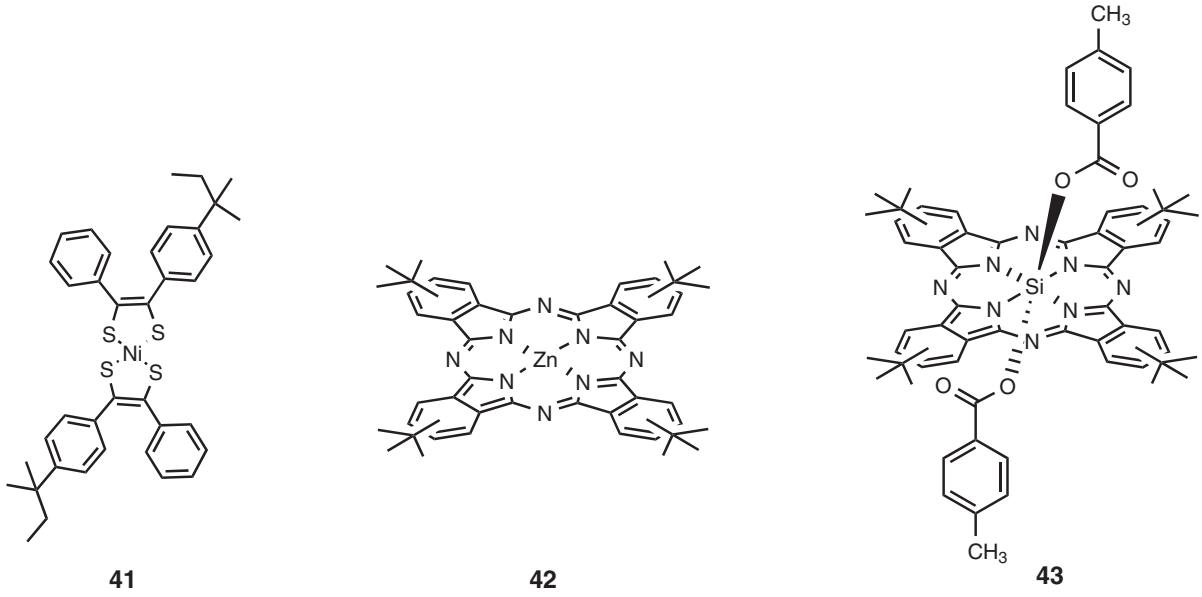


41 42 43

**Figure 9.** Chemical structure of metal-containing complexes, **41** TT-2324,[54] **42** ZnPc,[123] **43** SiPc.[123]

at rather high applied fields ($E_{ext}$ ~ 100 V μm$^{-1}$), the response time of these materials is in the multi-second domain (derived from fit to the gain-dynamics). Unfortunately, no 4WM- experiments were conducted on these materials.

#### *3.3.2.2. Metal-atom Containing Complexes as Sensitizers*

Metal coordinated organic macrocycles like porphyrins, phthalocyanines and naphthalocyanines are known to be efficient light harvesting molecules.[120] Their benefits include high photo-stability and large absorption cross-sections. Moreover, the use of different central atoms allows for the tailoring of oxidation and reduction potentials. To date, few studies have been undertaken to utilize these molecules in PR composites, among them ruthenium-phthalocyanine complexes for IR-sensitive high $T_g$ materials[121] and ruthenium- and osmium-based complexes in fully functionalized polymeric systems.[122]

Zinc- and silicon phthalocyanines (ZnPc **42**, SiPc **43**, see **Figure 9**) were incorporated in PVK-based PR composites by Gallego-Gomez et al.[123] The extraordinary high absorption of the blends allowed for holographic and photocurrent characterization of the materials at 633 nm with sensitizer concentrations as low as 0.002 wt.%. Since the radical anion of the phthalocyanines was found to constitute a hole-trap, which is well-known to be the case for $C_{60}$/PCBM[98] and TNF/TNFM[124] sensitizers, the use of little quantities of strong absorbing sensitizer (ca 0.1 wt.% SiPc and ZnPc compared to a 0.5 wt.% $C_{60}$), and thus the low density of recombination centres, leads to a dramatic enhancement of the phase-shift for both complexes compared to $C_{60}$ (58°, 31°, and 14° for SiPc, ZnPc and $C_{60}$, respectively, at $E_{ext}$ = 71 V μm$^{-1}$), the chief reason for the high gain values for the complex-sensitized materials in this study. The higher photocurrent yield, diffraction efficiency and dynamic performance of SiPc compared to ZnPc was explained on the basis of a higher charge generation efficiency due to a lower reduction potential of the SiPc-complex.

The strong NIR absorption of the Ni-dithiolene complex TT-2324 (**41**) allowed our group to prepare efficient $\lambda = 1064$ nm sensitive PF6TPD-based PR composites.[54] The material featured sub-second response times and complete internal diffraction efficiency. However, due the high absorption of the sensitizer and its unfavourable influence on the trapping landscape and the sensitivity when used in higher concentrations (above 1 wt.%), the performance was inferior to the results described for [84]PCBM sensitized materials in the same publication (see Section 3.3.2.1).

#### *3.3.2.3. Quantum Dots as Sensitizers*

The approach to combine nanotechnology and photonic materials holds great promise for the fabrication of novel and efficient nanophotonic devices and applications.[125–127] Much research effort was put into the development of inorganic nanoparticles or quantum dots (QD) for use as sensitizing agent in inorganic-organic hybrid PR composites. A recent review on nanoparticle blended PR systems can be found in Ref. [128]. Besides the availability of a huge number of inorganic semiconducting materials, exhibiting band-gap energies that cover the entire visible and NIR spectrum, the most apparent benefit of this approach is the possibility of tailoring of the spectral region of absorption of the QD through quantum confinement effects. By decreasing its dimensions beyond the associated Bohr radius, a hypsochromic shift of the absorption of the nanoparticle with regard to the bulk semiconducting material, and further an inverse correlation between the band-gap and the physical proportions of the particle is established.[129] Doping the semiconducting nanoparticles into organic hole-conductors is found to greatly enhance the photoconductivity. On the one hand, the generation of charges is facilitated, as indicated by the decrease

**Table 3.** Properties and results of a selection of QD particles and the respective photorefractive blends. Wavelength $\lambda$ of experiment, bandgap $E_g$ of the semiconductor in the bulk, QD size $d$ of the particle, organic shell, wt.% -content in the PR blend, absorption coefficient $\alpha$ at the working wavelength $\lambda$, gain coefficient $\Gamma$ and diffraction efficiency $\eta$ under steady-state conditions and fitting constants to dynamic transients.

| $\lambda$ [nm] | QD | $E_g$ [eV] | $d$ [nm] | Shell/ligand | Content [wt.%] | $\alpha$ [cm$^{-1}$] | $\Gamma$ [cm$^{-1}$](@ $E_{ext}$/ V µm$^{-1}$) | % $\eta$ (@ $E_{ext}$/ V µm$^{-1}$) | $\tau$ [s] (@ $E_{ext}$/ V µm$^{-1}$) | Ref. |
|---|---|---|---|---|---|---|---|---|---|---|
| 515 | CdS | 2.42 | 168 | *p*-thiocresol | 0.2 | 9 | 60 (119) | 8 (137) | 7.3[a] (80) | [151] |
| 633 | CdSe | 1.73 | n.s. | -/4-methylbenzenethiol | 1 | 143 | 35 (80) | 29 (60) | 0.09[a] (67) | [133] |
| | CdTe | 1.56 | 4 | -/py | 1 | 18 | 24 (30) | 20 (60) | 0.2[a] (60) | [146] |
| | NiS | 0.04 | 11 | -/py | 0.4 | 36 | 79 (80) | 37 (50) | 0. 5[a] (70) | [129] |
| 1310–1340 | HgS | 0.3[152]–0.5[153] | 10 | - | 1 | 10 | 4 (90) | - | - | [148] |
| | PbS | 0.41 | 6–8 | - | 2 | 69 | 185 (93) | - | 1.5[b,c] | [149] |
| 1550 | PbSe | 0.26 | 5 | - | 10 | 8 | 86 (59) | 40 (60) | 1.8[a] (40) | [150] |

[a]fast time constant from mono or bi-exponential fit; [b]gain dynamics; [c]stretched exponential fit.

of photoluminescence yield upon excitation,[130] on the other hand the mobility[126,131,132] of the blend system is increased.

Besides the chemical nature and the size of the QD, strong evidence in current literature[129,133–136] is given of a pronounced influence of the surface of the dot on the photoelectric parameters of the composite when doped into a hole-conducting polymer.

Since the first demonstration of a CdS-QD sensitized PR composite,[137] the most frequently used nanoparticle sensitizer in literature is CdSe. All PR measurements were done in PVK-based composites (except for p-PMEH-PPV **14** in[78] and an ECZ doped inert polymer in[138]). With one exception ($\lambda$ = 647 nm in Ref. [139]), CdSe-QDs were exclusively characterized at an operating wavelength of $\lambda$ = 633 nm, facilitating the comparison of different nanoparticle-sizes, concentrations and capping chemistry.

Capping ligands are introduced during QD synthesis to yield soluble, organophilic particles. Also, the size of the nanoparticle depends partly on the ratio of capping agent and QD-precursor in the reaction mixture.[134,140] The chemical nature of the capping ligand was found to dramatically influence the performance of the QD sensitized PR device. However, a relatively thin shell of the small molecule 4-methylbenzenethiol was ascribed to present only a thin barrier to charge transfer between host and QD, which resulted in astonishing fast PR-response[133] (see **Table 3**). Contrarily, the direct comparison of 1-hexadecylamine (HDA) capped CdSe QD[134] yielded two orders of magnitude higher sensitivity compared to tris-*n*-octylphosphine oxide (TOPO)-capped CdSe particles,[141] the former molecule forming the thicker capping. Photoluminescence studies on both particles exhibited bathochromic shifted spectral features regarding the excitonic peak for TOPO capped CdSe QD only, which indicates the presence of detrimental charge traps on the dot surface. This feature was not present in spectra of HDA-capped dots and was accounted for the better performance of HDA- over TOPO-capped particles despite their thicker capping. In a subsequent publication,[140] the group described the possibility of the HDA ligand to form parasitic absorbing complexes with the EHDNPB-chromophore of the composite, depending on the metal content of the dot surface and consequently the packing density of the ligands.

Ligand exchange from oleic acid (OA)-capped to pyridine (py)-capped NiS QDs,([129] see below) improved the performance of the PVK/7-DCST-based PR material, which was explained by the reduction of trapping centers originating from a lower density of QD surface defects. This enhancement translated into an increase of gain coefficients (see **Figure 10**) and a shift of the over-modulation field $E_{max}$ from $E_{ext}$ = 70 V µm$^{-1}$ (OA-capped) to $E_{ext}$ = 50 V µm$^{-1}$ (py-capped). It is noteworthy, that the quantum efficiency of the charge generation indeed was not affected by the ligand substitution.

Defect sites and dangling Se bonds on the dot surface may trap the hole in low-lying energetic states and present adverse recombination routes for the trapped electron and the hole. In order to reduce these surface effects, a 1-2 monolayers thick shell of a wider band-gap material (e.g. CdS[135] and ZnS[136]) was grown around the CdSe QD. The authors demonstrated increased PR sensitivity for both core/shell materials relative to a core-only QD under identical measurement conditions. The wider band-gap ZnS-shell (bulk band-gap $E_g$ = 3.6 eV) was found to be a more

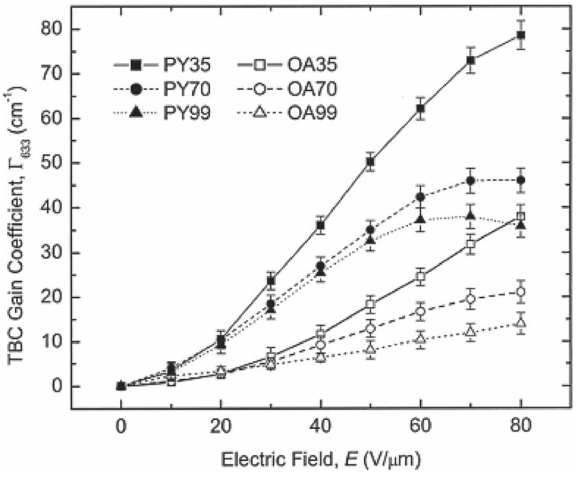


**Figure 10.** Steady-state gain coefficients for a series of oleic acid (OA)-capped (open symbols) and pyridine (py)-capped NiS-QDs. The nanoparticle concentrations in the composites were tailored to reveal absorption coefficients of $\alpha_{633nm} \approx 35$ cm$^{-1}$ (squares), $\alpha_{633nm} \approx 70$ cm$^{-1}$ (circles), $\alpha_{633nm} \approx 99$ cm$^{-1}$ (triangles) in the final PVK-blend. Reproduced with permission from.[129] Copyright 2008, American Institute of Physics.

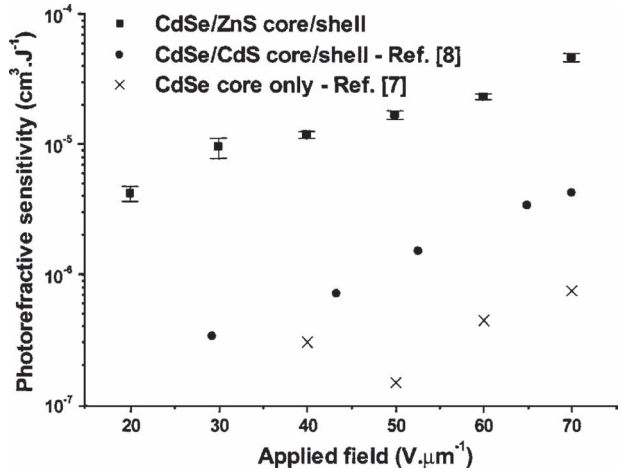


**Figure 11.** Semi logarithmic plot of the sensitivity of identical composites with sensitizer made from CdSe/ZnS[136] (squares), CdSe/CdS[135] (circles) and CdSe core-only[141] (all TOPO-capped) QDs, plotted against the applied electric field. The sensitivity is evaluated according to $S = \Delta n/\tau I\alpha$. Reproduced with permission.[136] Copyright 2005, American Institute of Physics.

efficient than the CdS-shell (bulk band-gap $E_g = 2.4$ eV), resulting in a one order of magnitude higher sensitivity (**Figure 11**).

The synthetic preparation procedure of the ZnS-shell (grown around identical CdSe QDs) was found to be of significant influence on the PR characteristics of the materials with regard to the index modulation and grating rise time.[142] Time- and field-resolved PL measurements on CdSe core-only and CdSe/ZnS core/shell sensitized composites and a subsequent rate-equation analysis allowed to assign the beneficial influence of the shell on a reduced recombination rate of the mobile hole and the charged QD.[143] Also, the influence of the NP size on charge generation and recombination was found to be absent in core/shell systems.

Without the use of organic capping, blending of uncapped QDs into the polymeric material usually results in the formation of nanoparticle aggregates. An alternative approach to obtain a homogeneous dispersion of QDs in the polymeric matrix is the chemical hybridization of PVK and QD.[130,144] The synthesis involves sulfonation of the PVK material and fabrication of a suitable precursor ($PVK(SO_3)_2Cd$), which is followed by the nanocomposite formation.[145] Benefits of this approach include enhancement of photoconductivity through higher charge generation efficiency and an increase of the lifetime of the charge carriers compared to the PVK/capped-QD blend,[144] which is ascribed to a higher interface quality. Subsequently, a two-fold increase of the gain coefficient $\Gamma$ was demonstrated for CdSe nanocomposites compared to the blend system of PVK and 4-methylbenzenethiol capped CdSe-QD.[130]

Another approach to uncapped ("naked") CdSe QD sensitizers, introduced by Li et al.,[138] was to exchange PVK in favour of a polymeric system offering better QD-solubility, such as the inert poly(syrene-co-acrylonitrile) (PSCA). ECZ was doped into the system to facilitate charge-transport. The authors demonstrated a 20% enhancement of photosensitivity (defined as photocurrent density over applied electric field and illumination intensity) over comparable py-capped CdSe-doped PVK-based systems. They attribute this finding to the reduction of the potential barrier of charge generation for uncapped QDs.

Apart from CdS and CdSe QDs, recently CdTe[146] and NiS[129] were introduced for $\lambda = 633$ nm sensitization, both of which feature similar results compared to the typical steady-state and dynamic PR characteristics of the former mentioned (see Table 3). For CdTe, a higher charge generation quantum efficiency compared to CdSe was demonstrated when doped into PVK. NiS was intentionally employed to circumvent the use of environmentally dubious heavy metals. A dependence of $\Gamma$ on the QD-concentration was ascribed to an influence of the NiS-QD on the trapping landscape of the material, rendering the charged QD a hole trapping species.[129] The obtained lower phase-shifts and gain coefficients for higher QD ratios are thus in accordance with similar experimental results on higher concentrations of organic sensitizers.[54,147]

The utilization of narrow band-gap semiconductor nanoparticles allowed sensitizing PR composites in the technically important spectral region of telecommunication bands. This spectral region ($\lambda$ = 1340–1550 nm) so far lacks in the availability of efficient linear absorbing organic dyes. Sensitization of a PVK-based PR composite at 1310 nm was initially demonstrated through the employment of HgS (10 nm) or PbS (50 nm) QDs at a content of 1 wt.% each.[148] For the PbS QDs, $\Gamma_p = 32$ V μm$^{-1}$ at 50 V μm$^{-1}$ was achieved. Due to a lower charge generation quantum efficiency and trap density, the HgS nanoparticles featured a roughly one order of magnitude lower gain coefficient (see Table 3). In a subsequent paper[149], the group further improved the response of the PbS QDs. The careful control of the nanoparticle dimension and the subsequent enhancement of the spectral response through operating the device at an absorption edge of the QD, efficient grating recording was demonstrated. The PVK/DEANST based composite achieved remarkable high gain values (net gain of $\Gamma_{net}$ = 115 cm$^{-1}$ at 93 V μm$^{-1}$). This constitutes the highest net gain value in a QD-containing PR composite so far. The response of the material is well within the second range, which might be further enhanced by the use of photoconductors with higher mobility than PVK.

The use of the lower band-gap semiconductor PbSe QDs of 5 nm diameter led to a PVK/DEANST-based sample sensitive at 1550 nm.[150] Here, the laser wavelength corresponds exactly to the first excitonic absorption peak of the nanoparticle. Impressive results reported include a net gain of 79 cm$^{-1}$ at 59 V μm$^{-1}$, a refractive index modulation of $\Delta n = 3.1 \times 10^{-3}$ corresponding to 40% internal diffraction efficiency and a fast rise time constant of 1.8 s at 40 V μm$^{-1}$, indicating the applicability of the material at this technologically important wavelength. It should be emphasized here, that the results were demonstrated at very low irradiance (total 100 mW cm$^{-2}$) cw-illumination.

A summary of the currently best results achieved with QD-sensitized PR materials is given in Table 3.

#### 3.3.2.4. Co-Sensitization

Recently, several material systems were doped with non-absorbing electron acceptors featuring a lower reduction potential than the sensitizer.[53,111,154–156] This approach is referred to as co-sensitizing in some publications.[111,154,155] In a combined

photo-EMF[154] and holographic[111] characterization, copper-doped $LiNbO_3$ nanoparticles (20 nm diameter, surface treated with dimethyldichlorosilane) were blended into PVK-based materials. In both investigations, the particles were found not to directly sensitize the PVK materials at 633 nm within a ratio from $10^{-7}$ to 5 wt.% content, due to the large band-gap of $LiNbO_3$ ($E_g$ = 3.8 eV) compared to other semiconductor materials discussed in the previous Section. In conjunction with TNF, the holographic performance was found to be optimized for a concentration as low as $10^{-3}$ wt.% $LiNbO_3$, giving rise to increased gain values compared to the un-doped reference material.[111] In concert with a rather constant steady-state refractive index modulation and a minor influence on dynamic performance, the nanoparticle dopant was found to enhance the phase-shift due to increased drift lengths of the mobile hole. This finding is supported by modulated photocurrent and photo-EMF measurements on the composites (without the use of chromophores in the blend).[154] Increased content of $LiNbO_3$ nanoparticles leads to an increase of photocurrent flow through the sample due to a growth of the mobility-lifetime product $\mu\tau$, which is due to a reduced recombination rate of the mobile hole and the excited nanoparticle. The charge generation rate was found to be unaffected by the particles, initial charge generation via the PVK/TNF complex was shown to be followed by electron-transfer to a particle in close proximity. The QDs are capable of accumulating several negative charges; as a consequence a cloud of trapped holes in its vicinity surrounds the charged particle in a core/shell manner. This leads to a bending effect on the HOMO-level of the PVK/crystal interface, which presents an energetic barrier to recombination. As obvious from the increased photocurrent amplitude, the longer lifetime of the mobile hole seems to overcompensate for the reduced hole-mobility, which concurrently results from the Coulomb attraction of the mobile hole by the charged QD.

A co-sensitizing effect was also demonstrated with organic materials. A 5wt.% PCBM sensitized PF6-TPD composite was doped with 1–5 wt.% benzoquinone (BQ **23**) by Köber et al.,[155] which was found not to generate charges at the working wavelength of 830 nm. Since BQ has the higher electron affinity than PCBM, the electron is transferred to BQ after charge generation on PCBM. The holographic characterization yielded an increase of $\Delta n$ and steady-state gain coefficients with increased BQ content, in conjunction with constant dynamic characteristics. In this case, the results clearly indicate an increase of the space-charge field $E_{SC}$ due to a higher steady-state charge density in the material, while maintaining a constant hole-displacement distance. Please note that only the first reduction of BQ is energetically favorable compared to the reduction of PCBM, thus each BQ is capable of holding a single charge. This explains the higher amount of co-sensitizer necessary to yield significant effects compared to the nanoparticle approach.

In a similar attempt, $Alq_3$ was introduced as electron trap into a composite material based on PATPD/7-DCST/$C_{60}$,[53] a liquid crystal containing composite (TPD/8OCB/TNF)[156] and a monolithic material based on ECYENPA (**71**).[157] As for the results described above, the doped materials featured significantly higher gain coefficients (increase from 232 $cm^{-1}$ to 424 $cm^{-1}$ for the monolithic material upon doping 2 wt.% $Alq_3$, 75% increase for the PATPD-based composite) and also faster response times. Also, a higher steady-state diffraction efficiency is reported (from 15% to 90% at 532 nm illumination at 42 V $\mu m^{-1}$).[53] $Alq_3$ is considered to be a very efficient electron trap, capable of reducing the recombination rates and thus enhancing the charge density in the material, the same mechanism considered above for the BQ-series. This assumption is further confirmed by a reduction of photocurrent in the materials with $Alq_3$ doping in comparison to un-doped reference materials.[53,156]

In conclusion, it should be emphasized, that the co-sensitizing procedure in all described cases does not induce any further absorption losses, e.g. the increase in gain-coefficients in the holographic characterization translates completely into an increase of the net gain.

#### *3.3.3. Redoxchemical Doping*

Dopants that may further affect the photoconductivity of PR composite were introduced into the material blends. The addition of dopants with lower oxidation potential (TPD) than the holeconductor (PVK) was investigated by Bittner et al.[158] The intention in this particular case was to increase the hologram dark-decay times and to enhance the multiplexing capability of PR composites.[159]

A systematic study of the influence of low ionization potential dopants on the PR characteristics were performed by Malliaras et al.,[160] where increasing amounts of low oxidation potential DEH was added to a PVK/EPNA/TNF composite. The holographic response time as well as the phase-shift $\varphi$ was found to drop significantly ($\tau^{-1}$ roughly by a factor of 10, $\varphi$ from 32° to 2°, respectively) with introduction of small amounts of DEH (up to 2 wt.%), which indicates that DEH in small concentrations act as traps for holes in the composite. At higher concentrations of DEH (2-20 wt.%), both response time and phase-shift was found to increase, even above the initial values found for the composite without DEH. This finding is in accordance with research performed by Pai et al.[161] on mobilities of PVK films doped with TPD, which indicates that the dopant in sufficient concentration provides an alternative path for charge transport. Interestingly, the amplitude of refractive index modulation was found to vary very little for all concentrations of DEH, enabling the possibility to tailor specific characteristics of the material by the introduction of hole-traps.

The redox-chemical doping of the hole-conductor in a TPD-PPV-based composite by the oxidation agent TBPAH[70] in small quantities (one molecule TBPAH for $10^4$ repeating units of the polymer) was found to greatly enhance the intermediate charge-carrier density and thus $E_{SC}$ of the material upon pre-illumination (see **Figure 12**). The effect is based on the availability of permanent charges in the material provided by the oxidation agent (roughly $4 \times 10^{16}$ $cm^{-3}$). The higher intermediate diffraction efficiency (factor 1.7) and the faster response time was accompanied by a lower quasi-steady-state index modulation due to higher dark current in the material and a reduced stability against dielectric breakdown.

### 3.4. Electro-optic Response

Today, compared to the number of publications focusing on the photoconductive properties of the materials, the research interest in PR electro-optical dyes (chromophores), which was the main

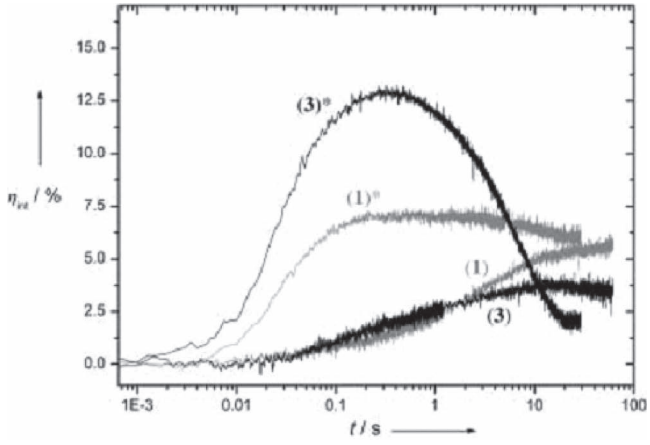


**Figure 12.** Changes of the dynamics of a TPD-PPV/DMNPAA/MNPAA/PCBM composite upon gating (marked with ∗) of a pristine (curve 1, grey) and a chemically doped (curve 3, black; oxidation yield approx. $4 \times 10^{16}$ cm$^{-3}$ permanent charges) sample. Gating refers to pre-illumination with 633 nm light ($I_{gate}$ = 2.3 W cm$^{-2}$, $t_{gate}$ = 995 ms) prior to the actual holographic recording. All curves were measured at $I_{WB}$ = 3.27 W cm$^{-2}$ and 50 V μm$^{-1}$ applied field. Reproduced with permission.[70] Copyright 2004, Wiley-VCH.

driver for material development in the early days of organic photorefractives, has dropped significantly. Here, we briefly review the implications of improving the electronic structure of chromophores in light of chemical modifications and the subsequent influence on composite formulation. Recent developments on chromophore molecules for PR composites, as well as PR low molecular weight glasses (see Section 3.4.4) are discussed.

### *3.4.1. Molecular Aspects*

Chromophores are incorporated into the PR material to translate the obtained space-charge field into a refractive index modulation. These molecules are comprised of an extended $\pi$-conjugated core, end-capped with substituents of electron donating and accepting capability, respectively. Thus, chromophore molecules exhibit a non-vanishing ground-state dipole momentum $\mu$ and a strong anisotropy of the polarizability along the long axis and the perpendicular axis of the molecule. The application of an external electric field is necessary to break centrosymmetry of the initially randomly oriented molecules in the bulk material to allow for second-order nonlinear effects (see Figure 3).

Microscopically, the overall effect in low-$T_g$ PR composite materials originates from the linear EO (Pockels)-effect through the hyperpolarizability $\beta$ and to a greater extent from a birefringence modulation through the polarizability anisotropy $\delta\alpha$ of the chromophore. A figure of merit (FOM) $F$ reflecting the peculiarities of low-$T_g$ PR composites, e.g. a description of the effect in terms of a Kerr-susceptibility according to the orientational enhancement mechanism,[17] is given by

$$F = \frac{1}{M}\left[9\mu\beta + \frac{2\mu^2\delta a}{k_B T}\right] \quad (1)$$

with $M$ the molecular mass of the chromophore molecule, $\mu$ the ground-state dipole momentum, $k_B$ Boltzmann's constant and $T$ the temperature.

Structural modifications to influence $\delta\alpha$ and $\beta$ are carried out by tuning the accepting and donating capability of the respective substituents and the structure of the $\pi$-conjugated main-axis of the chromophore. Structural modifications affecting $\delta\alpha$ and $\beta$ are quantifiable by UV-VIS spectra and electro-optical absorption measurements (EOAM)[162–166] of the chromophore in dilute solution. The obtained physical quantities (UV-VIS: absorption maximum $\lambda_{ag}$, spectrum integration yields the transition dipole $\mu_{ag}$, EOAM: ground-state dipole moment $\mu$ and dipole difference $\Delta\mu$ upon optical excitation) can be used to estimate $\delta\alpha$, $\beta$ and $F$.

The influence of donor-acceptor interaction on $F$ is described by the two-state model using the resonance parameter $c^2$. It denotes the linear combination of the wavefunctions of the two basic resonance structures of push-pull chromophores, i.e. neutral/polyene ($c^2 = 0$, D-A) and zwitterionic/betaine ($c^2 = 1$, $D^+$-$A^-$). Increasing the push/pull characteristics of the accepting/donating groups increases the polarity and the dipole moment $\mu$ of the chromophore as well as the value of $c^2$.

Several recent reviews and feature articles treated the influence of the chemical structure on the EO-properties of the chromophore in light of PR applications.[3,14,86,162,167,168] In 2002, Würthner et al.[162] presented a comprehensive compilation of chromophores, the influence of their structure on $c^2$, $\beta$, $\delta\alpha$, $\mu$ and $F$ and thus a recipe for high figure of merit PR chromophores. Three significant conclusions were drawn:

(1) Increasing the polarity of the push-pull system leads to an increase of $F$ until a $c^2$-value of 0.7-0.8. A plot on this correlation is depicted in **Figure 13**. Unfortunately, the high dipole

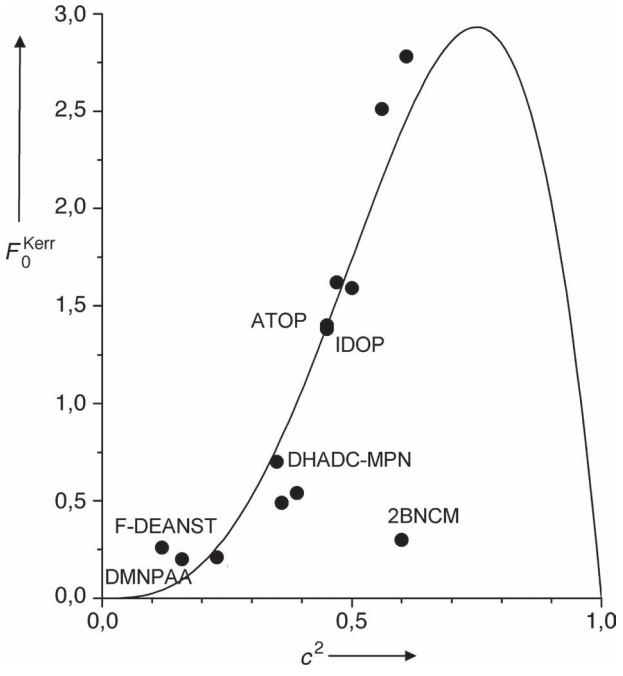


**Figure 13.** Figure of merit of chromophores in low-$T_g$ PR composites, plotted against the charge resonance mixing parameter $c^2$. For structures and nomenclature of unassigned data points, the reader is referred to the original publication. Reproduced with changes, with permission.[162] Copyright 2002, Wiley-VCH.

of materials with $c^2 > 0.5$ yielded high melting crystalline solids, which are hard to dissolve in rather non-polar polymeric hosts.

(2) A strong variation of $c^2$ was found by introducing aromatic and quinoid carbo- and heterocycles,[164,165] which significantly increased the polarizability of the $\pi$-conjugated system with respect to simple donor-acceptor substituted polyene structures.

(3) Increase of the chromophore-length was found to be less effective for optimizing $F$, which is due to the predominant influence of $\mu^2\delta\alpha$ on $F$, whereas extension of the polarizable chain segment chiefly effects $\mu\beta$. Moreover, extended polymethine chains impart new problems with regard to solubility, aggregation (see below), as well as decreased thermal stability. Finally, the higher molar mass $M$ adversely affects $F$.

It should be noted, that $\beta$ and $\delta\alpha$ of a molecule cannot be optimized independently.[13] Thus, due to its higher impact, emphasis is generally put on $\delta\alpha$. The polarizability anisotropy has its maximum at $c^2 = 0.5$ (here, $\beta = 0$), which describes an equal contribution of the polyene and betaine wavefunctions in the ground-state of the molecule. This particular situation is typically found in cyanine-dyes, hence chromophore structures featuring this particular charge resonance are referred to be in the cyanine-limit. Since the potential energy surfaces of the polyene and zwitterionic electronic state are very similar in cyanine dyes and the structures of the ground and excited state do not show a change of atomic core coordinates (and dipole moments), the absorption spectra of these molecules feature a sharp peak of high extinction. Thus, in comparison to broad absorption spectra of polyene structures, it is possible to operate the cyanine-chromophores closer to the resonance wavelength which feature higher values of $\beta$ and $\delta\alpha$ without the loss of material transparency (efficiency-transparency trade-off).

It is thus generally concluded,[86,162–165,169] that structures tuned near the cyanine-limit should yield optimized chromophores for the use in photorefractive composite materials with regard to traditional NLO-dyes.

As can be seen in **Figure 14** and **Table 4**, FOM-optimized chromophores in or near the cyanine-limit based on aminothienyl oxopyridone (ATOP **63**, **64**), indoline dimethine oxopyridone (IDOP **62**) and rigidized polyene derivatives (DHADC-MPN **65**) feature a dramatic increase of $F$ over traditional chromophore structures, e.g. azo dyes (DMNPAA **45**), amino-nitrostyrene structures (F-DEANST **53**, DANS **59**) and benzylidene-malononitriles (PDCST **50**). All structures are depicted in Figure 14.

### 3.4.2. Macroscopic Response

The "oriented gas model"[13,14] relates the microscopic properties of the chromophores to a bulk electro-optic response of the PR material. The resultant magnitude of the refractive index modulation depends, besides the microscopic properties, on the chromophore density in the bulk material and supra-molecular interactions of the chromophores, e.g. degree of orientation of the chromophore main-axis under the poling field versus dipolar aggregation.

The formation of dimer aggregates through anti-parallel orientation of the dyes yields species which are no longer able to orient in an applied electric field. Thus, the effective chromophore density of the composite is reduced in this case. Moreover, the dimer species may feature redox-potentials different from the pristine dye, with detrimental effects on the photoconductive properties of the composites (see below). The extent of dimerization and the associated Gibbs free dimerization energy of the dimers are accessible through concentration dependent UV/VIS absorption spectroscopy in solution.[162]

### 3.4.3. Chromophore Containing PR Composites

To translate the space-charge field into a macroscopic refractive index modulation amplitude $\Delta n$, composites with rather high chromophore content (usually 30-50 wt.%) have to be prepared. For similar chromophore content, the field necessary for complete diffraction efficiency should therefore be significantly lower for chromophores with higher $F$. The superior PR performance by utilizing ATOP as chromophore is demonstrated by Mecher et al.,[179] yielding complete internal diffraction efficiencies for a 40 wt.% ATOP doped PVK composite material at $\lambda = 790$ nm at applied fields as low as 23 V $\mu m^{-1}$. This compares favorably to a similar material doped with 50 wt.% DMNPAA, which requires an applied field of $E_{ext} = 71$ V $\mu m^{-1}$ for the same refractive index modulation.[178] Similarly, a DHADC-MPN (40 wt.%) doped PVK/TNF-material featured a roughly 5 times higher refractive index modulation compared to the same material doped with 40 wt.% DMNPAA, corresponding to a shift of $E_{max}$ from 65 V $\mu m^{-1}$ (DMNPAA) to 30 V $\mu m^{-1}$ (DHADC-MPN).[86]

The achievable content of chromophore molecules in the blend depends on the mutual solubility of chromophore and polymer, which is restricted due to their difference in polarity. Several approaches are discussed in the literature to increase the solubility of the chromophores in rather non-polar polymeric matrices like carbazoles, TPDs and PPVs. Often, aliphatic groups are attached to the chromophore to increase its solubility, albeit F is reduced due to the increase of the molar mass of the molecule. For example, the FOM of ATOP is subsequently reduced from 1.98 (see Table 4, all R are denoted methyl-group for calculation) to 1.35 for ATOP-4 (**64**)(R = butyl, butyl, ethylhexyl).[179] Nevertheless, it is observed empirically,[13] that the maximum content of chromophore that can be incorporated into a material scales with the alkyl content. Similarly, branched chromophores[181] and aromatic substitution of aliphatic endgroups[171] were discussed to increase the shelf lifetime of the materials. It should be pointed out, that substitutions on the NLO molecule may adversely affect the orientational mobility of the chromophore under applied fields.[171] Ref. [178] discusses doping of a second chromophore to enhance the polarity of the matrix in order to increase the solubility of a dye in the cyanine-limit. A 25 wt.%/25 wt.% mixture of ATOP-1 (**63**) and DMNPAA featured a complete internal diffraction efficiency at $E_{max} = 33$ V $\mu m^{-1}$ (PVK-based composite at 790 nm illumination), in comparison to a sample with 50 wt.% DMNPAA ($E_{max} = 71$ V $\mu m^{-1}$) and 20 wt.% ATOP-1 in PVK ($E_{max} = 65$ V $\mu m^{-1}$).

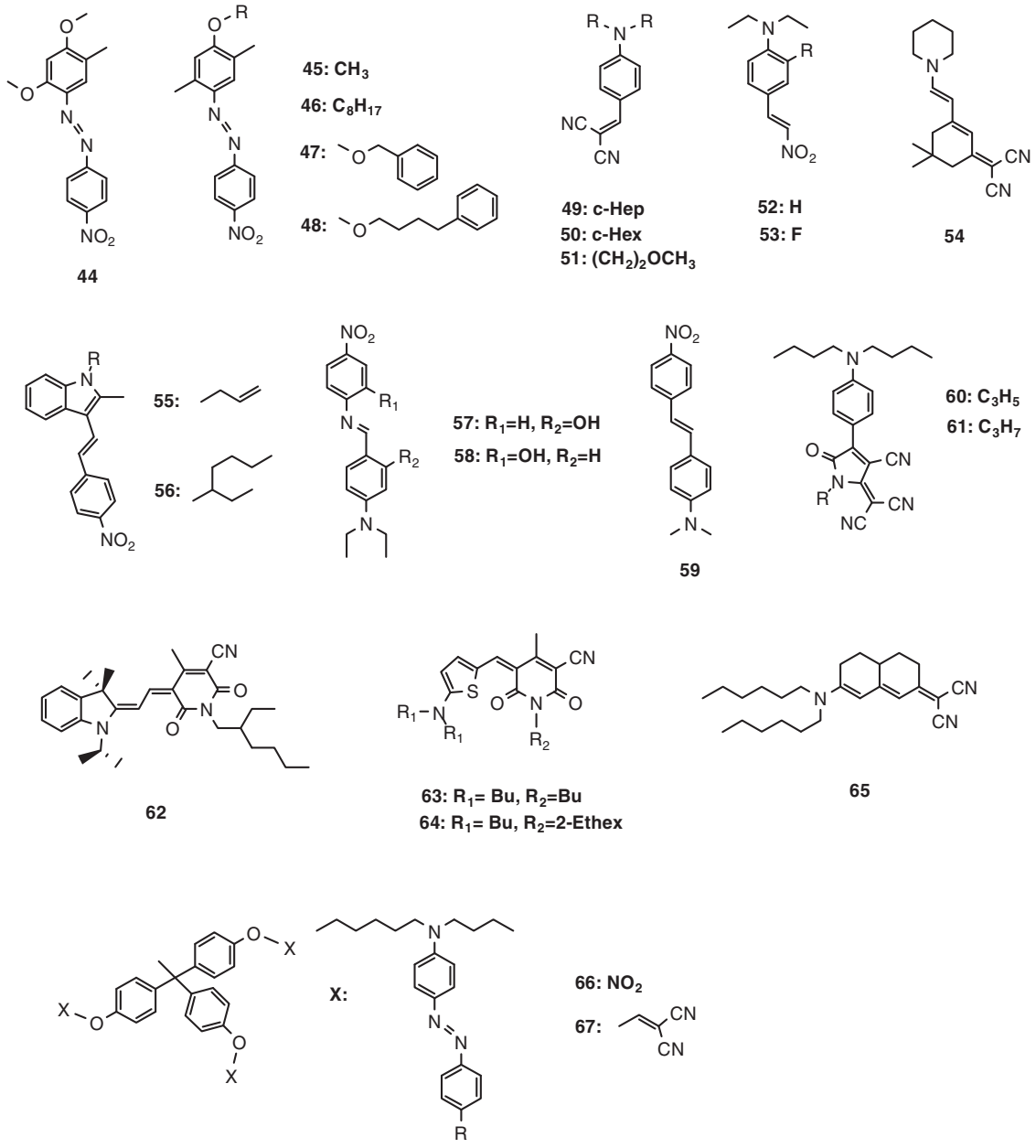


**Figure 14.** Structure of photorefractive chromophores: **44** MNPAA,[170] **45** DMNPAA,[62] **46** DMNPAPOE,[171] **47** DMNPAPBE,[171] **48** DMNPAPhBUE,[171] **49** 7-DCST,[46] **50** PDCST,[29,46] **51** AODCST,[46] **52** DEANST,[115] **53** F-DEANST,[82,162] **54** DB-IP-DC,[172,173] **55** NPEMI-A,[174] **56** NPEMI-E,[174,175] **57** H1,[176] **58** H2,[176] **59** DANS,[168,165] **60** DBA-TCP,[177] **61** DBP-TCP,[177] **62** IDOP-20,[162] **63** ATOP-1,[162,166,178] **64** ATOP-4,[162,179] **65** DHADC-MPN,[86,180] **66**,[181] **67**.[181]

The latter was found to be the optimum concentration for ATOP-1 in PVK without the doping of a second chromophore.

Besides structural characteristics, it should finally be noted, that the polarity of the surrounding medium influences all relevant NLO properties of the chromophores. A study of computational and experimental results on the influence of the medium polarity on FOM of high- and low-$T_g$ PR polymers is given in.[183]

Despite a sufficient initial solubility of the chromophore in the polymeric matrix, it should be pointed out that mixtures of polymers and low molecular weight dopants are inherently metastable. This fact is most obviously observable through partial crystallization of the low molecular weight components and the subsequent loss of transparency. Aggregation and phase-separation of the dipolar chromophores is thus a major concern in the design strategy of NLO molecules for PR composites. This is especially true for composite materials of low $T_g$, which offers high degree of diffusional freedom for the chromophore. Furthermore, these issues tend to aggravate in light of the higher polarity of optimized ($\mu^2\delta$a) chromophores with regard to traditional ($\mu\beta$) chromophores (see Table 4).

**Table 4.** Molecular parameters of some selected EO-chromophores, data taken from [a] Ref. [165], [b] Ref. [162] and [c] Ref. [166]. For ATOP, all R in Figure 14 are assumed to be methyl-groups.

| | $c^2$ | $\mu$ [$10^{-30}$Cm] | $\beta$ [$10^{-50}$ CV$^{-2}$m$^3$] | $\delta\alpha$ [$10^{-40}$ CV$^{-1}$m$^2$] | $F$ [$10^{-74}$ C$^2$V$^{-2}$m$^4$kg$^{-1}$mol] |
|---|---|---|---|---|---|
| DANS[a] | 0.09 | 25 | 133 | 28 | 0.42 |
| F-DEANST[b] | 0.12 | 21 | 78 | 22 | 0.27 |
| DMNPAA[b] | 0.16 | 21 | 56 | 22 | 0.20 |
| PDCST[c] | 0.22 | 29 | 52 | 25 | 0.48 |
| DHADC-MPN[b] | 0.35 | - | - | - | 0.7 |
| ATOP[b] | 0.45 | 47 | 27 | 55 | 1.98 |
| IDOP[b] | 0.45 | 43 | 30 | 61 | 1.58 |
| 2BNCM[c] | 0.59 | 31 | –9 | 19 | 0.30 |

Approaches to hinder the thermodynamically favored aggregation of the dipolar chromophores are the introduction of sterically demanding side-groups or branched structures (e.g. **66**, **67**),[181] the use of mixtures of chromophores (e.g. the 1:1 wt.% eutectic mixture of DMNPAA and MNPAA,[170] or a 4:1 mixture of DBDC/7-DCST,[184]) or incorporating chromophores of high structural similarity with the respective photoconducting host.[174] Alternatively, in order to reduce the tendency of the dipolar chromophores to form anti-parallel aggregates, a Hamilton receptor is employed to a merocyanine dye.[182] This substituent is attached to facilitate the formation of head-to-tail parallel ordered chromophores through multiple hydrogen bonds with the barbituric acid electron accepting group on the tail of a second dye. Cooperative orientation of these dyes is confirmed through electro-optic absorption measurements in solution; however, a PR characterization of this chromophore material has not been performed so far. Also, in some materials the structure of the chromophore structure itself was found to disfavor the anti-parallel aggregation of the dyes, which leads to lower dimerization energies than expected. The bulky dimethylmethylene unit in the central part of the IDOP chromophore and the bent shape of the ATOP molecule was found to disfavor close anti-parallel packing.[162] Similar arguments were discussed for the dimethyl-substituted ring-structure of the isophorone unit of the DB-IC-DC (**54**) chromophore.[172]

The electronic structure of the chromophore and its redox properties also influence the steady-state and dynamic properties of the materials. Restricting the discussion here to a hole-conducting host system, the chromophore may either present a trap for the mobile hole (lower oxidation potential than the host) or form a separate conduction path in high concentration,[185] co-participate in hole-conduction (similar oxidation potential) or be inert to the photoconduction process (higher oxidation potential than the hole conductor). Even for the latter case, the high concentration of dipolar molecules was found to severely reduce the charge carrier mobility of the host material due to their influence on the hopping site energy distribution, which was found to be proportional to the square-root of the dipole concentration and strength of the dipole momentum.[186]

Several publications investigated the influence of the chromophore ionization potential on the performance of the composite material.[22,29,61,185,187,188] The "trap"-case is found to be detrimental for the performance of the composites under prolonged exposure to the illuminating write beams, due to the accumulation of sensitizer radical anions and positively charged chromophore compensator trap sites.[29] A difference in trap density by one order of magnitude was found between chromophores featuring HOMO-levels above and below the HOMO-level of the hole-conductor.[29] Spectroscopic evidence for this aspect is given in.[98] Comparative studies on chromophores with ionization potentials above and below the HOMO-level of the charge-transport polymer can be found in[29,187,188] and,[22] the latter being supported by photoconductivity experiments and simulations. The best dynamic performance in this study was obtained for materials featuring oxidation potentials similar or slightly above the CTA, which implies a participation of the chromophore in the charge transport. Nevertheless, the currently fastest materials with stable and fully reversible dynamic properties[29,47,61,189] incorporate chromophores which do neither participate in charge generation, nor in transport, and do not absorb at the operational wavelength.

Conclusively, due to the comprehensive understanding of the underlying mechanisms of NLO-effects in PR composites, the systematic synthesis of organic molecules and their subsequent characterization by powerful methods like EOAM, there is currently a broad availability of high FOM chromophores for PR applications. Nevertheless, secondary implications of high FOM chromophores exist, which are due to their increased dipole moment, causing dipolar aggregation and diminished solubility in non-polar photoconductive matrices. Accordingly, recent publications on high performance PR composites, especially with regard to the dynamic performance, still utilize chromophores with rather moderate or low values of $F$, for example the DMNPAA/MNPAA-couple, 7-DCST etc. In Ref. [176], arylamine-derivatives of the traditional DANS-chromophore (H1 **57**, H2 **58**) were shown to exhibit 75% diffraction efficiency at low electric fields ($E_{max}$ = 32 V μm$^{-1}$, 633 nm illumination, PVK/$C_{60}$-based composite) at a low chromophore content of 25 wt.%, which is clearly competitive to blends containing high-FOM chromophores described above.

Finally, there exists an inherent trade-off between fast response-time and dynamic range of the composite due to the detrimental effects of content and polarity (and thus the FOM) of the chromophores[29] on the photoconductive properties of the CTA.

### *3.4.4. Multifunctional Materials/Organic LMW-Glasses*

The need for high concentration of chromophores in PR composites and the subsequent issues of solubility and stability led to the development of multifunctional LMW PR glasses. Here, the chromophore also serves as a CTA, the molecules form amorphous glassy materials with maximized chromophore content and reduced tendencies of phase-separation. Examples of this approach are materials based on the pyridone derivative 2BNCM (**68**),[190] DHADC-MPN (**65**),[180] DCDHF (**69**) -based

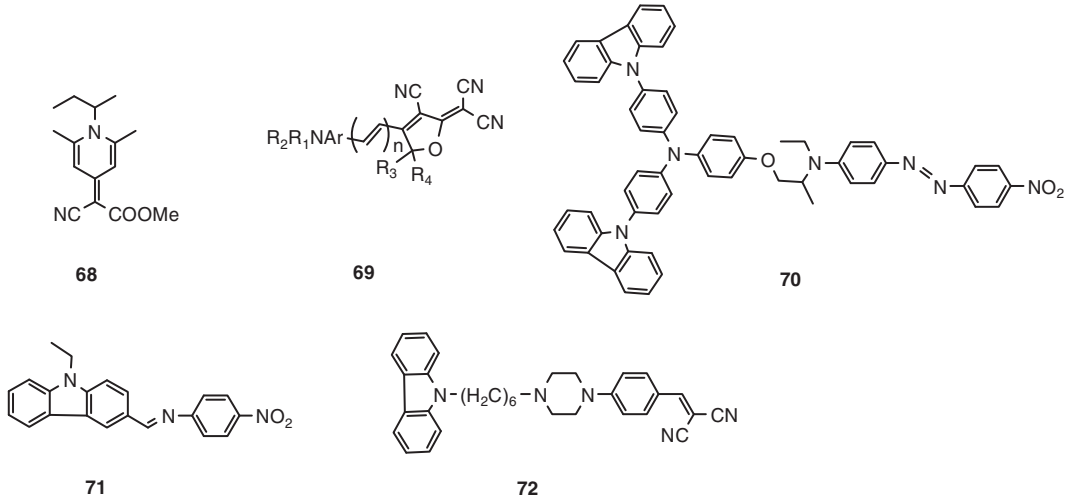


**Figure 15.** Structure of multifunctional organic glass-forming materials: **68** 2BNCM,[190] **69** DCDHF,[112,191,192] **70** DRDCTA,[193] **71** ECYENPA,[157] **72** Cz-C6-PDCST.[194]

glasses,[112,191,192] 2-methylindole-derivatives NPEMI-A (**55**) and NPEMI-E (**56**),[174,175] IDOP and ATOP-4,[162,179] see **Figure 15**. Some of the materials (DHADC-MPN, ATOP-4) were even shown to be trifunctional, e.g. also providing photosensitization at the respective write-beam wavelengths. A similar approach to organic glasses is the utilization of covalently bond structures of a monomeric hole-conductor moiety and chromophore as building block for LMW-organic glasses. Examples include ECYENPA (**71**),[157] DRDCTA (**70**)[193] and Cz-C6-DCST (**72**),[194] a hyperstructured cyclotriphosphazene molecular glass,[195] amongst others.

High gain coefficients of $\Gamma$ = 415 $cm^{-1}$ were achieved in a glassy material made of a mixture of two DCDHF (**69**)-based glasses sensitized by 1 wt.% TNFM at 830 nm NIR illumination,[192] which is clearly due to the benefit of high chromophore content provided by the glass approach. The combination of 99 wt.% ATOP-4 with 1 wt.% TNFM led to unprecedented steady-state diffraction performance, reaching complete internal diffraction efficiencies at external fields as low as 10 V $\mu m^{-1}$ at 790 nm. Due to the ability of merocyanines to provide hole-conducting capability and their intense, narrow absorption bands, Kronenberg et al.[56] recently fabricated bulk heterojunction organic solar cells from a wide range of merocyanines (including ATOP and IDOP) and PCBM. Under standard solar radiation, a blend of 30 wt.% ATOP-4 and 70 wt.%[60] PCBM (100 nm active layer thickness, 40 nm ITO/PEDOT:PSS anode, Al cathode) reached power conversion efficiencies (PCE) of roughly 1%. Mixtures of merocyanines and PCBM/$C_{60}$ currently feature PCEs of up to 3.0%/5.0%.[196] A feature article on this matter can be found in.[197]

An interesting variation of weight contents of low molecular weight glass forming multifunctional chromophore and a polymeric hole-conductor and thus a transfer from composite to LMW-material was recently described for NPEMI-A and NPEMI-E in[174] and,[175] respectively. Here, as both 2-methylindole-derivatives show a high mutual solubility in PVDMI (**3b**,see Figure 4) due to their structural similarity, composite samples of chromophore content between 0% and 99% chromophore (each material was doped by 1 wt.% TNFM sensitizer) were fabricated. The authors claim stable and transparent composites upon aging for all compositions. From composites of 50 wt.% NPEMI-A (NPEMI-E) to glassy materials of 99 wt.%, the $T_g$ of the films is found to drop from 50 °C (43 °C) to 18 °C (–3 °C), respectively. Photoconductivity and gain coefficients increased with increasing chromophore content for both material sets, but reached minimum (photoconductivity) and plateau-values (gain factors) for chromophore contents of around 90-95 wt.%, respectively (see **Figure 16**).

The authors took these findings as evidence for a collaborative effect in both composites at these chromophore contents, which is due to rapid variations of electro-optic parameters as a function of the mutual distance and intermolecular geometry of the chromophores.[174] This effect was found to affect both the photoconductive and PR behavior of the materials. Very high values for the gain coefficients were found, $\Gamma$ = 210 $cm^{-1}$ for NPEMI-A (99 wt.%) at $E_{ext}$ = 75 V $\mu m^{-1}$ and $\Gamma$ = 2027 $cm^{-1}$ for NPEMI-E (90 wt.%) at $E_{ext}$ = 90 V $\mu m^{-1}$ (all at 685 nm).

Despite the high promise of PR glasses, the approach presents some drawbacks that hinder the implementation of organic PR glasses in holographic applications, most pronounced the slow response time of the materials. To the best of our knowledge, only one organic LMW glass was demonstrated to exhibit holographic response times in the sub-second time domain (DRDCTA,[193]) which is clearly inferior to performance reached by the composite approach. This may either be due to orientational limitations and thus the $T_g$ of the material[191] or to the photoconductivity of the materials.[112]

Another problem of LMW-materials is high losses due to beam-fanning. Beam fanning is an inherent loss mechanism originating from amplification of scattered light and the subsequent formation of noise gratings.[198–200] This effect is most pronounced in strongly coupling media (e.g. materials featuring high gain coefficients).

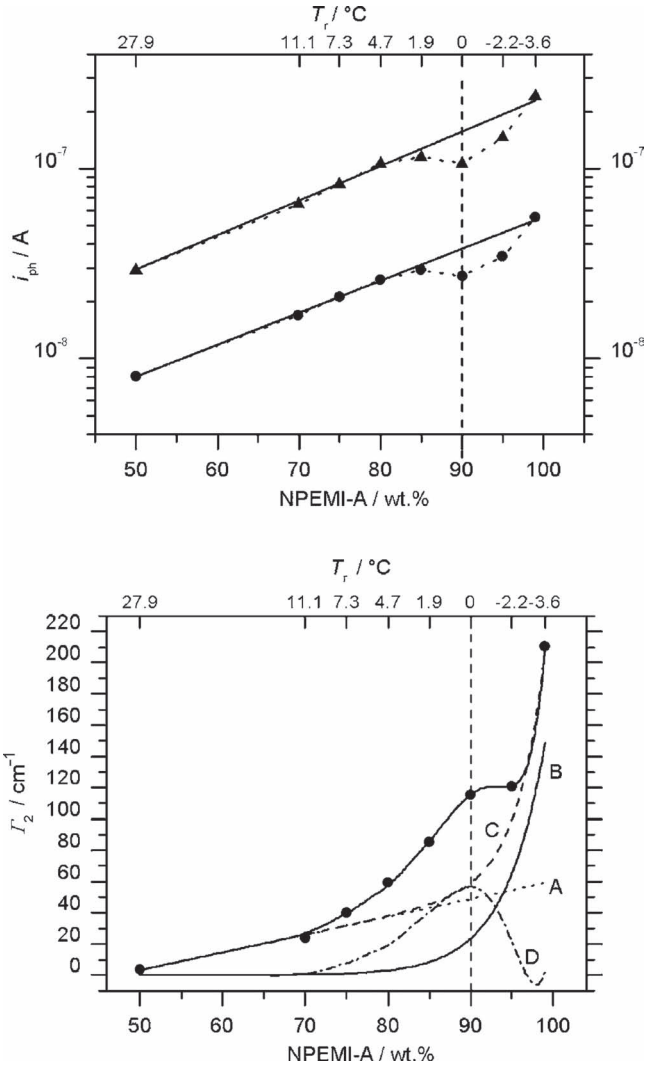


**Figure 16.** Photocurrent $i_{Ph}$ (upper plot) and Gain-values $\Gamma_2$ (lower plot) as a function of the composition of the NPEMI-A/PVDMI blend (upper plot $E_{ext}$ = 75 V µm$^{-1}$ (triangles) and $E_{ext}$ = 50 V µm$^{-1}$ (dots), lower plot $E_{ext}$ = 75 V µm$^{-1}$ (dots)). The dashed line indicates a reduced temperature $T_r = T_g - T_{RT} = 0$. Lines A–D in the lower plot are semi-empirical deconvolution functions of the polynomial fit to the data points, line D hereby represents the contribution of a "collaborative" effect. Reproduced with permission.[174] Copyright 2010, Wiley-VCH.

## 4. Physical Aspects

### 4.1. Geometry

The steady-state and dynamic performance of PR materials depend strongly on the recording geometry of the setup.[124,201–203] This is due to the influence of the geometry on the formation of the space-charge field, as well as the birefringence and electro-optic contributions of the chromophores. Two basic recording geometries can be distinguished: Transmission type, which to date is the most common recording scheme, and reflection geometry. In the former case, both write-beams impinge on the sample from the same side of the PR recording medium. Predictions for the PR behavior based on the adjustable geometric factors, tilt angle $\Psi$ and grating spacing $\Lambda$ (see Section 7.2.2), imply, that a performance increase is expected for both, increasing $\Psi$ and $\Lambda$, until external influences impose restrictions, e.g. high order diffraction and loss of resolution (high $\Lambda$), and increased absorption losses (large $\Psi$).

Reflection holograms are formed by counter-propagating beams in the material. This geometry correspondingly offers certain advantages with regard to low absorption losses for the reading beam, thus allowing for external (absorption-loss corrected) diffraction efficiencies near 100%, theoretically no oscillatory behavior of $\eta$ with increasing $\Delta n$ (oscillatory behavior was observed due to read out with crossed polarizations in[203]) and high projections of the applied electric field on the grating vector. Furthermore, high Bragg selectivity due to the short fringe spacing is achieved, which allows for hologram reconstruction by white light and the possibility to circumvent the beam walk-off effect in low coherence interferometry (see Section 5.5). Nevertheless, reflection type holograms were often found to be inferior in diffraction efficiency compared to transmission holograms, which is due to the limitations of the space-charge field for small grating spacings. Hence, materials with a strong saturation field (e.g. high number of traps) are needed to compensate the restrictions of small grating spacings.[201,203] Since the space-charge field is consequently very sensitive to changes in the number of traps, reflection gratings allow for a reliable calculation of the trap density and the saturation field.[124] An analysis of the geometrical dependence of the birefringence ($\Delta n_{BR}$) and the electro-optic ($\Delta n_{EO}$) contribution to the total refractive index modulation $\Delta n$ revealed, that in transmission-type gratings, both factors are always positive and thus add up. However, in the case of reflection geometries, $\Delta n_{BR}$ may become negative (for p-polarized read-out of the grating) at certain write-beam angles. Hence both contributions compete with each other and, depending on the chromophore, may cancel out. As pointed out in,[124] this implies a modification of the chromophore FOM introduced in Eq. 3.1 to be applicable for reflection gratings, and the use of optimized chromophores in the cyanine-limit, which have a strong emphasis of $\Delta n_{BR}$ over $\Delta n_{EO}$ (see Section 3.4). Moreover, due to the high Bragg-selectivity of reflection gratings, the Bragg-matched read-out angle was found to be sensitive to deterioration induced by the magnitude of the applied electric field.[203]

Up to now, the highest external diffraction efficiency of 30% in reflection gratings is achieved in a PVK/DMNPAA/MNPAA/TNFM- device (633 nm, 60 V µm$^{-1}$ applied field, see **Figure 17**). This corresponds to an internal diffraction efficiency of 65% in this particular material. Moreover, the grating formation was found to be faster by a factor of 5 in reflection geometry than in direct comparison to transmission gratings.[124] Due to the smaller fringe spacing in reflection gratings, hole displacement typically yields higher values of the phase-shift $\varphi$, which is significant for the amplitude of the coupling gain, since $\Gamma \approx \Delta n \sin \varphi$, see Equation 7.3.

Despite the type of employed geometry, the range of possible write-beam angles is limited due to the refractive index mismatch of air and the glass substrate of the plan-parallel sample configuration (for transmission gratings, $\Psi_{max} \approx 36°$). The influence of attached glass prisms and cylindrical glass hemispheres

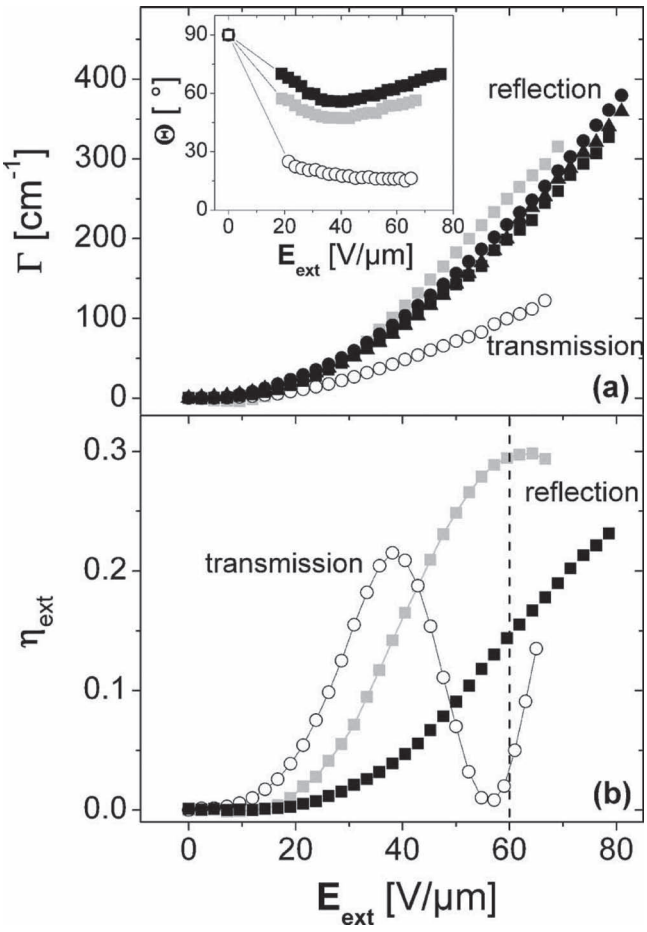


**Figure 17.** Comparison of reflection type (grey and black solid symbols, corresponding to two different reflection geometries) and transmission type (open symbols) behavior for a PVK/DMNPAA/MNPAA/TNFM-based material at 633 nm under steady-state conditions, a) gain coefficients $\Gamma$ (inset: phase-shift $\varphi$), different solid black symbols denote a variation of the grating contrast m. b) External diffraction efficiency. Reproduced with permission from.[124] Copyright 2007, American Institute of Physics.

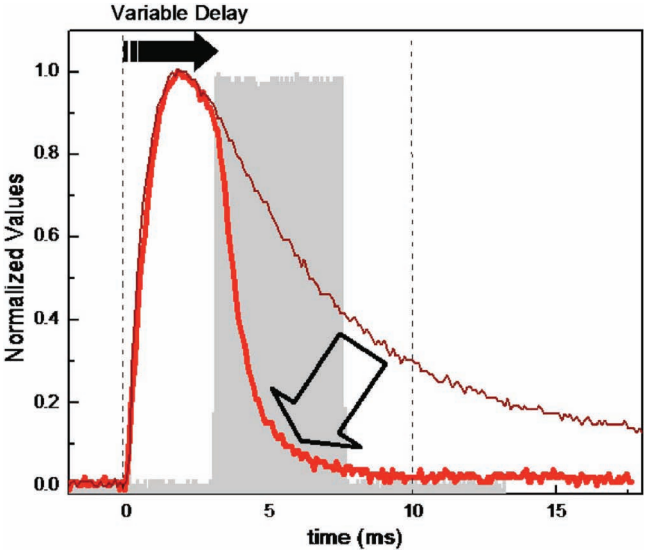


**Figure 18.** Normalized diffraction efficiency of a grating write-erase cycle. Upon pulsed illumination of the sample (pulse at first dashed line, see text for details of the writing procedure) and an adjustable time-delay (solid arrow) to reach a maximum of diffraction efficiency, the grating is erased (red line) by 5 ms uniform cw-illumination at 6 mJ cm$^{-2}$ exposure (gray window). The second dashed line indicates the end of the write-erase cycle, suggesting a possible operation of the device at 100 Hz. As comparison, the black line depicts the dark decay of the grating upon pulsed hologram formation. Reproduced with permission.[45] Copyright 2006, American Institute of Physics.

to increase the range of available write-beam angles are discussed by Sassa et al.[201] and Grunnet-Jepsen et al.,[204] respectively.

### 4.2. Pulsed Writing

For several applications, short or ultra-short light pulses are required to write PR gratings. For example, single-shot nano-second pulses allow for vibration-tolerant writing of gratings in holographic media. High intensity pulses were employed to enable two-photon absorption.[106,107,117] By employing 4 mJ cm$^{-2}$ 532 nm 1 ns pulses to a linear sensitized PATPD-based composite, a dramatic reduction in response time compared to cw-illumination was found.[45] The grating build-up time was found to be limited by the drift-mobility of the material or chromophore orientation (not specified by the authors), since the charge carriers are only formed during the overlap duration of the light beams. Maximum diffraction efficiency achieved was 56% at a build-up time of 300 μs (fast constant of bi-exp fit to the data, 95 V μm$^{-1}$ bias). Through pulsed illumination and time gated homogeneous illumination, gratings can be written and completely erased with a repetition rate of 100 Hz (see **Figure 18**).

If orientational limitations can be ruled out for the material under investigation, the grating build-up upon illumination by nano-second pulses is solely determined by the displacement of the mobile charge-carriers. This subsequently enables the measurement of the drift-mobility of the mobile charge carrier in the PR material. The corresponding technique is known as holographic time of flight (HTOF).[205–207]

### 4.3. Pre-Illumination

Homogeneous pre-illumination of the composites prior to the recording of the PR grating was discussed[22,28,47,57,64,70,71,208] as a method to increase the amplitude of $E_{SC}$ and the recording speed without increasing absorption losses of the composites. Pre-illumination was demonstrated at the same wavelength as the holographic experiment,[22,61,64,208] or at a shorter wavelengths (also denoted as "gating" in some publications) to increase the charge carrier generation rate through enhanced absorption and to take advantage of the higher quantum efficiencies at higher frequencies.[47,57,70,71] It should be explicitly noted here, that a series of write-erase cycles may indeed have the same effect on the dynamic behavior of the materials as pre-illumination, thus allowing for an estimation of the materials response under continuous illumination.

In any case, pre-illumination alters the initial conditions for grating formation in the composites, since a homogeneous density of trapped holes and ionized sensitizer radical anions is present in the material prior to the actual recording process. This was shown to have a significant impact on grating transients.[64,208] However, the resultant effects of pre-illumination on the grating formation rate and the corresponding steady-state values are strongly dependent on the material composition under investigation, especially with regard to their electronic structure. Thus, reports on pre-illumination experiments vary from decelerating grating build-up[61,209] to dramatic enhancements especially with regard to dynamic performance[71] and sensitivity.[47] Since no general description on the influence of pre-illumination is available so far, the obtained trends are described for each material study in detail below.

Usually, the pre-illumination process is reversible, with the relaxation time being dependent on the trap situation in the composite and illumination conditions (see below). Upon pre-illumination, the actual trap-depth and density as well as the nature of the incorporated sensitizer affect the response of the material to the subsequent holographic recording. Herlocker et al.[61] and Ostroverkhova et al.[22] studied the influence of the chromophore oxidation potential with regard to the CTA. Both found a more pronounced influence of pre-illumination on the behavior of the materials with the lower chromophore $I_p$. Here, the chromophores behave as compensation sites (and thus deep hole traps) for a growing density of sensitizer radical anions upon pre-illumination. Since sensitizer radical anions constitute recombination traps for holes, this effect is denoted as "optical trap activation",[209] which led to a significant reduction of PR performance in Ref. [61] under prolonged exposure.

The influence of the sensitizer on the impact of pre-illumination was studied in Ref. [47,70] for materials operated in the NIR (830 nm) and short (approx 1 s) pre-illumination pulses at 633 nm. It was shown,[70] that PVK-based materials (chromophore $I_p$ above CTA) sensitized with rather inefficient NIR sensitizers (TNF, PCBM) and thus charge generation limited performance experienced an increase of grating build-up speed upon pre-illumination (factor 15 and 16 increase of sensitivity for TNF and PCBM, respectively), whereas almost no influence was detected for efficiently sensitized and thus transport limited materials (PVK/TNFM, factor 0.8 change of sensitivity). A series of fullerene-sensitized PF6TPD-based materials demonstrated the influence of the reduction potential of the sensitizer on the significance of the pre-illumination procedure[47] (see plot b) in Figure 8). The decrease of the reduction potential by 400 mV (and thus increasing the acceptor strength, see Section 3.3.2.1), led to an increase of the sensitivity upon gating from $S = 3$ cm$^2$ J$^{-1}$ (worst acceptor) to $S = 35$ cm$^2$ J$^{-1}$ (best acceptor). Complementary photo-EMF measurements confirmed the intuitive notion that the better accepting capability led to reduced recombination rates, which eventually determine the density of charge carriers upon pre-illumination at the beginning of the actual measurement. Nevertheless, the performance increase upon pre-illumination compared to the non-pre-illumination case within this series was rather moderate (factor 1.6-2.3).

The strongest impact of pre-illumination to date was found for a TPD-PPV/DMNPAA/MNPAA composite doped with 1 wt.% PCBM[70,71], at a write-beam wavelength of $\lambda = 830$ nm and $\lambda = 633$ nm pre-illumination. A speed increase of factor 40, corresponding to a gain in sensitivity of a factor of 20, together with increased quasi steady-state diffraction efficiency values (factor 2) were achieved. Due to field dependence of the photogeneration efficiency ($\varphi \sim E^p$, $p \approx 2$) of PR composites, the authors were able to demonstrate a higher impact of pre-illumination for lower applied field strengths, which are bound to lower charge generation rates upon holographic recording. Moreover, pre-illumination fluence was found to reveal an asymmetry with regard to pre-illumination intensity and duration. Short pulses of high intensity were found to be favorably over longer pulses of lower intensity. This is appointed to the fact, that the grating build-up dynamics upon pre-illumination are not only determined by the number density of preformed charges, but also sensitive to their respective energetic state. This finding is further confirmed by chemical doping of the hole-conductor to provide the material with permanent charges,[70] which was shown to enhance the beneficial influence of pre-illumination (see Section 3.3.3). On the contrary, in Ref. [209], very long (60 min) pre-illumination exposure led to the non-reversible deceleration of grating formation.

The pre-illumination effects in TPD-PPV were further investigated by photocurrent measurements under various pulsed conditions,[28] which explained various aspects of the difference between pre-illuminated and non pre-illuminated samples. According to the authors, the grating buildup dynamics without pre-illumination are determined by trapping of the mobile charges in deep traps and the recombination with ionized sensitizer molecules. Upon intense pre-illumination however, the dynamics are determined by the generation and recombination kinetics, which accounts for the neutralization of ionized acceptor density in the dark regions of the interference pattern. However, a direct comparison of the impact of pre-illumination in TPD-PPV with other materials would require a wider photoelectric characterization of different material systems.

An unique illumination effect was found by Salvador et al.[57] upon utilizing 405 nm light, which coincided with the maximum absorption band of the incorporated chromophore in a PVK-based composite. Due to the high extinction of the light in the material the penetration depth was less than 100 nm, which allowed for continuous illumination of the sample without distortion of the grating recording by 830 nm write-beams. Gain transients were found to reverse their sign upon illumination (see **Figure 19**,b)), which was identified as complementary electron transport through the LUMO of the chromophore. Dynamic grating recording was accelerated (factor 2 at $E_{ext} = 57$ V μm$^{-1}$) with regard to non-illuminated samples.

## 5. Applications

Several exciting applications relying on the reversible holographic nature of organic PR materials were demonstrated during the last 5 years. In this Section, we review recent publications on several interesting topics, which make use of various different and unique properties of PR holography, together with the possibility of organic materials to be cast into various sizes and thicknesses. These applications are ranging from biomedical imaging to optical computing, image and signal processing, holographic filters and 3D display technology.

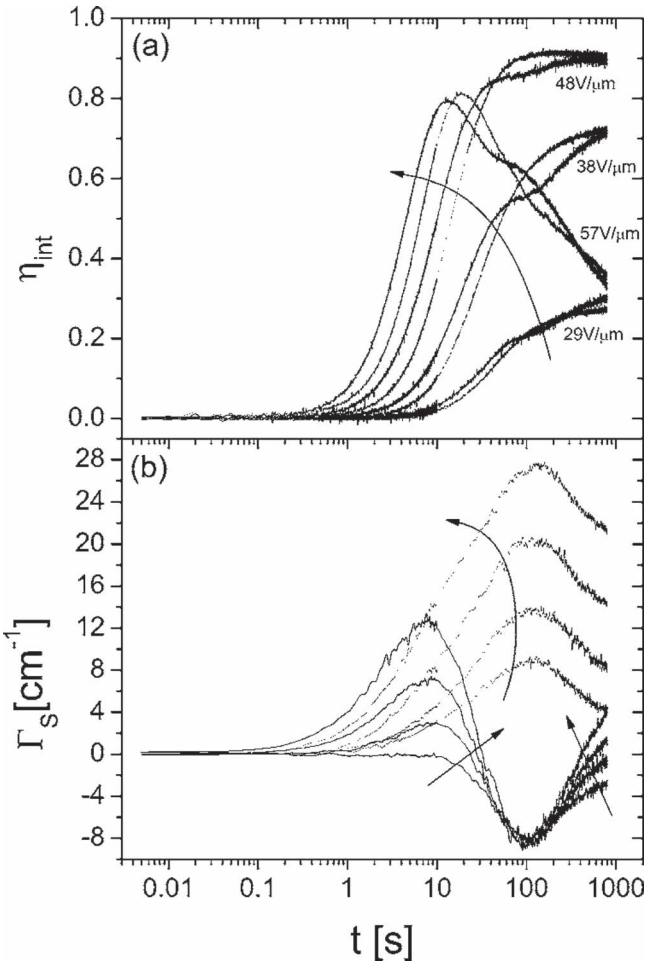


**Figure 19.** Dynamic transients of (a) diffraction efficiency $\eta_{int}$ and (b) gain $\Gamma_S$ of a PVK/DMNPAA/MNPAA/TNFM-material under 830 nm illumination ($I_g$ = 0.6 W cm$^{-2}$) and various applied fields (the arrow points in the direction of increased field strengths). Black curves refer to measurements with supplementary 405 nm illumination ($I$ = 3.9 W cm$^{-2}$), grey curves denote the NIR-illumination only references. Reproduced with permission.[57] Copyright 2007, American Institute of Physics.

### 5.1. Tunable Color Filter Through Surface Plasmon Resonance

A tunable color filter based on surface plasmon polariton (SPP) is demonstrated by Oh et al.[210] A SPP is an electromagnetic mode that can propagate along dielectric-metal interfaces and typically shows strong absorption at resonant wavelengths. This resonance can be tuned by changing the refractive index of the dielectric attached to the metal layer, or by varying the spatial frequency of a coupling grating. The device in Ref. [210] is operated by use of a PR polymer composite in the grating coupling configuration.

The authors added a 50 nm gold layer to the usual 100 μm PR sample (see **Figure 20**), which consisted of the polysiloxane-derivative PSX-Hz sensitized with 1wt.% TNF and the chromophore DB-IP-DC (30wt.%). Gratings were recorded in the PR composite by interfering two 633 nm light-beams, additionally the sample was illuminated by an incoherent p-polarized white light source, reflected light was recorded by a spectrometer. The SPP resonance wavelength was shifted from $\lambda_{SP}$ = 450 nm to $\lambda_{SP}$ = 288 nm by changing the period of the diffraction grating from $\Lambda$ = 0.541 μm to $\Lambda$ = 0.288 μm, respectively. The corresponding complementary color was reflected from the sample and detected, demonstrating the color filtering properties of the device.

### 5.2. Injection Locking of a Broadband Laser Source

The frequency-locking of a broad area laser-diode to a single-line Ti:Sapphire-laser by use of holographic feedback is demonstrated in.[211] The 105 μm NIR-sensitive composite based on the PATPD hole-conductor is used to write a reflection grating by interference of the single-line seed-laser, the spatially and spectrally poor quality broad area laser is incident onto the sample at Brewster's angle. Subsequently, the PR four wave-mixing grating diffracts light from the Ti:Sa into the phase-conjugate beam path of the broad area laser, leading to spectrally selective injection-locking. By this, the authors demonstrated locking of 98% of the broadband laser intensity to the frequency of the seed-laser, while the spatial mode distribution of the broad area laser is stabilized to its self-preferred pattern at this wavelength.

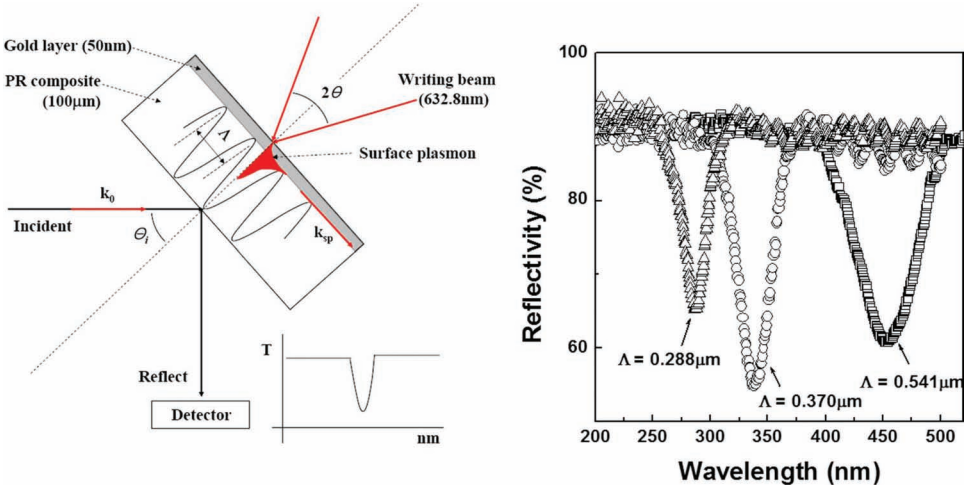


**Figure 20.** Left image: Experimental setup and sample structure. Right image: Reflectivity of the PR/SPP device depending on the grating spacing of the PR grating written in the composite material. Reproduced with permission.[210] Copyright 2009, Optical Society of America.

### 5.3. Dynamic Distortion Correction

Free-space communication systems are attractive for their inherent high information bandwidth, and moreover their speed and security advantages compared to the use of radio-frequency radiation. One necessity for laser-based information distribution systems is the removal of phase-distortions originating from the propagation through aberrating media, e.g. the atmosphere. One process to deal with these distortions is to generate the phase-conjugate beam of the aberrated object beam through the four wave mixing process. Li et al. discuss a simple model:[212] A receiver station sends an information-less beam through the aberrating medium to the sending station, adding distortions to the beam. The sending station phase-modulates the information onto the beam and redirects it to the receiver station by use of a phase-conjugating mirror. Through the characteristic propagation of the phase-conjugated wave, which is basically the time-reversal of the propagation before reflection, non-aberated information can be obtained at the receiver station. For this application, both fast response of the holographic medium and high diffraction efficiencies are key requirements. The authors demonstrated this technique through four wave-mixing in a 105 μm thick PATPD-based composite at 633 nm illumination. The phase-conjugate object-beam is obtained through diffracting the phase-conjugate (simply retro-reflected) reference beam from a grating written in the PR polymer. The authors were able to correct phase-aberations induced by a peri-dish and an oil-filled phase plate (simulating atmosphere-like wave-front disturbance) in the propagation direction of the object beam. Dynamic correction was demonstrated by displacing the phase-plate (equivalent to moving the object itself) by 0.3 mm/s.

A drawback of the setup described above is the fact that the beam has to propagate twice through the distortion. This problem was overcome by adding the read-out to the object beam[213]. This was achieved by tilting of the polarization of the signal beam (polarized perpendicular) to contain a small amount of parallel polarized light (forming the read-beam). The object could thus be recovered without forming the phase-conjugate as the p-polarized light portion simply reads out the grating. The experimental demonstration was performed at 633 nm in a 110 μm PVK:7-DCST:ECZ:$C_{60}$ (49.5:35:15:0.5 wt.%) sample. Dynamic correction of the number "3" of an Air Force test pattern by displacing a phase-aberator up to 0.1 mm/s was successfully demonstrated. Since the response-time of the holographic material is strongly affecting the performance the correcting capabilities of the setup, in this case the dynamic filtering is limited by the inferior dynamic capability of the PVK-based sample with regard to the experiment described above.

Future research in this category will certainly aim to develop fast materials with high diffraction efficiencies at telecommunication bands (O-band: 1260-1360 nm, C-band: 1530-1565 nm).

### 5.4. Image Processing Operations

Organic PR materials are suitable components for optical computing applications, due to the inherent parallel processing capability of the holographic material. A well-known example is the optical correlation of 2-dimensional data sets through the 4-wave mixing process. This is equivalent to the comparison of a set of spatially encoded information pages in a database with an image containing a specific search pattern. A possible application is the personal identification through searches in image databases. In Refs. [85,214], the use of embossed phase masks to encode the information on the beams is anticipated, due to their inherent resistance to counterfeit. Two different correlator layouts are proposed, the matched filter (or vander Lugt) and the Joint Fourier Transform (JFT) architecture. For a comprehensive overview on both working principles, the reader is directed to Ref. [215].

To date, correlators based on organic PR materials were demonstrated in the matched filter[85,216] and JFT,[217] configuration. A setup performing both operations interchangeably is shown in.[218] As discussed in,[215] the implementation of volume holographic materials in the JFT configuration imposes a decrease of the achievable space-bandwidth product due to restrictions from the necessity of obeying the Bragg-condition. Recently, an edge-enhanced shift-invariant matched filter-correlator based on PATPD was demonstrated.[219] Here, shift invariance is given through the low Bragg selectivity (and thus high angular bandwidth) of the very thin (37 μm) PR-device, which nevertheless was shown to exhibit high diffraction efficiencies.[184] Successful correlation of images stored in a static holographic storage material with horizontal and vertical displaced input images were demonstrated.

Another example for the necessity of a thin holographic medium (with respect to PR-crystals) is the demonstration of an image cross-connector,[220] again realized in the PATPD-based composite. Here, reconfigurable connections between multiple input-output images are controlled in a purely optical manner by the four-wave mixing-process. For this application, the rather thin (100 μm) PR-material proofs to be superior over thick (mm) PR crystals with regard to image quality, due to the absence of distortions originating from the overlap of images diffracted from different locations in the thickness of the crystal material.

Finally, purely optical logic operations based on two-wave interactions were demonstrated in a PATPD-based PR-composite at 633 nm illumination.[221] XOR-, OR- and AND-gates were successfully demonstrated in a single optical setup. Logic operations were conducted by trans-illuminating a spatial light modulator (SLM), which first encodes a combination of white ("1") and dark ("0") pixels onto the PR-medium. In a subsequent step, a modulated signal or pump beam is interacting with the previously written grating, depending on the desired output on a CCD-detector. Again, the possibility of the organic material to show high coupling strength in a rather thin medium is a mandatory prerequisite to avoid crosstalk between "1"and "0"-pixels of the corresponding gates.

### 5.5. Holographic Depth-Resolved Imaging

Holography requires the formation of interference fringes through the interaction of at least two coherent light beams and is thus a valuable tool to discriminate coherent from incoherent light. A practicable application is Holographic Optical Coherence Imaging (HOCI), which provides depth resolved images

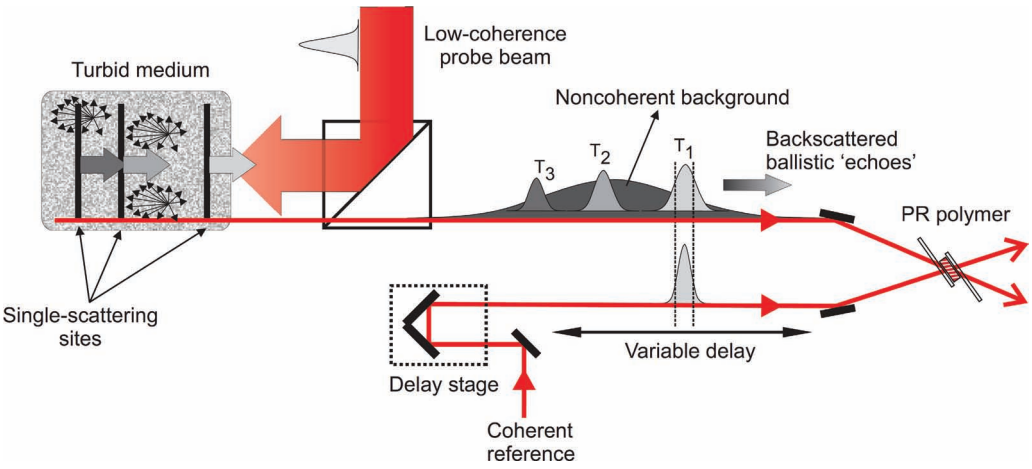


**Figure 21.** Principle of coherence gated imaging through turbid media by HOCI with a photorefractive holographic medium. Reproduced with permission.[69] Copyright 2009, Optical Society of America.

from turbid and highly scattering media by coherence gating. Here, the PR sample serves as a demodulator, discarding the multiply scattered light background from the information carrying coherent, so called ballistic photons of a light beam emerging from the highly scattering medium in question. The ballistic photons form a diffraction grating in the holographic medium by interference with a reference beam. The depth-discrimination of the ballistic photons is accomplished by introducing a delay-line in the reference beam. A sketch to clarify the main working principle is depicted in **Figure 21**.

For non-invasive imaging of biological samples like human tissue, this application requires NIR short-coherence light sources like femto-second lasers, superluminesence diodes (SLD) or swept source tunable lasers of the Littman-type.[222] This is on the one hand due to the transparency-window of biological tissue (roughly 700–900 nm), on the other hand because the effective depth-resolution is determined by the temporal coherence length of the light source. The lateral resolution is given by the optical setup and the recording geometry of the PR device and thus independent of the axial resolution of the system. The hologram formed during the imaging process can be read out in a parallel fashion without requiring any further computation steps, which means that in contrast to optical coherence tomography (OCT) technique, confocal scanning microscopy or HOCI by digital holography,[223] the PR holographic method provides whole-field images in a purely optical manner and in real-time (within the recording speed of the PR medium).

Imaging through scattering media in organic PR materials was first demonstrated in PVK-based systems at 800 nm cw-illumination,[86] followed by 633 nm and 785 nm cw-light[224] and depth resolved operation was performed by a 794 nm SLD.[225] A major drawback of PVK-based systems is the low sensitivity of the PR-material, due to the rather low hole-mobility of the PVK polymer. To meet the stringent requirements on the PR materials sensitivity for *in vivo* imaging purposes, our group recently employed a novel composite system based on the PF6-TPD hole-conductor, sensitized with an optimum concentration of 10 wt.% PCBM.[69,226] Considering identical measurement

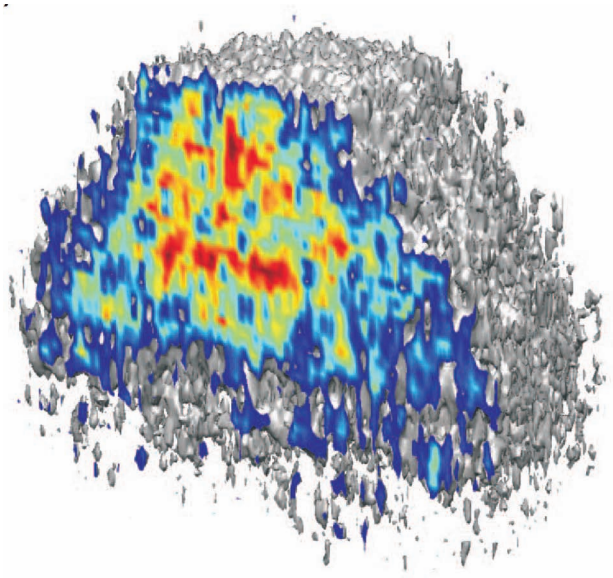

**Figure 22.** Volumetric rendering of data obtained from a 740 µm rat osteogenic sarcoma tumor spheroid. The color coding resembles tissue morphology variations inside the tumor, which are due to necrosis and microcalcification of cells in the tumor center. The resolution obtained is 12 µm and 10 µm for the axial and lateral direction, respectively, with a dynamic range of 20 dB. Reproduced with permission from[69] Copyright 2009, Optical Society of America.

conditions under 830 nm cw-illumination, the PF6-TPD based material reveals a 250-fold faster response (considering time needed to reach 10% internal diffraction efficiency) compared to the well-known PVK/TNFM composition.[69] The high sensitivity of this novel material allowed for depth-resolved imaging of a biodegradable polyurethane foam with 500 ms image acquisition time[226] and a rat osteogenic sarcoma tumor spheroid with a data acquisition speed of $8 \times 10^5$ voxels $s^{-1}$ and a dynamic range of 20 dB[69](see **Figure 22**). Those numbers are comparable to holographic imaging operations performed

on semiconductor PR multiple quantum wells[227] and digital holography.[223]

Of major concern for the use of PR composites as the recording medium for HOCI are limitations imposed by the geometry of the holographic setup. The use of short coherence laser sources imposes the problem of beam walk-off, which describes the reduction of the field of view (FOV) or image resolution, depending on the PR sample to be used in the image or Fourier domain,[69,226] due to the small effective overlap area of the coherent beams in the PR device. The beam walk-off effect occurs in any off-axis configuration (e.g. spatial separation of object and reference beam), whenever the temporal coherence length is smaller than the beam diameter. The effect is thus very pronounced in the strongly tilted transmission setup with large separation angles between the write beams usually employed with PR composites. In depth resolved imaging from biological tissue or more generally volumetric translucent samples, the effect is intrinsically suppressed due to the availability of a distribution of object wavefronts accommodating the reference wave,[69] which is not the case for 3D structures composed of a stack of 2D substructures (for example a cake-shaped reflective object.[228]) Methods to suppress the beam walk-off in organic PPCs include tilting of the object,[69,226] the introduction of a demagnifying optical system in order to fit the complete image size into the effective interaction region of the write-beams in the composite material (which implies $d_{WB} = l_c$),[228] or to adopt a reflection geometry of counter-propagating object and reference waves in contrast to the usually employed transmission geometry.[228] However, despite some promising results of high performance acquired in reflection geometry,[124,203] the transition from transmission to reflection geometry is usually accompanied by a detrimental drop in material sensitivity (see Section 4.1).

### 5.6. Updateable 3D Holographic Display

One of the most striking and well-known abilities of holography is to record and display full parallax 3-dimensional images. Holographic displays are thus regarded as highly anticipated connections between digital data-sets acquired from 3 dimensional objects (e.g. scientific or medical data obtained by tomography, magnetic resonance, confocal imaging etc.) and natural perception by human vision without the need for special eyewear. Generally, all PR materials are principally capable of displaying dynamically refreshed 3-dimensional data sets, but PR crystals are usually hard to grow beyond some cubic centimeters, which render them inappropriate for display applications. PR composites in turn are easily prepared into various forms and sizes through established polymer preparation, for example techniques like injection molding.[229] Recently, Tay et al.[96] demonstrated an impressive 100 $cm^2$ updatable 3-dimensional holographic display. They were able to record a monochrome, horizontal parallax-only holographic image within 2–4 minutes onto the display, which was stable against dark decay (no coherent illumination incident on the display) for around 3 hours. The PR material in this study was based on the copolymer PATPD-CAAN (50 wt.%), with the plasticizer ECZ (20 wt.%) and the fluorinated dicyanostyrene chromophore FDCST (30 wt.%). A critical factor for display applications, apart from durability and high diffraction efficiency, is the ratio between hologram-write time and dark decay, which is usually unfavorable since both are roughly equal. The authors solved this problem by employing the "voltage kick-off" procedure.[96,230] The hologram is written at high applied field-strengths (90 V $\mu m^{-1}$), to take advantage of high charge-generation rates and fast response time, then switching to lower fields (40 V $\mu m^{-1}$), which corresponds to the steady-state maximum of diffraction efficiency and offers significantly reduced dark decay rates. The images on the display were produced by holographic stereography, by writing computer generated perspective slices (denoted as holographic pixels, or hogel in short form) by transillumination of a spatial light modulator in Fourier transform geometry onto the display. This technique is inherently applicable to display data from tomographic imaging systems. Total recording time per hogel was set between 0.5 and 2 seconds of 0.1W $cm^{-2}$ 532 nm illumination, resulting in a total write time of 1-4 min at 9 kV for a horizontal parallax only $10 \times 10$ $cm^2$ display. To display the content, the applied field was reduced to 4 kV and the composite was illuminated by a red LED or an expanded low power HeNe-laser. The information on the display was stable for 3 h or erasable by homogeneous 532 nm- illumination within 120 s. **Figure 23** depicts several 3D images, demonstrating the capabilities of the described display.

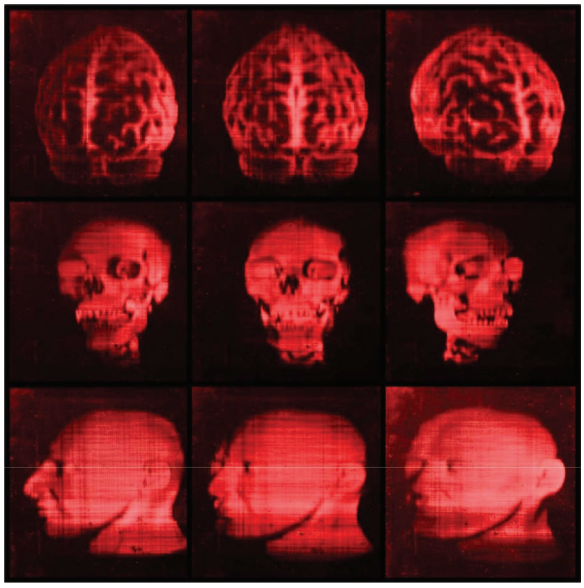

**Figure 23.** Images displayed by the photorefractive, 3D updatable holographic display. Reproduced with permission.[230] Copyright 2008, IEEE.

In a subsequent publication,[231] the same group enhanced the capabilities of the display (without changes to the photorefractive material) by employing a pulsed laser source (6 ns pulses, 50 Hz repetition rate) in order to reduce the complete recording time of a 100 $cm^2$ display with 1 mm hogel resolution to 2 s. Full parallax operation was demonstrated by spatially multiplexing of the recording beams by a holographic optical element lens array. Multi-color representation of display content was achieved by recording up to three angular multiplexed holograms, which are independently reconstructed by colored

LEDs. The quasi real-time operation of the display due to the improved recording conditions allowed for the demonstration of a holographic telepresence system.

For quasi real-time update of the display, previously inscribed information is simply over-written by new holograms. Some applications, however, may demand the stability of the information without continuous refreshing (through subsequent recording processes) of the hologram. A possible route to fixing of the PR grating and thus the information of the holographic display is demonstrated in Ref. [232]. Here, a high-$T_g$ PR material based on a multifunctional TPD/Cz/DCST copolymer is locally heated above $T_g$ by illumination with a $CO_2$-Laser for writing of the grating. After subsequent thermal relaxation, the orientation of the chromophores is "frozen" in the polymer matrix. The author presented optimizations regarding glass-substrate thickness and heating-laser exposure through solving heat transfer equations. Thermal fixing of gratings with an efficiency of 80% over 20 minutes (writing time 2 minutes with 7 s of heating by $CO_2$- Laser) was demonstrated.

## 6. Conclusions

In conclusion, remarkable progress has been achieved in the field of organic PR materials, which manifests itself in the demonstration of efficient new materials and impressive applications based on them. Several aspects of research are responsible for the performance enhancements of the materials in the course of recent years.

On the one hand, the broad understanding of the underlying physical phenomena, which are deduced from a wide array of holographic and secondary measurements, helped to gain insight into the photoconductive and electro-optic response of the materials. Still, this does not allow for prediction of the materials behavior in general, due to the complex interaction of the blend components in the amorphous material.

On the other hand, efforts in synthetic chemistry, material, and nanoparticle research led to the demonstration of a wide array of materials with unprecedented properties and performance. Since the electro-optic characteristics of the materials are understood quite well in terms of structure-property relationships, currently the photoconductive properties of the materials are identified as the main driver for further performance enhancements. Indicators of this trend are furthermore the deliberate utilization of materials from other branches of organic electronics in PR materials.

Organic PRs offer advantages over their inorganic counterparts in terms of cost, processability and the possibility to customize the material with regard to the desired application. The extensive research on material combinations and dopants thus allows for almost independent tuneability of specific material requirements, which cannot, due to the dependency on various material parameters, be optimized altogether in a single blend.

Much attention was recently devoted to fabricate materials with enhanced shelf lifetime by increased compatibility of the blend ingredients or the preparation of PR multifunctional materials and glasses. Moreover, the reduction of photoconductive fatigue caused by filling of deep trapping centers under pro-longed exposure to illumination was circumvented by adjusting the respective redox potentials of the components. Lifetimes of over a year and 1.6 million repeated write-erase cycles under working conditions were demonstrated, which, together with the low price of a typical PR sample, brings the materials close to requirements of commercial demand.

On the contrary, unlike other fields of organic electronics (e.g. OLEDs), organic PR materials are still not found in any commercialized product. Organic PR materials still present some drawbacks, which hinder the integration of the materials in photonic products. The most severe problem is the necessity for the application of strong applied dc-fields and thus the prevalent risk of dielectric failure of the sample. Although some efficient materials reduce the amplitude of the applied field to reach high diffraction efficiency through the utilization of high FOM chromophores or liquid crystals, still the response of the materials at low fields are inferior to demand. Hence, currently the only commercial aspect is the material itself (some material composite formulations are on the market for research purposes). It should be pointed out here, that this statement is also valid for inorganic PR crystals.

For some of the discussed applications in this review, fast computer-based setups and the tremendous progress in CCD, CMOS and SLM technology, backed by a steady efficiency enhancement mainly driven by the consumer market, offer efficient alternative routes for data processing, information gathering and display. Research interest in digital holography and computer generated holography has, thus, increased significantly during the last years. Nevertheless, the inherent parallel nature of optical recording and reconstruction from PR holographic media still holds promise for real-time applications with high bandwidth requirements.

### 6.1. Quo Vadis?

As indicated above, the research interest in the photoconductive properties of organic photorefractives is mainly driven by the necessity to create faster and thus more sensitive materials. Although materials with video-rate compatible response times (several ms) exist and the recent demonstration of pulsed writing operation, which led to fast time constants for grating build-up of only 300 μs, still dynamic performance needs to be enhanced to compete with alternative processes. Furthermore, research will definitely aim to enhance the performance of organic photorefractives especially at NIR wavelengths, which are required for applications based on telecommunication signals (1300 nm–1550 nm).

## 7. Experimental Techniques and Measurements

In this Section, we will describe techniques for measuring the refractive index grating formed through the PR effect, and discuss influences of external parameters on the performance of the material under field and time-dependent measurements.

### 7.1. Device Preparation

The most common preparation procedure for organic PR devices is the "melt-pressing"-technique. In the case of material blends,

the components in appropriate weight ratios are dissolved, the mixture cast on glass plates and heated to allow for evaporation of the solvent. Composite materials often are further homogenized by repeated melting-cooling cycles. The material is then placed between two facing ITO electrodes on glass substrates, heated until softening and finally pressed to the desired thickness, which is ensured by spacer materials (silica beads etc.). In Ref. [233], an additional 10 nm $SiO_2$-blocking layer was introduced between PR-material and ITO-coating to lower dark- and photocurrent-flow through the sample. The melt-pressing procedure is generally limited to materials with a suitable viscosity for preparation at temperatures below sublimation of some of the components or thermal damage. Moreover, the preparation of large-area samples proves to be complicated. A more suitable method for plasticized materials is injection molding.[229]

Typical device thicknesses d range between 30 µm and 200 µm.[13] As a general trade-off, the thickness hereby couples the interaction length of the beams in the material with the absolute value of the external applied field. A method to circumvent this restriction is the use of stratified media [88, 234], or to guide the beam in the polymer film.[235]

### 7.2. Holographic Wave-Mixing

#### 7.2.1. Holographic Thickness

The diffractive properties of the refractive index change formed in the PR material are evaluated by holographic wave-mixing experiments. A critical factor is the Q-factor of the material, which categorizes the holographic medium as thin ($Q < 1$, Raman-Nath regime, angle-independent formation of several diffraction orders) or thick ($Q >> 1$, Bragg regime). $Q$ is given by

$$Q = \frac{2\pi\lambda d}{\Lambda^2} \tag{2}$$

and thus depends on the laser wavelength $\lambda$, thickness of the material d, and through the grating spacing $\Lambda$ on the geometry of the setup ($\Lambda = \lambda/(2n \sin(\theta))$, with n the refractive index of the material and $2\theta$ the inter-beam angle). We restrict the discussion here to thick materials (volume holograms), for which the Bragg-condition is valid and only a single diffraction order is relevant for the description of the material performance. The thickness of the medium d relative to the grating spacing $\Lambda$ also determines the extent of the Bragg-condition. The angular selectivity of the grating is approx given by $\Delta\theta = \Lambda/2d$.[203]

#### 7.2.2. Geometry

**Figure 24** depicts a sketch of a typical wave-mixing setup. The z-axis corresponds to the direction of the applied dc-field. In the case that both write-beams illuminate the material from the same direction relative to the sample (depicted in Figure 24), a transmission grating ($\cos\theta_1\cos\theta_2 >$) is formed in the material. Reflection gratings ($\cos\theta_1\cos\theta_2 < 0$) are formed with beams illuminating the sample from opposite sides. A typical feature for transmission gratings in organic PR media is the tilt angle $\Psi$, which is the angle formed by the bisecting line of the write-beams and the z-axis. This tilt provides a component of the

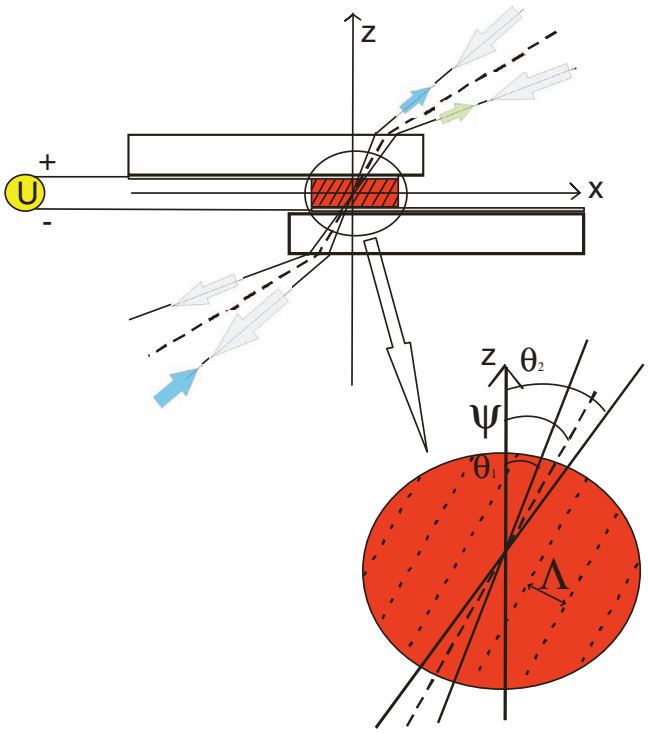


**Figure 24.** Setup and geometric parameters of a typical transmission geometry wave-mixing experiment, open arrows indicate the write-beams with internal angles $\theta_1$ and $\theta_2$ inside the material with respect to the field direction z, blue the read-beam with a transmitted (blue) and diffracted (green) portion. The color-coding does not imply a wavelength statement. $\Psi$ denotes the tilt of the inter-beam angle (dashed line).

applied electric-field along the grating wave-vector, which allows the mobile charges to migrate from the bright to the dark regions of the interference pattern. Moreover, for a symmetric configuration ($\theta_1 = -\theta_2$), the effective electro-optic coefficient $r_{eff}$ is zero.

The dependence of the PR medium on changes of the geometry is discussed in Section 4.1.

#### 7.2.3. Two-Beam Coupling

As outlined above, the propagation of the beams writing the grating is affected by the phase-shift between the interference pattern and the index grating formed due to the PR effect. Since both beams are automatically Bragg-matched to the grating, a component of each beam diffracts in the direction of the other beam. Due to the phase-shift $\varphi$, for one of the write-beams the superposition with the diffracted component is constructively, for the other beam destructively, which results in an energy transfer from one beam to the other. The quantitative measure of this two-beam coupling (2BC) effect is the gain coefficient $\Gamma$ and given by

$$\Gamma = \left[\ln\left(I_1/I_{1,0}\right)\cos\theta_1 - \ln\left(I_2/I_{2,0}\right)\cos\theta_2\right] d^{-1} = \frac{2\pi}{m\lambda}\Delta n \sin\varphi \tag{3}$$

$m = 2(I_1 I_2)^{0.5}/(I_1 + I_2)$ denotes the holographic contrast, $I_1$ and $I_2$ describe the intensity of the write-beams within the material,

the subscript 0 refers to the intensity at zero applied field. The direction of the gain and thus the sign of $\Gamma$ depend on the polarization of the write-beams and the direction of the applied electric field, which moreover allows for the determination of the sign of the majority carrier. Due to the asymmetry of the employed chromophores in the material and thus the birefringence of the poled polymer composite, the magnitude of the gain coefficients differ significantly for s and p-polarizations of the write-beams. For applications based on gain-derived amplification of a write-beam, gain values have to be corrected for absorption losses in the composite. The net gain is thus given by $\Gamma_{net} = \Gamma - \alpha$. For applications relying on amplification of one beam, the product of net gain and interaction length is of further relevance.

Due to the necessity of a phase-shift to obtain asymmetric energy transfer between the write-beams, the gain was usually treated as an unambiguous fingerprint of the PR effect. Recently however, huge gain-values were found for a non-PR sol-gel material due to photoinduced isomerization of azo-chromophores.[236]

### 7.2.4. Four-Wave Mixing

The four-wave mixing process (4WM) relies on diffracting a Bragg-matched read-beam off the grating formed by the interaction of the write-beams. In most cases, the read-beam is of the same wavelength (degenerate 4WM) and thus counter propagates one of the write-beams (since the material is birefringent, this is true for the same polarizations of WBs and RB, only). The intensity of the read-beam is usually strongly (roughly a factor 100) reduced in intensity to allow for quasi non-destructive read-out of the index grating. The internal diffraction efficiency $\eta_{int}$ is defined as the ratio between the diffracted $I_d$ intensity and the transmitted $I_t$ read-beam intensity:

$$\eta_{int} = \frac{I_d}{I_d + I_t} \quad (4)$$

The external diffraction efficiency $\eta_{ext} = \exp(-\alpha * d/\cos\Psi)\eta_{int}$ accounts for absorption losses $\alpha$ of the sample. The coupled wave equations[237] relate the diffraction efficiency to the refractive index modulation. For transmission gratings, $\eta \sim \sin^2(\Delta n\, C)$, $C$ being a constant containing geometrical parameters and the laser wavelength.

### 7.2.5. Evaluation of Wave-Mixing Processes and Underlying Physical Phenomena

**Figure 25** displays typical field- and time-dependent 4WM and field-dependent 2BC data. To compare the holographic performance of the materials, usually the respective values at a certain applied field are given in publications. For the diffraction efficiency in the case of transmission-type gratings, often the point of over-modulation ($E_{max}$) is taken as means for comparing different materials, the lower the applied field strength at over-modulation, the better the material. Please note, that a direct comparison between materials characterized by different research groups is often difficult, due to different setup parameters employed, as geometry, film thickness, beam intensities etc. The concurrent measurement of field-dependent diffraction efficiency and gain coefficients allows for a direct calculation of the phase-shift.

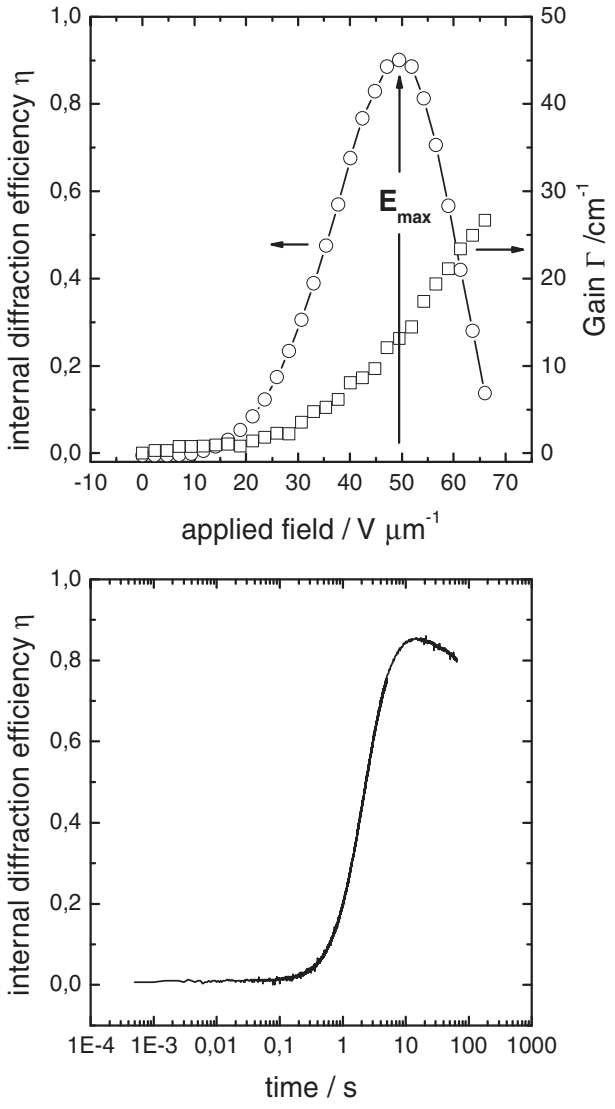


**Figure 25.** Experimental data of field dependent 4WM (circles) and 2BC (squares) (a) and time dependent 4WM (b) data. Measurements were conducted on a PVK/DMNPAA/MNPAA/TNFM material[57] under 830 nm illumination, 0.64 W cm$^{-2}$ irradiance. Response time was measured at 56.6 V µm$^{-1}$ applied field.

There are several means of quantifing the dynamic behavior of the materials reported in the literature. The transients (diffraction efficiency or the calculated dynamic index modulation) are either quantified by exponential fitting procedures (bi-exponential or stretched exponential fits[238]) or by extracting time-values at certain diffraction efficiency conditions (e.g., $\tau_{50}$, time to reach 50% of the steady-state diffraction efficiency). Please note that the quality of the fitting procedure might depend on the respective speed-limiting mechanism in the composite, e.g. the photoconductivity (charge generation or

**Table 5.** Overview on measurement techniques to probe physical quantities with regard to PR behavior.

| quantity | technique |
|---|---|
| chromophore orientation/amplitude of space-charge field | PR-ellipsometry[239–242] |
| glass-transition temperature | differential scanning calorimetry, photoconductivity[243] |
| charge-carrier mobility | time-of-flight,[22,206] holographic time-of-flight,[205–207] photo-electromotive force,[34] dc-photoconductivity[28,29] |
| photoelectric parameters relevant to the PR effect | photo-electromotive force (charge carrier lifetime, dielectric relaxation time, diffusion length, primary charge carrier generation efficiency),[34] pulsed photoconductivity (recombination and trapping coefficients),[28] spectroscopy (trap density)[98] |
| charge generation efficiency | xerographic discharge,[22,242] dc-photoconductivity[29] |
| phase-shift | moving-grating technique,[244,245] direct calculation from $\Delta n/\Gamma$[158] |
| dispersion of $\Delta n$ | interferometry[246] |

transport) and the orientational mobility of the chromophore. Whenever we have stated response times, we provided the information about the respective quantification procedure.

Several secondary measurements are described in the literature to further probe PR gratings and their underlying photo-physical processes. **Table 5** provides an overview over the respective techniques.

## Appendix

### Glossary

| | |
|---|---|
| 2BC | two-beam coupling |
| 4WM | four-wave mixing |
| CCD | charge-coupled device |
| CMOS | complementary metal-oxide semiconductor |
| CNT | carbon nanotubes |
| CTA | charge-transport agent |
| cw | continuous wave |
| EMF | electromotive force |
| EO | electro-optic |
| EOAM | electro-optical absorption measurement |
| FOM | figure-of-merit |
| FOV | field-of-view |
| HOCI | holographic optical coherence imaging |
| HOMO | highest occupied molecular orbital |
| HTOF | holographic time-of-flight |
| LC | liquid crystal |
| JFT | joint Fourier transform |
| LMW | low-molecular weight |
| LUMO | lowest unoccupied molecular orbital |
| MC | Monte-Carlo (simulation) |
| MQW | multiple quantum wells |
| NIR | near infrared |
| NLO | nonlinear optic |
| OCT | optical coherence tomography |
| OEM | orientational enhancement mechanism |
| OFET | organic field effect transistor |
| OLED | organic light emitting diode |
| OPV | organic photovoltaic devices |
| PCE | power conversion efficiency |
| PDLC | polymer-dispersed liquid crystals |
| PL | photoluminescence |
| PPC | photorefractive polymer composite |
| PR | photorefractive |
| QD | quantum dots |
| SLD | superluminesence diode |
| SLM | spatial light modulator |
| SPP | surface plasmon polariton |
| TOF | time-of-flight |
| TPA | two-photon absorption |

### Chemical Structures

| | |
|---|---|
| 2BNCM | *N*-2-butyl-2,6-dimethyl-4*H*-pyridone-4-ylidenecyanomethylacetate |
| 7DCST | 4-homopiperidino-benzylidenemalononitrile |
| 8OCB | 8-pertyloxy-4′-cyanobiphenyl |
| $Alq_3$ | tris(8-hydroxyquinoline) |
| AODCST | 2-[4-bis(2-methoxyethyl)amino]benzylidenemalononitrile |
| ATOP | aminothienyldioxocyanopyridine (ATOP1: 1-alkyl-5-[2-(5-dialkylaminothienyl)methyl-ene]-4-alkyl-[2,6-dioxo-1,2,5,6-tetrahydropyridine]-3-carbonitrile) |
| BBP | butyl-benzylphthalate |
| BQ | *p*-benzoquinone |
| $Cl_2Q$ | 2,5-dichloro-*p*-benzoquinone |
| Chloranil | 2,3,5,6-tetrachloro-*p*-benzoquinone |
| COANP | 2-cyclooctylamino-5-nitropyridine |
| DANS | 4-(*N*,*N*-dimethylamino)-4′-nitrostilbene |
| DAST | 4-*N*,*N*-diethylamino-4′-*N*′-methyl-stylbazolium toluene-*p*-sulfonate |
| DBM | 2-[2-{5-[4-(di-*n*-butylamino)phenyl]-2,4-pentadienylidene}-1,1-dioxido-1-benzothien-3(2*H*)-ylidene]malononitrile |
| DBDC | 3-(*N*,*N*-di-*n*-butylaniline-4-yl)-1-dicyanomethylidene-2-cyclohexene |
| DB-IP-DC | 2-{3-[(*E*)-2-(dibutylamino)-1-ethenyl]-5,5-dimethyl-2-cyclohexenylidene}-malononitrile |
| DDQ | 2,3-dichloro-5,6-dicyano-*p*-benzoquinone |
| DEANST | 4-I(*N*,*N*-diethylamino)-*β*-nitrostyrene |
| DEH | 4-(diethylamino)benzaldehyde diphenylhydrazone |
| DHADC-MPN | 2-*N*,*N*-dihexylamino-7-dicyanomethylidenyl-3,4,5,6,10-pentahydronaphthalene |
| DMNPAA | 2,5-dimethyl-4-*p*-nitrophenylazoanisole |
| DOP | dioctylphthalate |

| | |
|---|---|
| DPP | diphenylphthalate |
| ECYENPA | (9-ethyl-9*H*-carbazol-3-ylmethylent)-(4-nitrophenyl)-amine |
| EHDNPB | 1-(2-Ethylhexyloxy)-2,5-dimethyl-4-(4-nitrophenylazo)benzene |
| EPNA | *N*,*N*-diethyl-para-nitroaniline |
| FDEANST | 3-fluoro-4-*N*,*N*-diethylamino-$\beta$-nitrostyrene |
| HDA | 1-hexadecylamine |
| IDOP | 1-alkyl-5-[2-(1,3-dihydro-1-alkyl-3,3-dimethyl-[2H] indol-2-ylidene)ethylidene]-4-alkyl-2,6-dioxo-1,2,5,6-tetrahydropyridine-3-carbonitrile |
| MDCETPD | *N*-(4-[2,2-dicyanoethenyl]phenyl)-*N*′-phenyl-*N*,*N*′-bis(4-methylphenyl)-[1,1′-biphenyl]-4,4′-diamine |
| MNBA | 4-nitrobenzylidene-3-acetamino-4-methoxyaniline |
| MNPAA | 3-methoxy-4-*p*-nitrophenylazoanisole |
| MQ | 2,6-dimethyl-*p*-benzoquinone |
| NPP | *N*-(4-nitrophenyl)-(s)-prolinol |
| PATPD | poly(acrylic tetraphenyldiaminobiphenol) |
| PCBM | phenyl-$C_{61}$-butyric acid methyl ester |
| PF6-TPD | poly(*N*,*N*′-bis(4-hexylphenyl)-N'-(4-(9-phenyl-9H-fluoren-9-yl) phenyl)-4,4′-benzidine) |
| PSX | poly[methyl-3-(9-carbazolyl)propylsiloxane] |
| PVDMI | poly-*N*-vinyl-2,3-dimethylindole |
| PVK(PVCz) | poly-(*N*-vinylcarbazole) |
| PVI | poly-N-vinylindole |
| py | pyridine |
| SiPc | bis(*p*-methylbenzoate)(2,9,16,23-tetra-*tert*-butyl-phthalocyaninato)silicon |
| TOPO | tri-*n*-octylphosphine oxide |
| TeNFM | 2,4,5,7-tetranitro-9H-fluorine-9yilden-malonitrile |
| TFB | poly-(9,9'-dioctylfluorene-co-*N*-4-(butylphenyl)-diphenylamine) |
| TNF | 2,4,7-trinitrofluorenone |
| TNFM (TNFDM) | (2,4,7-trinitro-9-fluorenyl-idene)-malononitrile |
| TCNQ | 7,7,8,8-tetracyanoquinodimethane |
| TCNE | tetracyanoethylene |
| TPBAH | tri-(4-bromphenyl)-aminium hexachloroantimonate |
| ZnPc | (2,9,16,23-tetra-*tert*-butyl-phthalocyaninato)zinc |

## Acknowledgements

Funding was provided by the Deutsche Forschungsgemeinschaft (DFG), Volkswagen Foundation and the German ministry of science and education (BMBF). The authors would like to express their sincere gratitude to all collaborators and alumni (PhDs and student workers) involved in the research on photorefractive materials in our workgroup. The authors moreover thank Dr. Anne Köhnen (University of Cologne) for careful revision of the manuscript.

Received: February 3, 2011
Published online: September 13, 2011

[1] A. Ashkin, G. D. Boyd, J. M. Dziedic, R. G. Smith, A. A. Ballmann, H. J. Levinstein, K. Nassau, *Appl. Phys. Lett.* **1966**, *9*, 72–74.
[2] S. Ducharme, J. C. Scott, R. J. Twieg, W. E. Moerner, *Phys. Rev. Lett.* **1991**, *66*, 1846–1849.
[3] J. Thomas, R. A. Norwood, N. Peyghambarian, *J. Mater. Chem.* **2009**, *19*, 7476–7489.
[4] O. Ostroverkhova, W. E. Moerner, *Chem. Rev.* **2004**, *104*, 3267–3314.
[5] Y. Zhang, R. Burzynski, S. Ghosal, M. K. Casstevens, *Adv. Mater.* **1996**, *8*, 111–125.
[6] W. E. Moerner, A. Grunnet-Jepsen, C. L. Thompson, *Ann. Rev. Mater. Sci.* **1997**, *27*, 585–623.
[7] B. Kippelen, N. Peyghambarian, *Adv. Polym. Sci.* **2003**, *161*, 87–156.
[8] S. J. Zilker, *ChemPhysChem* **2000**, *1*, 72–87.
[9] T. Sasaki, *Polym. J.* **2005**, *37*, 797–812.
[10] Q. Wang, L. Wang, L. Yu, *Macromol. Rapid Commun.* **2000**, *21*, 723–745.
[11] B. Kippelen, K. Meerholz, N. Peyghambarian, in *Nonlinear Optics Of Organic Molecules and Polymers* (Eds: H. S. Nalwa, S. Miyata), CRC Press **1997**.
[12] K. Meerholz, B. Kippelen, N. Peyghambarian, in *Photonic Polymer Systems* (Eds: D. L. Wise, G. E. Wnek, D. J. Trantolo, T. M. Cooper, J. D. Gresser), Marcel Dekker **1998**.
[13] R. Bittner, K. Meerholz, in *Photorefractive Materials and Their Applications II: Materials* (Eds: P. Günter, J.-P. Huignard), *Springer Series In Optical Science*, Vol. *114*, Springer, Berlin **2006**, 419–486.
[14] B. Kippelen, in *Photorefractive Materials and Their Applications II: Materials* (Eds: P. Günter, J. P. Huignard), *Springer Series In Optical Science*, Vol. *114*, Springer, Berlin **2006**, 487–534.
[15] G. Montemezzani, C. Medrano, M. Zgonik, P. Günter, in *Nonlinear Optical Effects and Materials* (Ed: P. Günter), *Springer Series In Optical Sciences*, Vol. *72*, Springer, Berlin **2000**, 301–373.
[16] F. Simoni, L. Lucchetti, in *Photorefractive Materials and Their Applications* (Eds: P. Günter, J. P. Huignard), *Springer Series In Optical Science*, Vol. *114*, Springer, Berlin **2006**, 571–603.
[17] W. E. Moerner, S. M. Silence, F. Hache, G. C. Bjorklund, *J. Opt. Soc. Am. B* **1994**, *11*, 320–330.
[18] D. Hertel, H. Bässler, *ChemPhysChem* **2008**, *9*, 666–688.
[19] N. Tessler, Y. Preezant, N. Rappaport, Y. Roichman, *Adv. Mater.* **2009**, *21*, 1–21.
[20] V. Coropceanu, J. Cornil, D. A. da Silva Filho, Y. Olivier, R. Silbey, J.-L. Brédas, *Chem. Rev.* **2007**, *107*, 926–952.
[21] H. Bässler, *Physica Status Solidi (b)* **1993**, *175*, 15–56.
[22] O. Ostroverkhova, K. D. Singer, *J. Appl. Phys.* **2002**, *92*, 1727–1743.
[23] J. S. Schildkraut, Y. Cui, *J. Appl. Phys.* **1992**, *72*, 5055–5060.
[24] J. S. Schildkraut, A. V. Buettner, *J. Appl. Phys.* **1992**, *72*, 1888–1893.
[25] N. V. Kukhtarev, V. B. Markov, S. G. Odulov, M. S. Soskin, V. L. Vinetskii, *Ferroelectrics* **1979**, *22*, 949–960.
[26] B. Yuan, X. Sun, C. Hou, Y. Li, Z. Zhou, Y. Jiang, C. Li, *J. Appl. Phys.* **2000**, *88*, 5562–5569.
[27] Y. Cui, B. Swedek, N. Cheng, J. Zieba, P. N. Prasad, *J. Appl. Phys.* **1999**, *85*, 38–43.
[28] L. Kulikovsky, D. Neher, E. Mecher, K. Meerholz, H.-H. Hörhold, O. Ostroverkhova, *Phys. Rev. B* **2004**, *69*, 125216.
[29] E. Hendrickx, Y. Zhang, K. B. Ferrio, J. A. Herlocker, J. Anderson, N. R. Armstrong, E. A. Mash, A. P. Persoons, N. Peyghambarian, B. Kippelen, *J. Mater. Chem.* **1999**, *9*, 2251–2258.
[30] J.-W. Oh, C. Lee, N. Kim, *J. Chem. Phys.* **2009**, *130*, 134909.
[31] C. Lee, M. Yang, N.-S. Lee, N. Kim, *Chem. Phys. Lett.* **2006**, *418*, 54–58.
[32] C. Lee, S. Park, M. Yang, N. Lee, N. Kim, *Chem. Phys. Lett.* **2006**, *422*, 106–110.
[33] M. Samiullah, *J. Appl. Phys.* **2010**, *107*, 113525.
[34] M. C. Gather, S. Mansurova, K. Meerholz, *Phys. Rev. B* **2007**, *75*, 165203.
[35] S. Mansurova, S. Stepanov, V. Camacho-Pernas, R. Ramos-Garcia, F. Gallego-Gómez, E. Mecher, K. Meerholz, *Phys. Rev. B* **2004**, *69*, 193203.
[36] M. B. Klein, in *Photorefractive Materials and Their Applications II: Materials* (Eds: P. Günter, J. P. Huignard), *Springer Series In Optical Science*, Vol. *114*, Springer, Berlin **2006**, 241–284.
[37] M. Zgonik, M. Ewart, C. Medrano, P. Günter, in *Photorefractive Materials and Their Applications II: Materials* (Eds: P. Günter,

J. P. Huignard), *Springer Series In Optical Science*, Vol. *114*, Springer, Berlin **2006**, 205–235.
[38] K. Buse, J. Imbrock, E. Krätzig, K. Peithmann, in *Photorefractive Materials and Their Applications II: Materials* (Eds: P. Günter, J. P. Huignard), *Springer Series In Optical Science*, Vol. *114*, Springer, Berlin **2006**, 83–121.
[39] H. Hatano, Y. Liu, K. Kitamura, in *Photorefractive Materials and Their Applications II: Materials* (Eds: P. Günter, J.P. Huignard), *Springer Series In Optical Science*, Vol. *114*, Springer, Berlin **2006**, 127–159.
[40] A. A. Grabar, M. Jazbinšek, A. N. Shumelyuk, Y. M. Vysochanskii, G. Montemezzani, P. Günter, in *Photorefractive Materials and Their Applications II: Materials* (Eds: P. Günter, J. P. Huignard), *Springer Series In Optical Science*, Vol. *114*, Springer, Berlin **2006**, 327–362.
[41] M. Cronin-Golomb, M. B. Klein, in *Handbook Of Optics*, Vol. *II*, 2nd Ed. (Ed: M. Bass), Mcgraw-hill, New York **1994**, Ch. 39.
[42] K. Shcherbin, in *Photorefractive Materials and Their Applications II: Materials* (Eds: P. Günter, J. P. Huignard), *Springer Series In Optical Science*, Vol. *114*, Springer, Berlin **2006**, 391–414.
[43] D. D. Nolte, *J. Appl. Phys.* **1999**, *85*, 6259–6289.
[44] D. D. Nolte, S. Iwamoto, K. Kuroda, in *Photorefractive Materials and Their Applications II: Materials* (Eds: P. Günter, J. P. Huignard), *Springer Series In Optical Science*, Vol. *114*, Springer, Berlin **2006**, 363–370.
[45] M. Eralp, J. Thomas, S. Tay, G. Li, A. Schülzgen, R. A. Norwood, M. Yamamoto, N. Peyghambarian, *Appl. Phys. Lett.* **2006**, *89*, 114105.
[46] D. Wright, M. A. Díaz-García, J. D. Casperson, M. DeClue, W. E. Moerner, R. J. Twieg, *Appl. Phys. Lett.* **1998**, *73*, 1490–1492.
[47] S. Köber, F. Gallego-Gómez, M. Salvador, F. B. Kooistra, J. C. Hummelen, K. Aleman, S. Mansurova, K. Meerholz, *J. Mater. Chem.* **2010**, *20*, 6170–6175.
[48] R. Jones, S. C. W. Hyde, M. J. Lynn, N. P. Barry, J. C. Dainty, P. M. W. French, K. M. Kwolek, D. D. Nolte, M. R. Melloch, *Appl. Phys. Lett.* **1996**, *69*, 1837–1839.
[49] K. Jeong, L. Peng, D. D. Nolte, M. R. Melloch, *Appl. Opt.* **2004**, *43*, 3802–3811.
[50] M. Talarico, A. Golemme, *Nat. Mater.* **2006**, *5*, 185–188.
[51] D. Gong, Z. Zhou, Q. Meng, C. Hou, *Optics and Lasers In Engineering* **2007**, *45*, 170–174.
[52] M. Talarico, R. Termine, A. Golemme, *Appl. Phys. Lett.* **2007**, *91*, 081110.
[53] C. W. Christenson, J. Thomas, P.-A. Blanche, R. Voorakaranam, R. A. Norwood, M. Yamamoto, N. Peyghambarian, *Opt. Express* **2010**, *18*, 9358–9365.
[54] S. Köber, J. Prauzner, M. Salvador, F. B. Kooistra, J. C. Hummelen, K. Meerholz, *Adv. Mater.* **2010**, *22*, 1383–1386.
[55] J. Schelter, G. F. Mielke, A. Köhnen, J. Wies, S. Köber, O. Nuyken, K. Meerholz, *Macromol. Rapid Commun.* **2010**, *31*, 1560–1567.
[56] N. M. Kronenberg, M. Deppisch, F. Würthner, H. W. A. Lademann, K. Deing, K. Meerholz, *Chem. Commun.* **2008**, 6489–6491.
[57] M. Salvador, F. Gallego-Gómez, S. Köber, K. Meerholz, *Appl. Phys. Lett.* **2007**, *90*, 154102.
[58] L. Wang, M.-K. Ng, L. Yu, *Phys. Rev.B* **2000**, *62*, 4973–4984.
[59] W. You, S. Cao, Z. Hou, L. Yu, *Macromolecules* **2003**, *36*, 7014–7019.
[60] M. Angiuli, F. Ciardelli, A. Colligiani, F. Greco, A. Romano, G. Ruggeri, E. Tombari, *Appl. Opt.* **2006**, *45*, 7928–7937.
[61] J. A. Herlocker, C. Fuentes-Hernandez, K. B. Ferrio, E. Hendrickx, P.-A. Blanche, N. Peyghambarian, B. Kippelen, Y. Zhang, J. F. Wang, S. R. Marder, *Appl. Phys. Lett.* **2000**, *77*, 2292–2294.
[62] K. Meerholz, B. L. Volodin, B. Kippelen, N. Peyghambarian, *Nature* **1994**, *371*, 497–500.
[63] N. Tsutsumi, W. Miyazaki, *J. Appl. Phys.* **2009**, *106*, 083113.
[64] E. Mecher, C. Bräuchle, H.-H. Hörhold, J. C. Hummelen, K. Meerholz, *Phys. Chem. Chem. Phys.* **1999**, *1*, 1749–1756.
[65] C.-S. Choi, I. K. Moon, J.-W. Oh, N. Kim, *Mol. Cryst. Liq. Cryst.* **2007**, *472*, 401–405.
[66] I. K. Moon, C.-S. Choi, N. Kim, *J. Photochem. Photobiol. A: Chem.* **2009**, *202*, 57–62.
[67] I. K. Moon, C.-S. Choi, N. Kim, *Optical Materials* **2009**, *31*, 1017–1021.
[68] U. Hofmann, A. Schreiber, D. Haarer, S. J. Zilker, A. Bacher, D. D. C. Bradley, M. Redecker, M. Inbasekaran, W. W. Wu, E. P. Woo, *Chem. Phys. Lett.* **1999**, *311*, 41–46.
[69] M. Salvador, J. Prauzner, S. Köber, K. Meerholz, J. J. Turek, K. Jeong, D. D. Nolte, *Opt. Express* **2009**, *17*, 11834–11849.
[70] E. Mecher, F. Gallego-Gómez, K. Meerholz, H. Tillmann, H.-H. Hörhold, J. C. Hummelen, *ChemPhysChem* **2004**, *5*, 277–284.
[71] E. Mecher, F. Gallego-Gómez, H. Tillmann, H.-H. Hörhold, J. C. Hummelen, K. Meerholz, *Nature* **2002**, *418*, 959–964.
[72] N. Tsutsumi, T. Murao, W. Sakai, *Macromolecules* **2005**, *38*, 7521–7523.
[73] D. Wright, U. Gubler, W. E. Moerner, M. S. DeClue, J. S. Siegel, *J. Phys. Chem. B* **2003**, *107*, 4732–4737.
[74] K. Ogino, T. Nomura, T. Shichi, S.-H. Park, H. Sato, T. Aoyama, T. Wada, *Chem. Mater.* **1997**, *9*, 2768–2775.
[75] C. Fuentes-Hernandez, J. Thomas, R. Termine, G. Meredith, N. Peyghambarian, B. Kippelen, S. Barlow, G. Walker, S. R. Marder, M. Yamamoto, K. Cammack, K. Matsumoto, *Appl. Phys. Lett.* **2004**, *85*, 1877–1879.
[76] J. Thomas, C. Fuentes-Hernandez, M. Yamamoto, K. Cammack, K. Matsumoto, G. A. Walker, S. Barlow, B. Kippelen, G. Meredith, S. R. Marder, N. Peyghambarian, *Adv. Mater.* **2004**, *16*, 2032–2036.
[77] H. J. Bolink, C. Arts, V. V. Krasnikov, G. G. Malliaras, G. Hadziioannou, *Chem. Mater.* **1997**, *9*, 1407–1413.
[78] D. Jong Suh, O. Ok Park, T. Ahn, H.-K. Shim, *Opt. Mater.* **2002**, *21*, 365–371.
[79] I.K. Moon, C.-S. Choi, N. Kim, *Org. Electron.* **2009**, *10*, 1521–1528.
[80] O. Zobel, M. Eckl, D.R.P. Strohriegl, M. Eckl, P. Strohriegl, D. Haarer, *Adv. Mater.* **1995**, *7*, 911–914.
[81] P. M. Borsenberger, D. S. Weiss, *Organic Photoreceptors for Xerography*, Marcel Dekker **1998**.
[82] M. C. J. M. Donckers, S. M. Silence, C. A. Walsh, F. Hache, D. M. Burland, W.E. Moerner, R.J. Twieg, *Opt. Lett.* **1993**, *18*, 1044–1046.
[83] E. Hendrickx, D. Van Steenwinckel, A. Persoons, *Appl. Opt.* **2001**, *40*, 1412–1416.
[84] A. Goonesekera, D. Wright, W.E. Moerner, *Appl. Phys. Lett.* **2000**, *76*, 3358–3360.
[85] B. L. Volodin, B. Kippelen, K. Meerholz, B. Javidi, N. Peyghambarian, *Nature* **1996**, *383*, 58–60.
[86] B. Kippelen, S. R. Marder, E. Hendrickx, J. L. Maldonado, G. Guillemet, B. L. Volodin, D. D. Steele, Y. Enami, Sandalphon, Y. J. Yao, J. F. Wang, H. Röckel, L. Erskine, N. Peyghambarian, *Science* **1998**, *279*, 54–57.
[87] M. B. Klein, G. D. Bacher, A. Grunnet-Jepsen, D. Wright, W. E. Moerner, *Opt. Commun.* **1999**, *162*, 79–84.
[88] A. Grunnet-Jepsen, C. L. Thomson, W. E. Moerner, *Science* **1997**, *277*, 549–552.
[89] Y. Zhang, T. Wada, H. Sasabe, *J. Mater. Chem.* **1998**, *8*, 809–828.
[90] H. J. Bolink, V. V. Krasnikov, G. G. Malliaras, G. Hadziioannou, *J. Phys. Chem.* **1996**, *100*, 16356–16360.
[91] R. Bittner, T. K. Däubler, D. Neher, K. Meerholz, *Adv. Mater.* **1999**, *11*, 123–127.
[92] R. Bittner, C. Bräuchle, K. Meerholz, *Appl. Opt.* **1998**, *37*, 2843–2851.

[93] J. C. Ribierre, L. Mager, F. Gillot, A. Fort, S. Méry, *J. Appl. Phys.* **2006**, *100*, 043103.
[94] N. Tsutsumi, H. Kasaba, *J. Appl. Phys.* **2008**, *104*, 073102.
[95] R. Angelone, C. Caste, V. Castelvetro, F. Ciardelli, A. Colligiani, F. Greco, A. Mazzotta, G. Ruggeri, *e-Polymers* **2004**, *075*, 1–15.
[96] S. Tay, P.-A. Blanche, R. Voorakaranam, A. V. Tunç, W. Lin, S. Rokutanda, T. Gu, D. Flores, P. Wang, G. Li, P. St Hilaire, J. Thomas, R. A. Norwood, M. Yamamoto, N. Peyghambarian, *Nature* **2008**, *451*, 694–698.
[97] O.-P. Kwon, S.-J. Kwon, M. Jazbinšek, S.-H. Lee, P. Günter, *Polymer* **2005**, *46*, 10301–10310.
[98] A. Grunnet-Jepsen, D. Wright, B. Smith, M. S. Bratcher, M. S. Declue, J. S. Siegel, W. E. Moerner, *Chem. Phys. Lett.* **1998**, *291*, 553–561.
[99] E. Hendrickx, B. Kippelen, S. Thayumanavan, S. R. Marder, A. Persoons, N. Peyghambarian, *Chem. Phys.* **2000**, *112*, 9557–9561.
[100] M. Eralp, J. Thomas, S. Tay, G. Li, G. Meredith, A. Schülzgen, N. Peyghambarian, G. A. Walker, S. Barlow, S. R. Marder, *Appl. Phys. Lett.* **2004**, *85*, 1095–1097.
[101] J. A. Quintana, P. G. Boj, J. M. Villalvilla, J. Ortíz, F. Fernández-Lázaro, A. Sastre-Santos, M. A. Díaz-García, *Appl. Phys. Lett.* **2005**, *87*, 261111.
[102] J. A. Quintana, J. M. Villalvilla, P. G. Boj, L. Martín-Gomis, J. Ortiz, F. Fernández-Lázaro, Á. Sastre-Santos, M.A. Díaz-Garciía, *Adv. Funct. Mater.* **2009**, *19*, 428–437.
[103] Y. Wang, A. Suna, *J. Phys. Chem. B* **1997**, *101*, 5627–5638.
[104] J.-W. Oh, I. K. Moon, N. Kim, *J. Photochem. Photobiol. A: Chem.* **2009**, *201*, 222–227.
[105] N. Tsutsumi, Y. Ito, W. Sakai, *Chem. Phys.* **2008**, *344*, 189–194.
[106] S. Tay, J. Thomas, M. Eralp, G. Li, B. Kippelen, S.R. Marder, G. Meredith, A. Schülzgen, N. Peyghambarian, *Appl. Phys. Lett.* **2004**, *85*, 4561–4563.
[107] S. Tay, J. Thomas, M. Eralp, G. Li, R. A. Norwood, A. Schülzgen, M. Yamamoto, S. Barlow, G. A. Walker, S. R. Marder, N. Peyghambarian, *Appl. Phys. Lett.* **2005**, *87*, 171105.
[108] L. Martín-Gomis, J. Ortiz, F. Fernández-Lázaro, Á. Sastre-Santos, B. Elliott, L. Echegoyen, *Tetrahedron* **2006**, *62*, 2102–2109.
[109] L. Martín-Gomis, F. Fernández-Lázaro, Á. Sastre-Santos, J. A. Quintana, J. M. Villalvilla, P. Boj, M. A. Díaz-García, *Synt. Met.* **2007**, *157*, 1064–1070.
[110] J. Ortiz, F. Fernández-Lázaro, Á. Sastre-Santos, J. A. Quintana, J. M. Villalvilla, P. Boj, M. A. Díaz-García, J. A. Rivera, S. E. Stepleton, C. T. Cox, L. Echegoyen, *Chem. Mater.* **2004**, *16*, 5021–5026.
[111] E. Śliwińska, S. Mansurova, U. Hartwig, K. Buse, K. Meerholz, *Appl. Phys. B* **2009**, *95*, 519–524.
[112] O. Ostroverkhova, D. Wright, U. Gubler, W. E. Moerner, M. He, A. Sastre-Santos, R. J. Twieg, *Adv. Funct. Mater.* **2002**, *12*, 621–629.
[113] W. D. Gill, *J. Appl. Phys.* **1972**, *43*, 5033–5040.
[114] C. A. Walsh, D. M. Burland, *Chem. Phys. Lett.* **1992**, *195*, 309–315.
[115] Y. Zhang, Y. Cui, P. N. Prasad, *Phys. Rev.B* **1992**, *46*, 9900–9902.
[116] A. V. Vannikov, R. W. Rychwalski, A. D. Grishina, L. Y. Pereshivko, T. V. Krivenko, V. V. Savel'ev, V. I. Zolotarevskii, *Opt. Spectrosc.* **2005**, *99*, 643–648.
[117] P.-A. Blanche, B. Kippelen, A. Schülzgen, C. Fuentes-Hernandez, G. Ramos-Ortiz, J. F. Wang, E. Hendrickx, N. Peyghambarian, S. R. Marder, *Opt. Lett.* **2002**, *27*, 19–21.
[118] A. D. Grishina, L. Y. Pereshivko, L. Licea-Jimenez, T. V. Krivenko, V. V. Savel'ev, R. W. Rychwalski, A. V. Vannikov, *High Energy Chem.* **2008**, *42*, 378–384.
[119] A. V. Vannikov, A. D. Grishina, *High Energy Chem.* **2007**, *41*, 162–175.
[120] H. Ali, J.E. van Lier, *Chem. Rev.* **1999**, *99*, 2379–2450.
[121] A. D. Grishina, F. Y. Konnov, Y. G. Gorbunova, Y. Y. Enakieva, L. Y. Pereshivko, T. V. Krivenko, V. V. Savel'ev, A. V. Vannikov, A. Y. Tsivadze, *Russ. J. Phys. Chem. A* **2007**, *81*, 982–989.
[122] Z. Peng, A.R. Gharavi, L. Yu, *J. Am. Chem. Soc.* **1997**, *119*, 4622–4632.
[123] F. Gallego-Gómez, J. J. M. Villalvilla, M. A. Díaz-García, L. Martín-Gomis, F. Fernández-Lázaro, A. Sastre-Santos*Chem. Mater.* **2009**, *21*, 2714–2720
[124] F. Gallego-Gómez, M. Salvador, S. Köber, K. Meerholz, *Appl. Phys. Lett.* **2007**, *90*, 251113.
[125] P. N. Prasad, *Nanophotonics*, Wiley-Interscience **2004**.
[126] P. N. Prasad, *Curr. Opin. Solid State Mater. Sci.* **2004**, *8*, 11–19.
[127] D. V. Talapin, J.-S. Lee, M. V. Kovalenko, E. V. Shevchenko, *Chem. Rev.* **2010**, *110*, 389–458.
[128] X. Li, J. W. M. Chon, M. Gu, *Australian J. Chem.* **2008**, *61*, 317–323.
[129] T. M. Fears, C. Anderson, J. G. Winiarz, *J. Chem. Phys.* **2008**, *129*, 154704.
[130] J. H. Park, O. Ok Park, *Appl. Phys. Lett.* **2006**, *89*, 193101.
[131] K. Roy Choudhury, J. G. Winiarz, M. Samoc, P. N. Prasad, *Appl. Phys. Lett.* **2003**, *82*, 406–408.
[132] K. Roy Choudhury, M. Samoc, A. Patra, P. N. Prasad, *J. Phys. Chem. B* **2004**, *108*, 1556–1562.
[133] C. Fuentes-Hernandez, D. J. Suh, B. Kippelen, S. R. Marder, *Appl. Phys. Lett.* **2004**, *85*, 534–536.
[134] F. Aslam, D. Binks, M. Rahn, D. P. West, P. O'Brien, N. Pickett, *J. Modern Opt.* **2005**, *52*, 945–953.
[135] D. J. Binks, S. P. Bant, D. P. West, P. O'Brien, M. A. Malik, *J. Modern Opt.* **2003**, *50*, 299–310.
[136] F. Aslam, D. M. D. Rahn, D. P. West, P. O'Brien, N. Pickett, S. Daniels*J. Chem. Phys.* **2005**, *122*, 184713.
[137] J. G. Winiarz, L. Zhang, M. Lal, C. S. Friend, P. N. Prasad, *J. Am. Chem. Soc.* **1999**, *121*, 5287–5295.
[138] X. Li, J. van Embden, J. W. M. Chon, R. A. Evans, M. Gu, *Appl. Phys. Lett.* **2010**, *96*, 253302.
[139] L. Ding, D. Jiang, J. Huang, G. Erdan, L. Liu, Z. Chai, D. Liu, *J. Phys. Chem. C* **2008**, *112*, 10266–10272.
[140] F. Aslam, D. J. Binks, S. Daniels, N. Pickett, P. O'Brien, *Chem. Phys.* **2005**, *316*, 171–177.
[141] D. J. Binks, D. P. West, S. Norager, P. O'Brien, *J. Chem. Phys.* **2002**, *117*, 7335–7341.
[142] F. Aslam, J. Stevenson-Hill, D. J. Binks, S. Daniels, N. L. Pickett, P. O'Brien, *Chem. Phys.* **2007**, *334*, 45–52.
[143] F. Aslam, D. M. Graham, D. J. Binks, P. Dawson, N. Pickett, P. O'Brien, C. C. Byeon, D.-K. Ko, J. Lee, *J. Appl. Phys.* **2008**, *103*, 093702.
[144] C. L. Yang, J. N. Wang, W. K. Ge, S. H. Wang, J. X. Cheng, X. Y. Li, Y. J. Yan, S. H. Yang, *Appl. Phys. Lett.* **2001**, *78*, 760–762.
[145] S. Wang, S. Yang, C. Yang, Z. Li, J. Wang, W. Ge, *J. Phys. Chem. B* **2000**, *104*, 11853–11858.
[146] J. G. Winiarz, *J. Phys. Chem. C* **2007**, *111*, 1904–1911.
[147] D. Van Steenwinckel, E. Hendrickx, A. Persoons, *J. Chem. Phys.* **2001**, *114*, 9557–9564.
[148] J. G. Winiarz, L. Zhang, J. Park, P. N. Prasad, *J. Phys. Chem. B* **2002**, *106*, 967–970.
[149] K. Roy Choudhury, Y. Sahoo, S. Jang, P. N. Prasad, *Adv. Funct. Mater.* **2005**, *15*, 751–756.
[150] K. Roy Choudhury, Y. Sahoo, P. N. Prasad, *Adv. Mater.* **2005**, *17*, 2877–2881.
[151] J. G. Winiarz, L. Zhang, M. Lal, C. S. Friend, P. N. Prasad, *Chem. Phys.* **1999**, *245*, 417–428.
[152] C.-Y. Moon, S.-H. Wei, *Phys. Rev.B* **2006**, *74*, 045205.
[153] I. Chakraborty, D. Mitra, S. P. Moulik, *J. Nanoparticle Res.* **2005**, *7*, 227–236.
[154] S. Mansurova, K. Meerholz, E. Śliwińska, U. Hartwig, K. Buse, *Phys. Rev. B* **2009**, *79*, 174208.

[155] S. Köber, J. Prauzner, M. Salvador, K. Meerholz, in *Photorefractive Materials, Effects and Devices: Control Of Light and Matter, PR09 Topical Meeting Technical Digest* **2009**, P1–46.
[156] Q. Wei, Y. Liu, Z. Chen, M. Huang, J. Zhang, Q. Gong, X. Chen, Q. Zhou, *J. Opt. A: Pure and Appl. Opt.* **2004**, *6*, 890–893.
[157] J. Zhang, Z. Chen, Y. Liu, M. Huang, Q. Wei, Q. Gong, *Appl. Phys. Lett.* **2004**, *85*, 1323–1325.
[158] R. Bittner, K. Meerholz, G. Steckman, D. Psaltis, *Appl. Phys. Lett.* **2002**, *81*, 211–213.
[159] G. J. Steckman, R. Bittner, K. Meerholz, D. Psaltis, *Opt. Commun.* **2000**, *185*, 13–17.
[160] G. G. Malliaras, V. V. Krasnikov, H. J. Bolink, G. Hadziioannou, *Appl. Phys. Lett.* **1995**, *66*, 1038–1040.
[161] D. Pai, J. Yanus, M. Stolka, *J. Phys. Chem.* **1984**, *88*, 4714–4717.
[162] F. Würthner, R. Wortmann, K. Meerholz, *ChemPhysChem* **2002**, *3*, 17–31.
[163] F. Würthner, R. Wortmann, R. Matschiner, K. Lukaszuk, K. Meerholz, Y. DeNardin, R. Bittner, C. Bräuchle, R. Sens, *Angew. Chem.* **1997**, *109*, 2933–2936.
[164] F. Würthner, C. Thalacker, R. Matschiner, K. Lukaszuk, R. Wortmann, *Chem. Commun.* **1998**, 1739–1740.
[165] S. Beckmann, K.-H. Etzbach, P. Krämer, K. Lukaszuk, R. Matschiner, A. J. Schmidt, P. Schuhmacher, R. Sens, G. Seybold, R. Wortmann, F. Würthner, *Adv. Mater.* **1999**, *11*, 536–541.
[166] R. Wortmann, C. Glania, P. Krämer, K. Lukaszuk, R. Matschiner, R. J. Twieg, F. You, *Chem. Phys.* **1999**, *245*, 107–120.
[167] S. R. Marder, *Chem. Commun.* **2006**, 131–134.
[168] S. R. Marder, B. Kippelen, A. K.-Y. Jen, N. Peyghambarian, *Nature* **1997**, *388*, 845–851.
[169] B. Kippelen, F. Meyers, N. Peyghambarian, S. R. Marder, *J. Am. Chem. Soc.* **1997**, *119*, 4559–4560.
[170] K. Meerholz, Y. De Nardin, R. Bittner, *Mol. Cryst. Liq. Cryst.* **1998**, *315*, 99–104.
[171] D. J. McGee, J. Y. Fukunaga, T. Zielinski, M. Yang, C. Salter, *J. Appl. Phys.* **2005**, *97*, 103102.
[172] H. Chun, I. K. Moon, D.-H. Shin, N. Kim, *Chem. Mater.* **2001**, *13*, 2813–2817.
[173] H. Chun, I. K. Moon, D.-H. Shin, S. Song, N. Kim, *J. Mater. Chem.* **2002**, *12*, 858–862.
[174] R. Angelone, F. Ciardelli, A. Colligiani, F. Greco, P. Masi, A. Romano, G. Ruggeri, *ChemPhysChem* **2010**, *11*, 460–465.
[175] R. Angelone, F. Ciardelli, A. Colligiani, F. Greco, P. Masi, A. Romano, G. Ruggeri, J.-L. Stehlé, *Appl. Opt.* **2008**, *47*, 6680–6691.
[176] J. L. Maldonado, Y. Ponce-de-León, G. Ramos-Ortíz, M. Rodríguez, M. A. Meneses-Nava, O. Barbosa-García, R. Santillán, N. Farfán, *J. Phys. D: Appl. Phys.* **2009**, *42*, 075102.
[177] W. G. Jun, M. J. Cho, D. H. Choi, *J. Kor. Phys. Soc.* **2005**, *47*, 620–624.
[178] K. Meerholz, Y. D. Nardin, R. Bittner, R. Wortmann, F. Würthner, *Appl. Phys. Lett.* **1998**, *73*, 4–6.
[179] F. Würthner, S. Yao, J. Schilling, R. Wortmann, M. Redi-Abshiro, E. Mecher, F. Gallego-Gómez, K. Meerholz, *J. Am. Chem. Soc.* **2001**, *123*, 2810–2824.
[180] E. Hendrickx, J. Herlocker, J. L. Maldonado, S. R. Marder, B. Kippelen, A. Persoons, N. Peyghambarian, *Appl. Phys. Lett.* **1998**, *72*, 1679–1681.
[181] V. E. Campbell, I. In, D. J. McGee, N. Woodward, A. Caruso, P. Gopalan, *Macromolecules* **2006**, *39*, 957–961.
[182] F. Würthner, J. Schmidt, M. Stolte, R. Wortmann, *Angew. Chem. Int. Ed.* **2006**, *45*, 3842–3846.
[183] G. Archetti, A. Abbotto, R. Wortmann, *Chem. A Eur. J.* **2006**, *12*, 7151–7160.
[184] M. Eralp, J. Thomas, G. Li, S. Tay, A. Schülzgen, R. A. Norwood, N. Peyghambarian, M. Yamamoto, *Opt. Lett.* **2006**, *31*, 1408–1410.
[185] D. P. West, M. D. Rahn, C. Im, H. Bässler, *Chem. Phys. Lett.* **2000**, *326*, 407–412.
[186] A. Goonesekera, S. Ducharme, *J. Appl. Phys.* **1999**, *85*, 6506-6514.
[187] M. A. Díaz-García, D. Wright, J. D. Casperson, B. Smith, E. Glazer, W. E. Moerner, L. I. Sukhomlinova, R. J. Twieg, *Chem. Mater.* **1999**, *11*, 1784–1791.
[188] D. Van Steenwinckel, E. Hendrickx, A. Persoons, K. Van Den Broeck, C. Samyn, *Chem. Phys.* **2000**, *112*, 11030–11037.
[189] S. Köber, F. Gallego-Gómez, M. Salvador, F. B. Kooistra, J. C. Hummelen, G. F. Mielke, O. Nuyken, K. Meerholz, in *Photorefractive Effects, Photosensitivity, Fiber Gratings, Photonic Materials and More (PR) 2007, OSA Technical Digest* **2007**, TuC6.
[190] P. M. Lundquist, R. Wortmann, C. Geletneky, R. J. Twieg, M. Jurich, V. Y. Lee, C. R. Moylan, D. M. Burland, *Science* **1996**, *274*, 1182–1185.
[191] O. Ostroverkhova, M. He, R. J. Twieg, W. E. Moerner, *ChemPhysChem* **2003**, *4*, 732-744.
[192] O. Ostroverkhova, W. E. Moerner, M. He, R. J. Twieg, *Appl. Phys. Lett.* **2003**, *82*, 3602–3604.
[193] S. J. Zilker, U. Hofmann, *Appl. Opt.* **2000**, *39*, 2287–2290.
[194] I. K. Moon, N. Kim, *Dyes and Pigments* **2008**, *76*, 353–357.
[195] L. Zhang, J. Shi, Z. Jiang, M. Huang, Z. Chen, Q. Gong, S. Cao, *Adv. Funct. Mater.* **2008**, *18*, 362-368.
[196] N. M. Kronenberg, V. Steinmann, H. Bürckstümmer, J. Hwang, D. Hertel, F. Würthner, K. Meerholz, *Adv. Mater.* **2010**, *22*, 4193–4197.
[197] F. Würthner, K. Meerholz, *Chem. A Eur. J.* **2010**, *16*, 9366–73.
[198] K. Meerholz, E. Mecher, R. Bittner, Y. De Nardin, *J. Opt. Soc. Am. B* **1998**, *15*, 2114–2124.
[199] O.-P. Kwon, M. Jazbinšek, P. Günter, S.-H. Lee, *Appl. Phys. Lett.* **2006**, *89*, 021905.
[200] T. Sassa, T. Muto, T. Wada, Y. Takeda, T. Fujihara, S. Umegaki, *Appl. Phys. Lett.* **2005**, *86*, 084103.
[201] T. Sassa, T. Muto, T. Wada, *J. Opt. Soc. Am. B* **2004**, *21*, 1255–1261.
[202] N. Tsutsumi, J. Eguchi, W. Sakai, *Chem. Phys. Lett.* **2005**, *408*, 269–273.
[203] M. Eralp, J. Thomas, S. Tay, P.-A. Blanche, A. Schülzgen, R. A. Norwood, M. Yamamoto, N. Peyghambarian, *Opt. Express* **2007**, *15*, 11622–11628.
[204] A. Grunnet-Jepsen, C. L. Thompson, W. E. Moerner, *J. Opt. Soc. Am. B* **1998**, *15*, 905–913.
[205] G. G. Malliaras, V. V. Krasnikov, H. J. Bolink, G. Hadziioannou, *Phys. Rev.B* **1995**, *52*, 14324–14327.
[206] S. J. Zilker, M. Grasruck, J. Wolff, S. Schloter, A. Leopold, M. A. Kol'chenko, U. Hofmann, A. Schreiber, P. Strohriegl, C. Hohle, D. Haarer, *Chem. Phys. Lett.* **1999**, *306*, 285–290.
[207] J. Wolff, S. Schloter, U. Hofmann, D. Haarer, S. J. Zilker, *J. Opt. Soc. Am. B* **1999**, *16*, 1080–1086.
[208] E. Mecher, R. Bittner, C. Bräuchle, K. Meerholz, *Synt. Met.* **1999**, *102*, 993–996.
[209] S. M. Silence, G. C. Bjorklund, W. E. Moerner, *Opt. Lett.* **1994**, *19*, 1822–1824.
[210] J.-W. Oh, J. Choi, N. Kim, *Appl. Opt.* **2009**, *48*, 3160–3164.
[211] P. D. van Voorst, M. R. de Wit, H. L. Offerhaus, S. Tay, J. Thomas, N. Peyghambarian, K.-J. Boller, *Opt. Express* **2007**, *15*, 17587–17591.
[212] G. Li, M. Eralp, J. Thomas, S. Tay, A. Schülzgen, R. A. Norwood, N. Peyghambarian, *Appl. Phys. Lett.* **2005**, *86*, 161103.
[213] J. G. Winiarz, F. Ghebremichael, J. Thomas, G. Meredith, N. Peyghambarian, *Opt. Express* **2004**, *12*, 2517–2528.
[214] T. Sato, N. Nagayama, M. Yokoyama, *Jpn. J. Appl. Phys.* **2004**, *43*, 8064–8068.
[215] M. Duelli, G. Montemezzani, M. Zgonik, P. Günter, in *Nonlinear Optical Effects and Materials*, *Springer Series In Optical Sciences*, Vol. *72*, Springer, Berlin **2000**, 375–436.

[216] C. Halvorsen, B. Kraabel, A. J. Heeger, B. L. Volodin, K. Meerholz, N. Peyghambarian, *Opt. Lett.* **1995**, *20*, 76–79.
[217] P. P. Banerjee, E. Gad, T. Hudson, D. McMillen, H. Abdeldayem, D. Frazier, K. Matsushita, *Appl. Opt.* **2000**, *39*, 5337–5346.
[218] D. Vacar, A. J. Heeger, B. Volodin, B. Kippelen, N. Peyghambarian, *Rev. Sci. Instrum.* **1997**, *68*, 1119–1121.
[219] A. Heifetz, G. S. Pati, J. T. Shen, J.-K. Lee, M. S. Shahriar, C. Phan, M. Yamamoto, *Appl. Opt.* **2006**, *45*, 6148–6153.
[220] A. Okamoto, K. Harasaka, H. Muranaka, T. Sano, A. Nishio, *J. Modern Opt.* **2007**, *55*, 311–322.
[221] D. Ishikawa, A. Okamoto, S. Honma, T. Ito, K. Shimayabu, K. Sato, *Opt. Rev.* **2007**, *14*, 246–251.
[222] N. Koukourakis, M. Breede, N. C. Gerhardt, M. Hofmann, S. Köber, M. Salvador, K. Meerholz, *Electron. Lett.* **2009**, *45*, 46–48.
[223] K. Jeong, J. J. Turek, D. D. Nolte, *Appl. Opt.* **2007**, *46*, 4999–5008.
[224] P. Dean, M. R. Dickinson, D. P. West, *Appl. Phys. Lett.* **2004**, *85*, 363–365.
[225] P. Dean, M. R. Dickinson, D. P. West, *Opt. Lett.* **2005**, *30*, 1941–1943.
[226] M. Salvador, J. Prauzner, S. Köber, K. Meerholz, K. Jeong, D. D. Nolte, *Appl. Phys. Lett.* **2008**, *93*, 231114.
[227] P. Yu, M. Mustata, L. Peng, J. J. Turek, M. R. Melloch, P. M. W. French, D. D. Nolte, *Appl. Opt.* **2004**, *43*, 4862–4873.
[228] M. Salvador, J. Prauzner, S. Köber, K. Meerholz, *Appl. Phys. B* **2011**, *102*, 803–807.
[229] J. A. Herlocker, C. Fuentes-Hernandez, J. F. Wang, N. Peyghambarian, B. Kippelen, Q. Zhang, S. R. Marder, *Appl. Phys. Lett.* **2002**, *80*, 1156–1158.
[230] P.-A. Blanche, S. Tay, R. Voorakaranam, P. Saint-Hilaire, C. Christenson, T. Gu, W. Lin, D. Flores, P. Wang, M. Yamamoto, J. Thomas, R. A. Norwood, N. Peyghambarian, *J. Display Technol.* **2008**, *4*, 424–430.
[231] P.-A. Blanche, A. Bablumian, R. Voorakaranam, C. Christenson, W. Lin, T. Gu, D. Flores, P. Wang, W.-Y. Hsieh, M. Kathaperumal, B. Rachwal, O. Siddiqui, J. Thomas, R. A. Norwood, M. Yamamoto, N. Peyghambarian, *Nature* **2010**, *468*, 80–83.
[232] G. Li, P. Wang, *Appl. Phys. Lett.* **2010**, *96*, 111109.
[233] W. Lv, Z. Chen, Q. Gong, *J. Opt. A: Pure Appl. Opt.* **2007**, *9*, 486–489.
[234] S. Tanaka, N. Nagayama, M. Yokoyama, *Mol. Cryst. Liq. Cryst.* **2004**, *424*, 233–239.
[235] M. Asaro, M. Sheldon, Z. Chen, O. Ostroverkhova, W. E. Moerner, *Opt. Lett.* **2005**, *30*, 519–521.
[236] F. Gallego-Gómez, F. del Monte, K. Meerholz, *Nat. Mater.* **2008**, *7*, 490–497.
[237] H. Kogelnik, *Bell Systems Tech. J.* **1969**, *48*, 2909–2947.
[238] L. Kador, R. Bausinger, A. Leopold, D. Haarer, W. Köhler, *J. Phys. Chem. A* **2004**, *108*, 1640–1643.
[239] W.-J. Joo, N.-J. Kim, H. Chun, I. K. Moon, N. Kim, C.-H. Oh, *J. Appl. Phys.* **2002**, *91*, 6471–6475.
[240] U.-J. Hwang, C.-S. Choi, N. Q. Vuong, N. Kim, *J. Chem. Phys.* **2005**, *123*, 244905.
[241] F. Gallego-Gómez, E. Mecher, K. Meerholz, in *Proceedings Of SPIE* (Ed: K. Meerholz), San Diego **2003**, 1–9.
[242] T. K. Däubler, R. Bittner, K. Meerholz, V. Cimrova, D. Neher, *Phys. Rev. B* **2000**, *61*, 13515–13527.
[243] J. A. Quintana, P. G. Boj, J. M. Villalvilla, M. A. Díaz-García, J. Ortiz, L. Martín-Gomis, F. Fernández-Lázaro, A. Sastre-Santos, *Appl. Phys. Lett.* **2008**, *92*, 041101.
[244] A. Grunnet-Jepsen, C. L. Thompson, W. E. Moerner, *Opt. Lett.* **1997**, *22*, 874–876.
[245] H. C. Pedersen, P. M. Johansen, T. G. Pedersen, *Opt. Commun.* **2001**, *192*, 377–385.
[246] T. Fujihara, T. Sassa, T. Kawada, J.-ichi Mamiya, T. Muto, S. Umegaki, *J. Appl. Phys.* **2010**, *107*, 023112.